Apolipoprotein A-I Mimetics for the Treatment of Niemann-Pick Disease

by

Maria Fawaz

A dissertation submitted in partial fulfillment
of the requirements for the degree of
Doctor of Philosophy
(Medicinal Chemistry)
in the University of Michigan
2020

Doctoral Committee:

Associate Professor Anna Schwendeman, Chair
Professor Heather Carlson
Professor Andrew Lieberman
Professor Nouri Neamati

Maria Fawaz

mvfawaz@umich.edu

ORCID iD: 0000-0002-4743-1444

Dedication

To

My Family

For their unconditional love and support

Acknowledgements

I would like to thank my PhD mentor Dr. Anna A. Shenderova Schwendeman for developing me into an independent scientist and helping me to become a stronger person. I came to Anna's laboratory with great enthusiasm, thirst for knowledge, and passion for science, but lacking some critical skills (experimental design, data analysis, and scientific writing among others). I struggled and learned, over and over, until I started to master new skills with my mentor's help. I really appreciate that Anna gave me many opportunities to present research at local, national and international conferences and also allowed me to go for an internship. That helped me to decide what I wanted to do after graduation and to become a very competitive scientist. Anna and I both came from Russia and she is my role model of a successful scientist, business woman, and mother. Thank you for all the wisdom that you pass to your students (especially during group meetings!). I am forever grateful!

Two chapters in my dissertation were possible because of our amazing collaborator Dr. Andrew Lieberman and his group at the University of Michigan, Department of Pathology. I would like to thank Dr. Lieberman not only for his scientific support, but also for being an incredibly positive and motivating person. In addition, I want to acknowledge Dr. Mark Schultz, a former post-doctoral fellow of Dr. Lieberman, for his contribution to the Niemann-Pick C manuscript presented in the Chapter 2. Over the past few years, Mark has become my cellular biology mentor. His love for science and fun personality are contagious.

Also, I would like to thank my dissertation committee including Dr. Heather Carlson, Dr. Andrew Lieberman, and Dr. Nouri Neamati for their time, support, and guidance.

I would like to thank the Department of Medicinal Chemistry, the Pharmacological Sciences Training Program (PSTP), the Cardiovascular Research and Entrepreneurship (CVRE) Program, and the American Foundation for Pharmaceutical Education (AFPE) for funding me over the course of my studies, allowing me to focus on research, and helping me to develop skills outside of my research area. I would not be able to get any of the aforementioned funding without countless recommendations of my advisor Dr. Anna Schwendeman, Dr. Peter Scott (my former supervisor and great supporter from the University of Michigan PET center), Dr. Xia Shao (colleague and mentor from the University of Michigan PET center), Dr. Heather Carlson, Dr. Andrew Lieberman, and Dr. John Tesmer (collaborator from Purdue University).

Working in the multinational laboratory of my advisor made my life as a student much more enjoyable. We had many awesome potlucks with dishes from China, Korea, Russia, and United States. I would like to thank our lab managers, Rose Ackermann and Karl Olsen, for their positive attitude and help with analytical and troubleshooting questions as well as animal research. I am very thankful to all current and former members of the Schwendeman Labs including Dr. Emily Morin, Dr. Wenmin Yuan, Dr. Rui Kuai, Jenny Shenkar, Dr. Jukyung Kang, Dr. Sang Kim, Alexander Benet, Dr. Dan Li, Dr. Jie Tang, Minzhi Yu, Troy Halseth, Lindsay Scheetz, Dr. Yayuan Liu, Dr. Ling Mei, Dr. Hongliang He, Dr. Lisha Liu, Dr. Kari Nieto, Jenna Walker, Dr. Avital Beig, Dr. Tina Li, Dr. Morgan Giles, and Ziyun Xia for their help with my projects and moral

support. Special thanks to my former undergraduate student, Rang Ming, who worked very hard on the Niemann-Pick project for almost two years. Also, I would like to acknowledge Dr. Sang Kim for his substantial contribution to the HDL manuscript presented in the Chapter 4 of this dissertation. Finally, huge thanks go to Troy Halseth for his help with the dissertation editing.

Special thanks to my friend Edwin Davila-Delgado, for sharing his past experiences with me and motivating me to grow.

Most importantly, I would like to thank my family. Without love and support of my husband Mike I would never be here writing the dissertation. My daughter Victoria is my biggest motivation in life. Although my mom, dad, and my sister are far away across the ocean, still they give me the tremendous emotional support and motivate me to never give up.

Table of Contents

List of Figures

List of Tables

Abstract

Niemann-Pick disease (NPD) is a fatal lipid storage disorder that results in an accumulation of unesterified cholesterol (type C) or sphingomyelin (types A and B) in late endosomes and lysosomes. Inherited defects in *NPC1* or *NPC2* genes are responsible for NPD type C (NPC) while mutations in *SMPD1* gene cause NPD types A (NPA) and B (NPB). To date, NPD management is largely symptomatic with only few therapies in clinical trials. Therefore, the main objective of this dissertation was to develop safe and effective therapeutics for the treatment of NPA/B and NPC. In NPD, the defects in cholesterol and sphingomyelin metabolism cause a panel of cellular problems including markedly decreased levels of high-density lipoproteins (HDL) responsible for the extracellular lipid transport. The body produces HDL as an 8-12 nm nanoparticle composed of a lipid membrane wrapped around by a belt of Apolipoprotein A-I (ApoA-I). Several synthetic HDL (sHDL) particles made of ApoA-I or ApoA-I mimetic peptides complexed with various phospholipids have been previously tested in patients for the treatment of atherosclerosis, where sHDL has been found safe at doses up to 100 mg/kg following intravenous administration. Applying the same strategy to NPD, we proposed that ApoA-I mimetics (peptide or sHDL) could be effective and rapidly translatable therapeutic approaches for the treatment of NPD.

In the second chapter, we investigated the therapeutic potential of ApoA-I mimetic peptides and sHDL in NPC. Nanoparticles, particularly 5A-SM sHDL, were effective at reducing cholesterol accumulations in human NPC cells and resulted in the

rescue of peripheral disease with intraperitoneal route in NPC1 mice. However, the correction of motor function was not detected. A direct brain administration of sHDL reduced cholesterol storage in neurons of NPC1 mice suggesting that the alternative delivery routes, treatment durations, or sHDL composition were still needed to be investigated.

In the third chapter, we used a similar strategy to NPC. We identified a peptide, 22A, and sHDL capable of reducing sphingomyelin levels in human NPA cells. Moreover, the ATP-binding cassette A1 transporter was found to be involved in sphingomyelin efflux from cells. Intravenous administration of 22A to wild type mice rapidly mobilized sphingomyelin from tissues into circulation. In addition to sphingomyelin, peptide and sHDL could both mobilize cholesterol, which was found to be elevated in NPA disease. Together, our data showed that ApoA-I mimetics might represent a novel therapeutic approach for NPA disease.

In the fourth chapter, we systematically evaluated the effect of both peptide sequence and phospholipid composition of sHDL on nanoparticle's ability to mobilize and esterify cholesterol *in vitro* and *in vivo*. Historically, sHDL drug discovery efforts were mainly focused on optimizing peptide sequences rather than understanding how both, peptide and lipid, influence sHDL pharmacokinetic and pharmacodynamic profiles. Two sets of sHDL were designed having either identical phospholipid but variable peptide sequences with different plasma stability, or identical peptide and phospholipids with variable fatty acid chain length and saturation. The results indicated that the phospholipid component in sHDL played a major role in cholesterol mobilization *in vivo* and should not be overlooked in the design of future sHDL.

In conclusion, the findings from these studies provide a solid foundation for the future development of ApoA-I mimetic peptides and sHDL for the treatment of Niemann-Pick disease.

Chapter 1: Introduction

1.1 **Apolipoprotein A-I (ApoA-I)**

Human ApoA-I is a highly α-helical polypeptide with a molecular weight of 28-kDa secreted by the liver and small intestine. ApoA-I functions to stabilize the phospholipid bilayer in high-density lipoproteins (HDL) as well as mediate lipid transport, receptor recognition, and activation of lecithin:cholesterol acyltransferase (LCAT) for the conversion of free cholesterol to cholesteryl ester [1, 2]. Biophysical and crystallographic studies suggest that lipid-free ApoA-I has two domains, N-terminal (1-187) and C-terminal (188-243), each having unique interactions with lipids and proteins. In solution, hydrophobic regions of ApoA-I face inward while hydrophilic regions interact with the aqueous environment. ApoA-I is an amphipathic alpha-helix composed of 22 and 11 amino acid repeats with most of them separated by the helix-breaking proline residue, which allows the protein to be flexible around the periphery of HDL particles [3]. Lipid-free and lipid-poor ApoA-I bind phospholipids and cholesterol via the ATP-binding cassette transporter A1 (ABCA1) on membranes, forming several classes (discoidal and spherical) of nascent HDL particles (Fig. 1-1). Mutations in ApoA-I lead to Tangier disease characterized by severe HDL deficiency confirming the critical role of ApoA-I in HDL biogenesis [4].

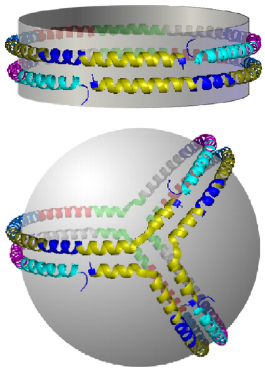

Figure 1-1 ApoA-I conformation on discoidal and spherical HDL particles. *ApoA-I is arranged in a double belt in disks and trefoil in spheres. Figure taken from [5].*

1.2 **High-Density Lipoproteins (HDL)**

High-density lipoproteins (HDL) are heterogeneous nanoparticles (7-12 nm in diameter) composed of proteins (apolipoproteins) and lipids that transport cholesterol in the intravascular and extravascular compartments. HDL particles are synthesized by the liver and intestine to mediate cholesterol transport from peripheral cells to the liver for excretion from the body via the reverse cholesterol transport (RCT). Epidemiological evidence suggests that the level of HDL in circulation is inversely correlated with the risk of coronary heart disease (CHD) [6]. There have been numerous unsuccessful attempts to develop therapies for the treatment of cardiovascular disease focused on raising HDL concentration in plasma. However, new evidence suggests that HDL composition may be as more important than its concentration. It has been recognized that HDL is not simply a cholesterol carrier, but rather a complex molecule with many functions including anti-inflammatory, anti-diabetic, anti-thrombotic, and anti-oxidant among many others yet to be discovered [7-9].

Approximately 70% of HDL protein is apolipoprotein A-I (ApoA-I), which plays a major role in the biogenesis and function of HDL [10]. When ApoA-I is secreted by the

liver (70%) and intestine (30%), it binds a cholesterol transporter, ABCA1, at the cell membrane and acquires phospholipids to form nascent HDL particles (pre-β HDL) as shown in Fig. 1-2. Subsequently, nascent HDL interacts with ABCA1 transporter to efflux cholesterol from cells. Another mechanism for cholesterol efflux described in the literature is based on the retroendocytosis pathway [11, 12]. Here, ApoA-I binds to the ABCA1 transporter at the plasma membrane followed by the ABCA1/ApoA-I complex internalization and transport to late endosomes/lysosomes (LE/Ls). In LE/Ls, ApoA-I picks up lipids, and then lipidated ApoA-I is resecreted from cells through exocytosis. These two pathways may operate simultaneously since ABCA1 is localized in both LE/Ls and the plasma membrane. Once HDL has acquired some cholesterol via ABCA1, it can interact with another lipid transporter called ATP-binding cassette transporter G1 (ABCG1) and efflux more cholesterol from cells. Then, nascent HDL interacts with lecithin:cholesterol acyltransferase (LCAT), an enzyme responsible for cholesterol esterification, leading to formation of larger mature HDL particles. Mature (spherical) HDL consists of apolipoproteins (45-55% by mass), phospholipids (26-32%), esterified cholesterol (15-20%), free cholesterol (3-5%), and triglycerides (5%). Mature HDL can deliver esterified cholesterol (EC) cargo directly to the liver for elimination through scavenger receptor class B type I (SR-BI), or it can transfer EC to low-density lipoproteins (LDL) by interacting with cholesterol ester transfer protein (CETP) for elimination by the liver following LDL receptor-mediated (LDL-R) uptake.

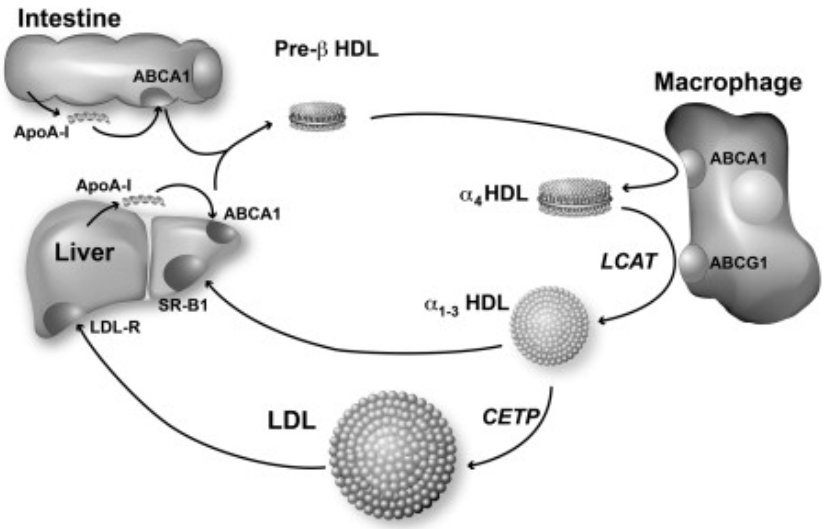

Figure 1-2 Reverse cholesterol pathway (RCT). *Figure taken from [13].*

1.3 **ApoA-I and ApoA-I Mimetic Peptide-based HDL Therapeutics**

ApoA-I-based HDL therapeutics. Human population studies have shown that HDL levels are inversely associated with CVD risk, where even a 1 mg/dL increase in HDL-cholesterol (HDL-C) translates into a 2-3% risk reduction for subsequent coronary events [14]. This data prompted a number of large clinical trials to investigate the role of drugs aimed at raising HDL-C levels to remove cholesterol from arterial plaques. Initially, HDL therapies were mainly based on the infusion of reconstituted HDL (rHDL) composed of purified human ApoA-I or ApoA-I_{Milano} (mutated, R173C) in complex with various phospholipids. The first rHDL product tested in humans was SRC-rHDL by ZLB Central Laboratory. ApoA-I isolated from human plasma was lipidated with soybean phosphatidylcholine (PC) using the cholate dialysis method [15]. Soybean PC was used in rHDL preparation because this was the only phosphatidylcholine available at high quality for parenteral use. A Phase I clinical trial in 40 healthy volunteers showed that SRC-sHDL at 40 mg/kg was safe and well tolerated [16, 17]. A Phase II trial of CSL-111

(ZLB Central Laboratory acquired by CSL Behring) in 183 patients showed toxicity at a dose of 80 mg/kg dose and reformulation of CSL-111 into CSL-112 with reduced lipid to protein ratio took place [18, 19]. CSL-112 was found to be safe and well-tolerated at doses up to 135 mg/kg and capable of acutely enhancing cholesterol efflux [20]. Currently, a Phase III clinical trial (ClinicalTrials.gov) for CSL-112 is still ongoing in 17,400 patients for the reduction of major adverse cardiovascular events.

The limited availability of human blood for ApoA-I purification necessitated the use of recombinantly produced protein in *E. coli*. In 1998, Esperion, developed a new rHDL formulation, ETC-216, composed of ApoA-I_{Milano} and 1-palmitoyl-2-oleoyl-sn-glycero-3-phosphatidylcholine (POPC) at 1:1 protein to lipid weight ratio. Five weekly infusions of ETC-216 at 15 and 45 mg/kg reduced coronary plaque volume by 4.2% and were safe and well tolerated at all doses [21]. Another rHDL product containing rhApoA-I was CER-001 (Cerenis) composed of rhApoA-I in complex with sphingomyelin (SM) and dipalmitoylphosphatidyl-glycerol (DPPG) at 1:2.7:0.1 ratio of ApoA-I:SM:DPPG by weight. Similar to ETC-216, CER-001 was non-toxic at all doses tested (3,6 and 12 mg/kg once per week for 6 weeks) [22, 23].

ApoA-I mimetic peptide-based HDL therapeutics. ApoA-I mimetic peptides are amphipathic α-helixes designed to mimic ApoA-I function. The first peptide, 18A, was developed by Anantharamaiah et al. and contained 18 amino acids sequence (DWLKAFYDKVAEKLKEAF) [24]. However, 18A peptide was not tested in humans. The non-lipidated ApoA-I mimetic peptide, D-4F (Ac-DWFKAFYDKVAEKFKEAF-NH_2), which was a modified version of 18A and made from all D-amino acids to ensure protection from proteolysis, was tested in the clinic. The first study of D-4F in high-risk cardiovascular

patients included a single oral administration of either 4.3 or 7.14 mg/kg, which were both ineffective. The second unsuccessful trial was based on 13 daily injections of D-4F and up to 7.14 mg/kg [25]. Another amphipathic ApoA-I mimetic peptide, ETC-642 (PVLDLFRELLNELLEALKQKLK), was developed by Esperion to be an activator of LCAT enzyme when reconstituted into rHDL. This peptide contained 22 amino acids complexed with SM and dipalmitoyl-phosphatidylcholine (DPPC) at 1:1:1 ETC-642:SM:DPPC ratio. The Phase I clinical trial of ETC-642 rHDL infusion in patients with stable atherosclerosis was found to be safe and tolerated up to 20 mg/kg dose. Further information for ETC-642 has not been made public [26]. Other ApoA-I mimetic peptides well-described in the literature include reverse 4F, ATI-5261, and 5A. All of these peptides showed great promise in animal models and need to be evaluated in humans to determine their efficacy [27].

1.4 **HDL in Niemann-Pick Diseases**

Niemann-Pick diseases (NPD) are rare and severe lipid storage disorders with no FDA-approved treatments. They are caused by loss of function mutations in endolysosomal enzymes leading to an accumulation of lipids and foam cell infiltration in tissues [28]. Mutations in the *SMPD1* gene cause NPD types A and B, where an abnormal accumulation of sphingomyelin originates from the insufficient activity of the acid sphingomelinase (ASM) enzyme [29]. Children with type A NPD die in infancy by age 3-4 while individuals with type B (non-neuropathic) survive into adulthood [30]. NPD type C is caused by mutations in *NPC1* (95% of cases) or *NPC2* genes, which encode proteins, NPC1 and NPC2, required for lysosomal export of unesterified cholesterol [31]. In addition

to cholesterol, sphingolipids (e.g., sphingomyelin and glycosphingolipids) also accumulate in late endosomes (LE) and lysosomes (Ls) together leading to progressive neurological dysfunction and death during childhood or later in life [32].

The accumulated cholesterol in LE/Ls originates from the uptake of LDL through receptor-mediated endocytosis on the plasma membrane [33]. LDL carrying cholesteryl ester traffics through endosomes/lysosomes, where the hydrolysis by acid lipase releases free cholesterol. Cholesterol homeostasis machinery senses elevated cholesterol levels via a negative feedback loop regulated by sterol regulatory element binding proteins (SREBPs) that directly activate genes involved in the synthesis and uptake of cholesterol and in lipogenesis [34]. Also, increases in cholesterol are recognized by liver X receptor (LXR) transcription factors [35]. Activation of LXR up-regulates a membrane transporter, ABCA1, which is responsible for cholesterol efflux from cells to nascent HDL. Compared to cholesterol, sphingomyelin in lysosomes comes not only from extracellular (lipoprotein endocytosis) but also from intracellular (autophagy, membrane recycling or phagocytosis) sources. Major molecular species of sphingomyelin are 16:0 and 24:1 [36]. Sphingomyelin and cholesterol have high affinity for one another and therefore reside together in raft and non-raft regions of the cell [37, 38]. The ABCA1 transporter mobilizes both cell phospholipids (e.g., phosphatidylcholine and sphingomyelin) as well as cholesterol to lipid-poor ApoA-I [39]. This transporter is located on membranes and traffics between the plasma membrane and membranes of intracellular vesicles, including LE/Ls [40, 41]. It has been shown in macrophages that free cholesterol from LE/Ls is the preferential source for ABCA1-mediated efflux that requires functional NPC2 protein, but not NPC1 [42, 43]. Thus, the ABCA1 transporter is a key mediator of cholesterol and

sphingomyelin exit from LE/Ls compartments and might represent a potential therapeutic target in Niemann-Pick diseases.

Niemann-Pick C. NPD type C is an autosomal recessive lysosomal storage disease characterized by an intracellular accumulation of unesterified cholesterol and sphingolipids (Fig. 1-3) [44-46]. NPC is a genetically and clinically heterogeneous neurovisceral disease affecting 1 in 89,000 individuals [47]. It occurs sporadically and causes progressive, disabling neurological symptoms such as vertical supranuclear gaze palsy, dysmetria, dysarthria, dysphagia, cerebellar ataxia, and seizures [48-50]. Most cases of NPC disease are diagnosed early in childhood (age 2-15 years), but increasing numbers of patients are now being recognized with adult (age > 15 years) onset of symptoms. In patients with adult onset, the disease typically presents with movement disorders, psychosis, and early cognitive decline. NPC is a result of mutations in one of two genes, *NPC1* (in 95% of cases) or *NPC2* (5% of cases), with clinically indistinguishable phenotypes [51]. The *NPC1* gene encodes for a large 1278 amino acid protein with 13 transmembrane helices [52]. The disease causing mutations mostly occur in the C-terminal cysteine-rich luminal domain (45%) with I1061T being the most frequent mutation, present in 15-20% of all disease alleles [53]. This particular mutation leads to NPC1 mislocalization and degradation related to protein misfolding [54]. The *NPC2* gene encodes a small 132 amino acid soluble lumenal protein, which binds cholesterol in 1:1 stoichiometry and, when mutated, it looses its ability to bind cholesterol [55]. Several groups have postulated a theory of “hydrophobic hand-off” transfer of cholesterol from NPC2 to NPC1 [52, 56]. In this model, NPC2 binds cholesterol in the lysosomal lumen followed by interaction with NPC1 to achieve cholesterol export from lysosomes. NPC

disease severity depends on the type of mutation an individual carries ranging from neonatal to adult.

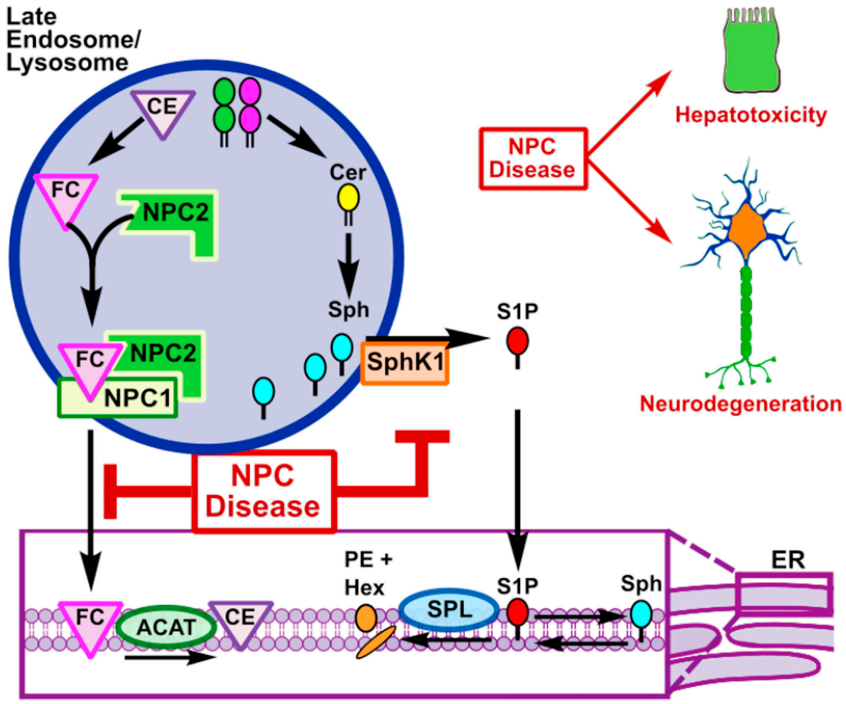

Figure 1-3 Cholesterol and sphingosine metabolism in NPC. *Abbreviations: GSL, glycosphingolipid; LDL; low density lipoprotein; LDLR, low density lipoprotein receptor; SM, sphingomyelin; Cer, ceramide; Sph, sphingosine; SphK1, sphingosine kinase 1; S1P. sphingosine-1-phosphate; S1PRs, S1P receptors; CE; cholesterol esters; FC, free cholesterol; ACAT, cholesterol acyltransferase; SPL, sphingosine-1-phosphate lyase; PE, phosphatidylethanolamine; Hex, hexadecenal. Figure taken from [44].*

Currently, there are no FDA-approved drugs for NPC. In the past, disease treatments have included palliative care such as anti-seizure medication, anticholinergic drugs for dystonia and tremor, and antidepressants or antipsychotics for mood disorders. However, fairly recently substrate reduction therapy aimed at decreasing the concentration of accumulated lipids in LE/Ls has been tested on patients. N-butyldeoxynojirimycin (miglustat) is a small imino sugar that inhibits the synthesis of glycosphingolipids (secondary to cholesterol) shown to accumulate in NPC cells and

cause decreased lysosomal calcium uptake leading to impaired endocytic function [57-59]. Miglustat is approved in Europe for NPC disease, but not in the United States due to inconclusive clinical data [60]. Hydroxypropyl-β-cyclodextrin (cyclodextrin), a pharmaceutical excipient that non-discriminatively binds cholesterol, is another drug currently being tested in patients [61]. The hydrophobic cavity of the cyclodextrin molecule is capable of accommodating cholesterol molecules, and incubation of NPC patient fibroblasts with cyclodextrin leads to a reduction in cellular cholesterol as measured by filipin staining [62]. Repeated subcutaneous (SC) administration of cyclodextrin at extremely high doses (4000 mg/kg) in mice decreases cholesterol levels in the liver and brain, slows Purkinje cell loss, and delays the onset of neurological disease when administered to mice before maturation of the blood-brain barrier (BBB) [63-65]. However, cyclodextrin has does not cross the BBB in adult animals and additional studies in a NPC feline model using repeated intracranial (IC) dosing show significant rescue of CNS symptoms, but fail to control peripheral disease [66, 67]. Thus, co-administration of cyclodextrin by IC (4000 mg/kg) and SC (1000 mg/kg) routes results in optimal disease control. However, high doses of cyclodextrin necessary for correction of neurological dysfunction in a NPC feline model are also associated with pulmonary toxicity and hearing loss owing to the non-specific nature of cyclodextrin as a cholesterol scavenger [68]. In human clinical trials, hearing loss has emerged as a dose-limiting toxicity following intrathecal administration, highlighting the urgent need for safer therapeutics, particularly ones amenable to peripheral administration [69-71].

Niemann-Pick A and B. NPA and NPB are caused by ASM deficiency that results in the progressive accumulation of sphingomyelin in lysosomes. ASM is a 70kDa

glycoprotein localized in lysosomes which operates at pH 4.5-5.5. ASM hydrolyzes SM derived from either the cellular membranes (recycling, autophagy or phagocytosis) or exogenous circulating lipoproteins (endocytosis) to phosphocholine and ceramide (Fig. 1-4) [72]. Sphingomyelin accumulation leads to systemic manifestations such as liver dysfunction, hepatosplenomegaly, infiltrative lung disease, and anemia [73]. Very low ASM activity (<5% of normal levels) in NPA makes this type of lysosomal storage disorder more severe, with sphingomyelin accumulations within visceral tissues and brain compared to non-neuropathic NPB type [74]. Currently, more than 180 mutations have been identified in *SMPD1* gene that cause NPA/B disease, with ΔR608, R496L, L302P, and H421Y being the most common [75]. Several animal models have been established to study ASM deficiency including ASM knockout, transgenic NPB, and knock-in NPA/B (deltaR608, R496L) models [75-78].

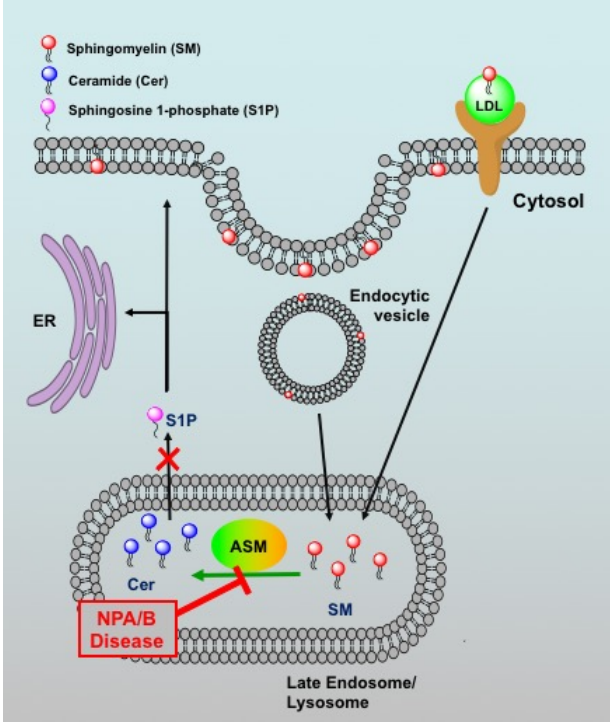

Figure 1-4 Schematic diagram of NPA/B molecular mechanism.

There are no FDA-approved therapies for NPA and NPB disease. However, the enzyme replacement therapy with recombinant human ASM (rhASM) is currently being tested in NPB patients [79, 80]. Rapid production of sphingomyelin catabolites (e.g., ceramide, sphingosine 1-phosphate) necessitates careful substrate debunking using lower doses (3 mg/kg) of rhASM to prevent toxicity. Dose escalation studies in patients have yielded positive results without serious adverse events; reductions in sphingomyelin storage, spleen and liver volumes as well as improvements in lipid profile, lung disease, and quality of life have been achieved [81]. Although rhASM treatment shows great promise for NPB patients, this therapy will require biweekly enzyme infusions, and it will not work for NPA patients with central nervous system symptoms [82]. Thus, it is critical to continue research to develop novel therapeutic strategies.

HDL Functionality in Niemann-Pick Disease. Cholesterol and sphingomyelin trafficking defects in NPD patients lead to markedly reduced (> 2-fold) HDL levels and a pro-atherogenic lipid profile characterized by elevated LDL and triglycerides as shown in Table 1-1 [83-85]. The underlying cause of HDL deficiency appears to have a different origin in NPC versus NPA/B. The cholesterol trafficking defect in NPC leads to impaired regulation of cholesterol synthesis and metabolism gene expression, including HMG-CoA reductase, HMG-CoA synthase, low density lipoprotein receptor (LDL-R), and LXR [84]. LXR regulates the expression of the ABCA1 transporter which in turn is responsible for the rate-limiting step of pre-β HDL formation [86, 87]. Therefore, low levels of ABCA1 in NPC lead to reduced concentration of circulating HDL. Similar to NPC, NPA/B patients have highly atherogenic lipid profiles manifested as elevated triglyceride and LDL-cholesterol along with low HDL-cholesterol levels [85]. However, ABCA1 transporter

expression is normal in these patients and therefore cannot be the reason for low HDL [83]. In turn, HDL in NPA/B patients is highly enriched with sphingomyelin, a known inhibitor of the LCAT enzyme [88]. Without LCAT being able to esterify cholesterol, small and immature HDL particles have a short circulation half-life and are quickly eliminated possibly by liver leading to their low overall levels in the periphery.

Table 1-1 Mean lipid concentrations in male and female NPA, NPB, and NPC1 patients *[84, 89].*

	Male, mean (md/dL)/(SD)	**Female, mean (md/dL)/(SD)**	**Desirable (mg/dL)**	**Abnormal (mg/dL)**
Cholesterol				
Type A	253 (65)	241 (47)	<170	>200
Type B	237 (71)	213 (52)		
Type C1	146 (33)	154 (37)		
HDL-C				
Type A	16 (5)	23 (12)	>45	<35
Type B	20 (7)	24 (11)		
Type C1	30 (10)	35 (11)		
LDL-C				
Type A	156 (57)	164 (54)	<110	>130
Type B	169 (62)	145 (49)		
Type C1	91 (32)	91 (43)		
Triglycerides				
Type A	207 (79)	198 (87)	<125	>125
Type B	235 (96)	169 (90)		
Type C1	126 (53)	152 (68)		

1.5 **Research Scope**

ApoA-I has been recognized as a key player in reverse cholesterol transport, the movement of cholesterol from peripheral tissues to the liver for elimination, where it solubilizes lipids to form HDL particles and acts as an activator of LCAT. ApoA-I is effective in promoting cholesterol efflux from arterial wall macrophages through the ABCA1 transporter. A number of ApoA-I-based therapeutics for the treatment of cardiovascular disease have reached clinical trials, with CSL-112 currently in Phase III. ApoA-I has been conventionally complexed with phospholipids such as soybean PC, POPC, DPPC or SM to form synthetic/reconstituted HDL (sHDL) in order to improve ApoA-I stability *in vivo*. The costly production of ApoA-I either purified from human blood or recombinantly produced in bacteria prompted a search for cheaper ApoA-I alternatives. One such product was ETC-642, was a 22 amino acid peptide with no sequence homology to ApoA-I that was able to form 8-12 nm HDL particles and efflux cholesterol from macrophages. To maximize cholesterol efflux through the ABCA1 transporter, another ApoA-I mimetic peptide, 5A, was developed and tested in pre-clinical animal models. Given that ApoA-I mimetic peptides are effective at solubilizing phospholipids and cholesterol efflux from cells, the work presented here will demonstrate the novel utility of ApoA-I mimetics (peptides and sHDL) for the treatment of a rare cholesterol and sphingomyelin storage disorder called Niemann-Pick disease. Moreover, peptide and phospholipid composition in sHDL will be examined to define the component of sHDL that drives its pharmacodynamics (cholesterol efflux) *in vivo*.

1.6 **Thesis Overview**

The main goal of this thesis is to explore the ability of ApoA-I mimetics to be tailored for cholesterol or sphingomyelin efflux in Niemann-Pick disease. To accomplish this, different ApoA-I mimetic peptides will be explored alone and in complex with phospholipids (sHDL) in Niemann-Pick type C and type A models. This thesis consists of five chapters focused on how the composition of ApoA-I mimetics (peptide and sHDL) influences its phospholipid and cholesterol efflux properties.

Chapter 1 is an introduction describing ApoA-I, its role in the formation of endogenous HDL and lipid transport. Then, a brief discussion of sHDL therapies is presented and followed by an overview of the Niemann-Pick disease. Finally, a literature review of what is known about HDL in Niemann-Pick disease concludes this chapter.

Chapter 2 of this thesis focuses on the discovery of an sHDL composition for the treatment of Niemann-Pick disease type C, which is characterized by excessive accumulation of cholesterol in late endosomes and lysosomes. Initial studies are focused on the design, optimization, and exploration of sHDL mechanism of action in primary human fibroblast cells. In this chapter, we demonstrate a dose-dependent rescue of cholesterol storage that is sensitive to sHDL lipid and peptide composition, enabling the identification of compounds with a range of therapeutic potency. This is accompanied by extensive characterization of sHDL efficacy in the mouse model of NPC1 disease. Findings from this study can be further used to optimize sHDL composition to maximize its therapeutic potential in NPC.

Chapter 3 assesses the utility of ApoA-I mimetics (peptides and sHDL) for the treatment of Niemann-Pick disease type A, which is characterized by excessive

accumulation of sphingomyelin in late endosomes and lysosomes. In this chapter, the efflux of sphingomyelin from primary NPA human fibroblast cells to ApoA-I mimetic peptide acceptors and sHDL is examined in two assays (radioactive and label-free). Lipid-free or lipid-poor ApoA-I mimetics are found to be efficacious at scavenging sphingomyelin from NPA cells. We also demonstrate that the ABCA1 transporter contributes to sphingomyelin efflux from cells. Finally, *in vivo* assessment of ApoA-I mimetic peptide and lipid-poor sHDL using wild type mice shows the ability of a peptide to mobilize sphingomyelin from tissues into circulation. Together, these studies provide proof-of-concept data to support the therapeutic potential of ApoA-I mimetics for the Niemann-Pick Disease type A. Findings from this work can be applied to *in vivo* model of NPA disease.

Chapter 4 presents a systematic evaluation of the effect of both peptide sequence and phospholipid composition of sHDL on particle's ability to mobilize and esterify cholesterol *in vitro* and *in vivo.* Historically, sHDL drug discovery efforts were focused on optimizing peptide sequences for interaction with cholesterol cellular transporters rather than understanding how both sHDL components, peptide and lipid, influence its pharmacokinetics (PK) and pharmacodynamic (PD) profiles. We designed two sets of sHDL having either identical phospholipid but variable peptide sequences with different plasma stability, or identical peptide and phospholipids with variable fatty acid chain length and saturation. Our data highlight the complexity of the reverse cholesterol transport and that the phospholipid composition of sHDL is the driving force for cholesterol mobilization *in vivo.* This work lays the foundation for future studies in appropriate disease models.

Chapter 5 is a summary of the dissertation main findings and future direction for the projects.

Chapters 2-4 were prepared in a manuscript format. Chapter 2 was published in *BMC Medicine*. The manuscript for Chapter 3 will be submitted for publication shortly after the dissertation defense. Chapter 4 was published in the *Journal for Pharmacology and Experimental Therapeutics*.

Chapter 2: Synthetic High-Density Lipoprotein Nanoparticles for the Treatment of Niemann-Pick Diseases

2.1 **Abstract**

Background: Niemann-Pick Disease type C is a fatal and progressive neurodegenerative disorder characterized by the accumulation of unesterified cholesterol in late endosomes and lysosomes. We sought to develop new therapeutics for this disorder by harnessing the body's endogenous cholesterol scavenging particle, high-density lipoprotein (HDL).

Methods: Here we design, optimize, and define the mechanism of action of synthetic HDL (sHDL) nanoparticles.

Results: We demonstrate a dose-dependent rescue of cholesterol storage that is sensitive to sHDL lipid and peptide composition, enabling the identification of compounds with a range of therapeutic potency. Peripheral administration of sHDL to *Npc1 I1061T* homozygous mice mobilizes cholesterol, reduces serum bilirubin, reduces liver macrophage size, and corrects body weight deficits. Additionally, a single intraventricular injection into adult *Npc1 I1061T* brains significantly reduces cholesterol storage in Purkinje neurons. Since endogenous HDL is also a carrier of sphingomyelin, we tested the same sHDL formulation in the sphingomyelin storage disease Niemann-Pick type A. Utilizing stimulated Raman scattering microscopy to detect endogenous unlabeled lipids, we show significant rescue of Niemann-Pick type A lipid storage.

Conclusions: Together, our data establish that sHDL nanoparticles are a potential new therapeutic avenue for Niemann-Pick Diseases.

2.2 **Background**

Niemann–Pick Disease type C is a fatal lysosomal storage disorder that causes progressive neurodegeneration along with visceral organ involvement. Symptom onset and disease severity are variable, but patients commonly develop hepatosplenomegaly, cognitive decline, and seizures, culminating in death in the second - third decades of life [90, 91]. Niemann-Pick C patients have loss-of-function mutations in the NPC2 (~5%) or, more commonly, NPC1 (~95%) proteins. In the late endosome/lysosomal compartment (LE/Lys), LDL derived unesterified cholesterol is bound by NPC2 and transferred to the transmembrane NPC1 protein [92, 93]. Using a poorly defined mechanism, NPC1 exports unesterified cholesterol from LE/Lys. Unesterified cholesterol then moves to other sites within the cell where it alters membrane dynamics or is utilized for steroid production [93]. In patients with Niemann-Pick C, mutations in NPC1/NPC2 prevent intracellular lipid trafficking and cause characteristic cholesterol storage [94]. A biochemically similar lipid storage disease arises from mutations in the gene encoding the lysosomal enzyme acid sphingomyelinase. Deficiency of enzyme activity causes Niemann-Pick Disease types A and B, in which the storage of sphingolipids and cholesterol in LE/Lys leads to hepatosplenomegaly and varying degrees of neurodegeneration [95].

Endogenous mechanisms to maintain cellular cholesterol homeostasis include the removal of excess cholesterol by high-density lipoprotein (HDL) particles.

Cholesterol is effluxed from peripheral cells by nascent HDL particles and esterified in plasma, and then mature HDLs travel to the liver where cholesterol is eliminated in the bile [96]. Recent work has taken advantage of endogenous HDL function for the development of synthetic HDL (sHDL) nanoparticles as potential therapeutics for cardiovascular diseases [19, 21, 97, 98]. These nanoparticles are composed of the HDL protein apolipoprotein A-1 (ApoA1) or ApoA1 mimetic peptides surrounding a lipid bilayer to form 10-12 nm diameter discoidal lipoprotein particles [99, 100]. Chemical synthesis of sHDL permits modifications that alter lipid and ApoA1 peptide composition and thereby impact potency, pharmacokinetics and safety [101-104]. sHDL nanoparticles were initially designed for removal of cholesterol from lipid-laden atherosclerotic plaques. In clinical trials involving ~2,000 cardiovascular disease patients, sHDL was safe and well-tolerated [19, 21, 23, 105-107], and a large phase III clinical trial in 17,400 patients is currently ongoing (https://clinicaltrials.gov/ct2/show/NCT03473223).

Here, we developed and optimized a sHDL nanoparticle which significantly reduces the accumulated cholesterol in Niemann-Pick type C cells. The sHDL contains a 37-amino acid ApoA1 mimetic peptide, termed 5A, and sphingomyelin (SM); these nanoparticles were originally developed for the treatment of atherosclerosis. 5A-SM sHDL at 1:1.15 (wt/wt) peptide:lipid ratio is safe in primates, and with established sterile manufacturing, this sHDL is well positioned for rapid clinical translation [108, 109]. We show that 5A-SM sHDLs are non-toxic and effective at reducing cholesterol storage in Niemann-Pick C patient fibroblasts and brain slice cultures from *Npc1* mutant mice. We establish that 5A-SM requires the ATP-binding cassette transporter 1 (ABCA1) to efflux

stored cholesterol. *In vivo* studies using *Npc1* mutant mice show evidence of target engagement and rescue of peripheral phenotypes and neuronal cholesterol storage. Furthermore, we show that 5A-SM also rescues sphingomyelin storage in Niemann-Pick type A fibroblasts. Together, these studies provide proof-of-concept data to support the therapeutic potential of sHDL for the Niemann-Pick Diseases.

2.3 **Methods**

Mice

All *Npc1*-I1061T mice [110] were backcrossed to C57BL/6 (≥10 generations). Approximately equal number of males and females were used for all experiments and littermates were used when available. Mice were randomly assigned to vehicle or experimental groups. All procedures involving mice were approved by the University of Michigan Committee on Use and Care of Animals (PRO00008133) and conducted in accordance with institutional and federal guidelines.

Reagents

2-hydroxypropyl-β-cyclodextrin (H-107) and amiloride (A7410) were from Sigma. EndoH (P0702) and PNGaseF (P0704) were from New England Biolabs. Dynasore (14061) was from Cayman Chemical; Human HDL (J64903) and acetylated LDL (J65029) were from Alfa Aesar. 5A peptide (DWLKAFYDKVAEKLKEAF-P-DWAKAAYDKAAEKAKEAA, 4078379) was from Bachem Americas (Torrance, CA). 22A peptide (PVLDLFRELLNELLEALKQKLK) was synthesized by Genscript (Piscataway, NJ). Lipids including egg-sphingomyelin (SM, Coastome NM-10), 1,2-

dimyristoyl-*sn*-glycero-3-phosphocholine (DMPC, Coastome MC-4040), and 1-palmitoyl-2-oleoyl-*sn*-glycero-3-phosphocholine (POPC, Coastome MC-6081) were from NOF America Corporation. 1,1'-Dioctadecyl-3,3,3',3'-tetramethylindodicarbocyanine, 4-chlorobenzenesulfonate salt (DiD, D7757) and 4-(4-(dihexadecylamino)styryl)-*N*-methylpyridinium iodide (DiA, D3883) were from Invitrogen. Cholesteryl [1,2,6,7-3H(N)] linoleate (ART 1203) and sphingomyelin [choline methyl-3H] were from American Radiolabeled Chemicals (Saint Louis, MO). N-[6-[(7-nitro-2-1,3-benxoxadiazol-4-yl)amino]-sphingosine-1-phosphocholine (NBD-Sphingomyelin, 810218P) was from Avanti Polar Lipids (Alabaster, AL).

Antibodies

(Antigen, dilution, vendor, cat. no.): NPC1, 1:500, Abcam, ab134113; Actin, 1:4000, Sigma, A544; LAMP1, 1:100, Developmental Studies Hybridoma Bank University of Iowa, H4A3; Calbindin, 1:500-1:2,000, Sigma, 02724; GFAP, 1:500, Dako, z0344; IBA1, 1:250, Abcam, ab5076; NeuN, 1:500, Millipore, abn78; EEA1, 1:400, abcam, ab2900; F4/80, 1:400, abcam, ab6640.

sHDL synthesis

sHDL particles were prepared using a lyophilization method where peptide (5A or 22A) and lipid (SM, DMPC or POPC) were dissolved in acetic acid at 1:1.5 wt/wt ratio and then lyophilized together for 24 hr. HDL was fluorescently labeled by adding 4 μg DiD or DiA per 1 mg peptide directly to the acetic acid mixture of peptide and SM. The resulting lyophilized dry pellet was re-hydrated in PBS, pH 7.4, to a final peptide concentration of

10 mg/mL, vortexed, and thermocycled 3 X between 55° C and room temperature to generate sHDL particles. pH was adjusted to 7.4 and sHDLs were sterile filtered using 0.22 μm Millipore filters. Labeling of 5A peptide in sHDL (5A-SM-DiA) with AlexaFluor 647 dye was performed using Invitrogen protein labeling kit (A20173). Purification of 5A-SM-DiA-Alexa647 post-labeling was done on the size-exclusion column supplied in the kit, and the final concentration of sHDL was determined according to the manufacturer's instructions using plate reader measurements (SynergyTM NEO HTS Multi-Mode Microplate Reader, Bio-Tek).

sHDL characterization

Fluorescently labeled sHDL particles were analyzed by UPLC (Waters Aquity UPLC BEH125 sec 1.7 μm, 4.6 x 150 mm column) equipped with UV (220 nm) and fluorescence detectors (ex/em 644/665 nm DiD, 456/590 nm DiA, 650/665 nm AlexaFluor647). The hydrodynamic diameters of sHDL were determined by dynamic light scattering on Zetasizer Nano ZSP, Malvern Instruments (Westborough, MA). The volume intensity average values were reported. Transmission electron microscopy images were obtained on an FEI Morgagni electron microscope run at 100 kV at a magnification of 22,000 x (2.1Å/pixel) and then recorded on a Gatan Orius charge-coupled device camera. sHDL samples (3 μL of 2 μg/ml) were adsorbed for 1 minute to a glow discharged 400-mesh copper grid covered with carbon-coated colloidion film (Structure Probe). The grids were washed twice and then negatively stained in 0.07% uranyl formate. 22A and 5A peptides, SM, POPC, and DMPC lipids combined at 1:0.5, 1:1 and 1:2 wt/wt ratios were described previously[101, 102].

Cells

Cell lines were obtained from the NIGMS Human Cell Repository at the Coriell Institute for Medical Research. GM08399 was used as a control (CTRL) cell line. Niemann-Pick C cell lines with mutations in the *NPC1* gene: GM18453 (I1061T/I1061T), GM17912 (P1007A/T1036M), GM03123 (I1061T/P237S); Niemann-Pick A (NPA) cell line with mutation in the *SMPD1* gene GM00112 (L302P/L302P). Cells were cultured in MEM, PSG, and 20% FBS [111].

Treatments

Endocytosis inhibitors: Cells were pretreated with dynasore (80 μM) or amiloride (1 mM) for 30 minutes. Cell culture media was replaced with fresh media containing vehicle (saline), dynasore, or amiloride along with 5A-SM-DiD for two hr. ImageJ was used to quantify DiD label intensity inside cells.

sHDL in cells: Cells were plated 24 hr before treatment. At the start of treatment, cell culture media was replaced with media containing vehicle or sHDL. Culture media containing vehicle or sHDL was refreshed after 24 hr.

sHDL treatment of brain slices: Slices were treated with fresh particles/media daily at a concentration of 5 mg/ml for a period of four days.

siRNA transfection

Predesigned ON-TARGETplus SMARTpools containing 4 individual siRNAs per target sequence (Dharmacon Non-targeting SMARTpool D-001810-10-05, ABAC1 L-

004128-00, SR-B1 L-010592-00) were transfected using TransIT-X2® (Mirus) reagent at t=0 and t=24 hrs. Imaging or RNA analysis occurred 48 hr after the first transfection [111].

Western blot

A bullet blender (Next Advance) was used to homogenize cell lysates. Protein concentrations were normalized by DC™-protein assay (Bio-Rad) and equal amounts of protein were loaded into 4-12 % gradient SDS PAGE gels (Invitrogen). After electrophoresis and transfer onto a PVDF membrane, immunoreactivity was detected by ECL (Thermo Scientific) and imaged using an iBright (Thermo Fisher Scientific). ImageJ was used to quantify band intensity [111]. For Endoglycosidase H assay, lysates were separated into three reactions containing: negative control (NT), EndoH (E) (NEB P0702L), or PNGaseF (P) (NEB P0704L) [111]. After a 3 hr incubation at 37º C samples were loaded on SDS PAGE gels as indicated above.

Filipin Staining

After treatment, cell membranes were labeled with wheat germ agglutinin® (Thermo Fisher). Cells were fixed in 4% PFA for 20 min, washed 3 X in PBS, and 1 X in glycine. Unesterified cholesterol was labeled with filipin labeling solution for 2 hr. Filipin labeling solution: 5% FBS + 0.4% DMSO+ 0.03 mg/ml (tissue) or 0.1 mg/ml (cells) filipin. Slides were washed 3 X with PBS and mounted with ProLong® Gold (Thermo Fisher) [111].

RT-qPCR

RNA was converted to cDNA using the High Capacity Reverse Transcription kit (Applied Biosystems 4368814). Quantitative real-time PCR (RT-qPCR) was conducted in technical triplicates using 15 ng cDNA, TaqMan™ probes (Thermo Fisher) for human *HMGCR* (Hs 00168302), *HMGCS1* (Hs 00940429), *ABCA1* (Hs 01059118), *ABCG1* (Hs 00245154), *LDLR* (Hs 01092524), *NPC1* (Hs 00264835), *SCARB1* (SR-B1) (Hs 00969821), *SREBF-2* (SREBP) Hs 01081778, *GAPDH* (loading control) (4325792), and mouse *HMGCS* (Mm 01304569). RT-qPCR was performed using an ABI 7900HT Sequence Detection System and relative expression calculated by the 2^ (-delta delta Ct) method using SDS software.

Immunofluorescence staining

Cells were washed 3 X with HBSS and fixed with 4% PFA for 20 min at room temperature. Cells were washed with PBS and glycine before addition of blocking solution (0.02% saponin, 5% normal goat serum (NGS), 1% BSA) for 1 hr. Slides were incubated with primary antibodies overnight at 4º C, washed with PBS + 0.02% saponin and incubated with secondary antibody for 1 hr [111]. Slides were mounted with Vectashield + DAPI (Vector Laboratories). For slice culture: slices were floated in HBSS+/+ in 6 well plates containing Netwell™ Inserts (Corning). Samples were fixed in 4% PFA and 0.1% Triton X-100 for 1 hr, rinsed 3 X in PBS, then treated for 10 min of 1.5 mg/ml glycine. After three washes in PBS, slices were blocked in PBS containing 5% NGS for 1 hr at room temperature. Slices were labeled with primary antibody (diluted in blocking) overnight. The following day, slices were washed 3 X in PBS and

labeled with Alexa conjugated secondary (1:500) for 1 hr. After 3 washes in PBS, slices were stained with filipin labeling solution for 2 hr, washed 3 X PBS and mounted in ProLong Gold (ThermoFisher) and imaged by confocal microscopy. Calbindin was used to outline Purkinje cells and filipin intensity was calculated using ImageJ.

Preparation of cerebellar organotypic slice cultures

Cerebellar organotypic slice cultures were prepared using 300 μM thickness sagittal brain slices [112]. Four slices per brain were used in each set of experiments, split evenly between control and experimental medium. Two slices were placed together on a cell culture insert (Millipore; 0.4 μM pore size, 30 mm diameter) which contained 1.2 ml slice culture medium (either control or experimental) and was pre-incubated at 37° C in 95% O_2/ 5% CO_2 in a 6-well plate. Control medium contained 50% minimal essential medium with Earle's salts, 25% horse serum, 25% Hank's balanced salts solution, 25 mM HEPES, 2 mM L-glutamine, 6.5 mg/ml glucose. Experimental medium was prepared by adding nanoparticles at a concentration of 5 mg/ml to the aforementioned control medium. Every 24 hr, cell culture inserts were transferred to a new 6-well plate which was pre-incubated at 37° C in 95% O_2/ 5% CO_2 with control or experimental medium, as described above. Imaging and analysis of Purkinje neuron cholesterol content was performed after 96 total hours of incubation. In all cases, wild type and NPC samples were matched so that slices were prepared on the same day and using the same reagents.

Stereotaxic mouse ICV bolus delivery

Stereotaxic administration of nanoparticles into the right lateral ventricle via an intracerebral ventricular (ICV) injection was performed on mice under vaporized

isoflurane anesthesia according to IACUC guidelines. 6-7-week-old mice received a single ICV bolus injection of sHDL or vehicle using established protocols [111, 113]. Each anesthetized mouse received a small scalp incision to expose the skull and a small burr hole was drilled relative to Bregma suture: anterior-posterior +0.3 mm, medio-lateral -1.0 mm. A beveled needle (7758-04, Hamilton, Reno, NV) connected to a 10 µL syringe (7653-01, Hamilton, Reno, NV) was placed dorso-ventral -3.0 mm at a rate of 1 mm/sec. A three-minute wait was allotted for the brain to seal around the needle and prevent backflow of treatment around the injection site. A total of 10 µL vehicle or sHDL at a concentration of 100 mg/ml was delivered at an infusion rate of 0.5 µL/sec using an injection pump (UMC4, World Precision Instruments, Inc., Sarasota, FL). Five minutes after the infusion was completed, the needle was retracted at a rate of 1 mm/sec and the incision site was sutured with synthetic non-absorbable sutures (1011209, Henry Schein, Melville, NY). Mice were recovered in a temperature controlled-environment and following surgery, the mouse weight, grooming activity, and home cage activity were recorded for up to 7 days according to IACUC guidelines.

Microscopy

Epifluorescence: Filipin was imaged on a Zeiss Axio Imager Z1 microscope with an automated stage. Cells were focused in the green channel (wheat germ agglutinin) and 16 tiled images were captured per experiment. Images with ≥ 90% cell confluence were quantified using NIH ImageJ software [111].

Confocal imaging of cells: Fluorescently labeled sHDL particles were imaged on a Nikon A-1 confocal microscope. Co-localization coefficients were calculated using

Nikon elements software (Pearson). Brightness and contrast was applied equally across the entire image to both control and experimental groups using Photoshop.

Macrophages were outlined in F4/80-stained sections of liver and area was quantified using ImageJ by an investigator blinded to genotype and treatment.

Confocal imaging of tissue: One-week post intraventricular injection, vehicle or 5A-SM treated mice were perfused with saline and tissues were placed in 4% PFA overnight. The liver and right hemisphere of the brain were embedded in OCT, frozen, and cut into 7μm thick sections. Sections were permeabilized (0.1% triton/10% NGS/1% BSA in PBS) for 10 min and placed into blocking buffer (10% NGS/1% BSA in PBS) for 50 min. Sections were placed in primary antibody overnight at 4°C, washed three times in PBS for 5 min, then incubated in secondary antibody for 1 hr at room temperature. Sections were stained with filipin and imaged on a Nikon A-1 confocal microscope. Purkinje neuron soma were defined using a calbindin-DK28 antibody and filipin was quantified using ImageJ.

Stimulated Raman scattering (SRS) microscopy: Cell monolayers were imaged at 2845 cm^{-1} Raman shift wavenumber to generate a greyscale image channel. Images acquired at the 2845 cm^{-1} are chemically selective for lipids, stimulating vibrational resonance of the CH_2 symmetric stretching mode [114]. Individual fields-of-view (FOVs) for lipid quantification were generated and quantified using a two-layer automated thresholding method to avoid selection bias. Over a full 2 mm X 2 mm SRS image, a 250-pixel X 250 pixel sliding window with 100-pixel step size was used to detect FOVs with greater than 90% cellular confluence. Mean background pixel intensity values for each image were used to set the FOV threshold for background (i.e. media) and

foreground (i.e. cells). Only FOVs with a foreground/background ratio greater than 90% were included for lipid quantification. After selection of FOVs, a second thresholding procedure was used to segment intracellular lipid droplets, which have high 2845cm^{-1} SRS signal compared to the remainder of the intracellular contents. For each FOV, a ratio between the area of intracellular lipid to total intracellular space was calculated and normalized to the number of cells within each image.

Amplex Red

The Amplex® Red Cholesterol Assay Kit A12216 (Invitrogen) was used to quantify total free cholesterol following the manufacturer's instructions.

Cell death

Cell viability was assessed using Promega CellTiter 96 Aqueous One Solution cell proliferation colometric assay (G3580). Briefly, Niemann-Pick C cells were cultured in 96-well plates at 10,000 cells per well for 24 hr, washed 3 X with PBS, and treated as indicated with compounds diluted in media for 24 hours. Cells were washed 3 X with PBS, and re-suspended in media supplemented with Promega CellTiter 96 reagent (20 µl reagent per 100 µl of media). After 45 min incubation at 37^{o} C, absorbance was read at 490 nm using a microplate reader. Each treatment was performed in triplicate and the average absorbance reading of non-treated (Veh) cells was set to 100%. The percent viability was determined by dividing the average absorbance of treated over non-treated cells and multiplying by 100.

Sphingomyelin loading

C6-NBD sphingomyelin was dissolved in 100 % ethanol to make a 10 mM stock solution. Cells were treated with 40 μM C6-NBD sphingomyelin in cell culture media overnight. The following day (t=0), wells were briefly washed 2 X with PBS and fresh media without C6-NBD sphingomyelin was added. At t=0 and t=24 hr, cells were treated with fresh media containing vehicle (saline) or 5A-SM.

Radioactive cholesterol efflux assay

Preparation of [^{3}H]cholesteryl linoleate-loaded acLDL

Cholesteryl [1,2,6,7-3H(N)] linoleate (60 Ci/mmol) was loaded into acetylated human LDL (acLDL) according to procedure adapted from Brown *et al* [115]. Briefly, 30 μCi (0.5 nmol) cholesteryl [1,2,6,7-3H(N)] linoleate in toluene was evaporated to dryness under a stream of nitrogen gas. Then, a thin film of cholesteryl [1,2,6,7-3H(N)] linoleate was dissolved in 10 μl DMSO followed by the addition of 100 μl acLDL (5 mg of protein/ml). The mixture was incubated for 2 hr at 37° C with gentle shaking to incorporate cholesteryl [1,2,6,7-3H(N)] linoleate into acLDL and then dialyzed at 4° C against 20 mM Tris/HCl, 0.3 mM EDTA, 0.15 M NaCl, pH 7.4 using 3.5K MWCO slide-A-Lyzer mini device (ThermoFisher 88400). Cholesteryl [1,2,6,7-3H(N)] linoleate-acLDL mixture routinely contained 90-95% of starting radioactivity as determined by scintillation counting before and after dialysis.

Cholesterol efflux assay

Niemann-Pick C fibroblast cells were grown in culture media until confluency. On day 1, 75,000 cells were plated in 24-well plates and grown for 24 hr in 0.5 ml culture

media. On day 2, cells were washed with PBS, pH 7.4, 1 X at room temperature and grown overnight in media containing lipoprotein-deficient serum (10% v/v) in DMEM to upregulate LDL receptors. On day 3, cells were washed with PBS, pH 7.4, 2 X and labeled with cholesteryl [1,2,6,7-3H(N)] linoleate-acLDL for 24 hr in DMEM (no phenol red)/BSA (1 mg/ml)/P-S media (0.5 ml) containing 1 µCi of [^{3}H]Cholesteryl linoleate per 1 ml media. On day 4, labeled cells were washed with PBS, pH 7.4, 3 X to remove cholesteryl [1,2,6,7-3H(N)] linoleate not taken up by cells. Radioactive cholesterol was effluxed from cells for 24 hr using vehicle (media), 5A peptide (0.75 mg/ml), 5A-SM HDL, 5A-DMPC, 5A-POPC (0.75 mg/ml) or cyclodextrin (1 mM) diluted in DMEM/BSA/P-S. On day 5, media from each well was transferred into separate Eppendorf tubes and centrifuged at 3,000 rpm for 10 min to remove any detached cells. The remaining cells on the plate were lysed with 0.1% SDS/ 0.1M NaOH solution for 2 hr at room temperature. Radioactive counts of media and cell fractions were measured separately using a Perkin Elmer liquid scintillation counter. Percent cholesterol effluxed from cells was calculated by dividing media counts by the total sum of media and cell counts and then multiplying by 100%. Non-specific cholesterol efflux by vehicle was subtracted from all data.

In vivo cholesterol mobilization

Total serum cholesterol concentrations from seven week old Niemann-Pick C mice pre- and 2 h post-treatment with 100 mg/kg 5A-SM i.p. were analyzed enzymatically by a colorimetric cholesterol oxidase assay (Wako Chemicals, Richmond, VA) using microplate reader.

Distribution of mobilized cholesterol in lipoproteins

Serum samples from Niemann-Pick C mice collected at baseline and 2 h post treatment with 100 mg/kg 5A-SM i.p. were analyzed to assess the cholesterol distribution between VLDL, LDL and HDL lipoprotein fractions. Separation of lipoproteins from serum was performed on a Waters HPLC system equipped with a Superose 6, 10/300 GL column (GE Healthcare, Piscataway, NJ) and a fraction collector. Serum samples were injected onto the HPLC and eluted with saline solution pH 7.4 at 1 ml/min. Eluent fractions containing different lipoproteins were post-column reacted in the HPLC with an enzymatic solution for total cholesterol detection [116].

Radioactive sphingomyelin efflux assay

Cells (40,000 cells/well) were cultured for 24 hr in 24-well plates and then incubated with 1 μCi (80 Ci/mmol) sphingomyelin [choline methyl-3H] per 1 ml media. After 24 hr, cells were washed with PBS, pH 7.4, 3 X followed by the treatment with vehicle or 0.75 mg/ml 5A-SM in culture media. Radioactivity in media and cells was counted using a PerkinElmer scintillation counter. Percent sphingomyelin effluxed from cells was calculated by dividing media counts by the total sum of media and cell counts and then multiplying this number by 100%. Non-specific sphingomyelin efflux by vehicle was subtracted from all data.

Serum analysis

Whole blood was collected and allowed to clot for 5 min in BD microtainer® SST gold cap tubes (365967). Tubes were centrifuged for 5 min at 3,000 X *g* to remove the

clot. Liver enzymes were blindly analyzed by the University of Michigan In-Vivo Animal Core.

Statistics

Significance ($P<0.05$) was determined by Graphpad Prism 7.0. Figure legends indicate when unpaired Student's two tailed t-test, one-way, or two-way ANOVA with Tukey or Bonferroni posthoc analysis were used. All error bars are s.e.m. Graphpad outlier analysis was used to remove one outlier per group for Purkinje neuron filipin quantification.

2.4 **Results**

Design and synthesis of sHDL nanoparticles

ApoA1 enwraps lipids into 10-12 nm nanodiscs forming endogenous HDL [117]. These particles contain a heterogeneous mixture of saturated and unsaturated phospholipids, with each lipid having distinct cholesterol binding properties [118]. Relative to full-length ApoA1 protein, use of synthetic ApoA1 mimetic peptide is beneficial due to the ease of manufacturing, enhanced quality control, and lower cost [99]. We utilized the ApoA1 mimetic peptide 5A, which is designed to maximize cholesterol efflux by ABCA1 [108]. Using phospholipids with differing affinities for cholesterol [119], we developed a panel of sHDLs containing various 5A:lipid formulations, including sphingomyelin (SM), a saturated phospholipid (DMPC, 1,2-dimyristoyl-sn-glycero-3-phosphocholine), or an unsaturated phospholipid (POPC, 1-palmitoyl-2-oleoyl-glycero-3-phosphocholine).

All sHDLs (5A-SM, 5A-POPC, and 5A-DMPC at 1:1.5 wt/wt ratio) were prepared by co-lyophilization and thermocycling (Figure 2-1a) [101]. The lyophilization and thermocycling processes are highly efficient, and we did not detect marked differences in the expected and actual ratios of peptide to lipid (Table 2-1). sHDL particles had an average diameter of 10-12 nm (5A-SM and 5A-DMPC) as determined by dynamic light scattering (Figure 2-1b). Hydrophobic uncomplexed lipids spontaneously form ≥100 nm liposomes. Large liposomes were not detected by dynamic light scattering (data not shown) indicating a highly efficient incorporation of lipids into sHDL. sHDLs also exhibited the expected size and disc-like morphology by transmission electron microscopy (Figure 2-1c). sHDL "stacking" by transmission electron microscopy is likely an artifact of sample preparation since dynamic light scattering revealed monomeric sHDL in solution.

sHDLs rescue cholesterol storage in Niemann-Pick type C fibroblasts

To assess the activity of sHDL on Niemann-Pick type C patient cells, we used the fluorescent dye filipin to label accumulated unesterified cholesterol. We analyzed filipin staining intensity in Niemann-Pick C fibroblasts following treatment with vehicle, 5A peptide alone, or sHDLs composed of 5A-POPC, 5A-SM, or 5A-DMPC. Treatment with 5A peptide alone did not significantly alter filipin intensity over 48 hrs (Fig. 2-2a, 2-2b). In contrast, both 5A-SM and 5A-DMPC significantly rescued stored cholesterol in a dose- and time-dependent manner in three independent lines of Niemann-Pick C primary fibroblasts (Fig. 2-2a, 2-2b, 2-3a). sHDL composed of 5A-POPC yielded a more modest and less consistent rescue, demonstrating that lipid composition impacts

biological activity. The beneficial effects of sHDL treatment were confirmed using an amplex red assay to measure total cellular cholesterol (Fig. 2-2c). Assessment of cell viability following treatment showed no significant changes, except for mild toxicity from 5A-DMPC (Figure 2-3b). Taken together, these studies demonstrate sHDL activity and tolerability, and given the investigational new drug status of 5A-SM, prompted further analysis of SM-containing sHDLs.

Although the lipid content of sHDL is a strong determinant of cholesterol efflux, the composition of the ApoA1 mimetic peptide is also important for sHDL function [104]. In order to investigate the impact of the ApoA1 mimetic peptide on sHDL's ability to reduce cellular cholesterol storage, nanoparticles were prepared with another peptide, 22A [105, 120]. Both 5A and 22A peptides have no sequence homology with endogenous ApoA1 and were optimized differently: 5A peptide was selected to maximally efflux cholesterol by ABCA1, while 22A peptide was selected to maximize cholesterol esterification within sHDLs in plasma [103, 105, 108].

Raising the lipid to peptide ratio increases sHDL's size and its capacity to accept cholesterol [102]. It is generally believed that larger sHDL particles efflux cholesterol through scavenger receptor B-1 (SR-B1) [121]. To examine the effect of peptide sequence and peptide:lipid ratio on cholesterol removal, we generated a panel of sHDLs containing 5A or 22A and various peptide:SM ratios. Filipin analysis revealed significant cholesterol reducing activity of sHDLs containing 5A-SM but not 22A-SM. Moreover, we found that a 1:1.5 wt/wt ratio of 5A:SM was optimal at reducing filipin intensity (Figure 2-2d).

To determine which cholesterol transporter is primarily responsible for 5A-SM mediated removal of unesterified cholesterol from Niemann-Pick C cells, we performed expression analysis of NPC patient fibroblasts. In contrast to ABCG1, expression of ABCA1 and SR-B1 were readily detected by qPCR (Figure 2-3c). Next, we treated primary fibroblasts with non-targeting siRNAs (siNT), or siRNAs targeting SR-B1 (siSR-B1) or ABCA1 (siABCA1). 5A-SM efficiently rescued cholesterol storage after treatment with either siNT or siSR-B1, but not after treatment with siABCA1 (Figure 2-2e). As siRNAs significantly reduced expression of target genes (Figure 2-3d), this analysis confirmed that 5A-SM requires ABCA1 to function. Notably, increasing cholesterol content of 5A-SM reduced its effect on clearance of unesterified cholesterol (Figure 2-2f). Consistent with this observation, incubation with a heterogeneous pool of human plasma HDL (HuHDL) containing nascent (cholesterol poor) and mature (cholesterol loaded) HDL failed to reduce cellular cholesterol levels (Figure 2-2f). These data contrast the observation that the cholesterol reducing agent 2-hydroxypropyl-beta cyclodextrin (cyclodextrin) preloaded with cholesterol remains effective at reducing unesterified cholesterol in Niemann-Pick C cells [122-124], and raise that possibility that sHDL and cyclodextrin have distinct mechanisms of action.

5A-SM induces the expression of cholesterol regulatory genes

To more fully define the biological responses triggered by sHDLs, we treated Niemann-Pick C fibroblasts with increasing doses of cyclodextrin or 5A-SM and analyzed the expression of cholesterol regulatory genes. A 48 hr treatment with cyclodextrin did not alter the expression of *HMGCR, HMGCS1,* or *LDLR* (Figure 2-4a).

This is consistent with previous research showing cyclodextrin causes a transient decrease then restoration in cholesterol biosynthetic genes by 48 hrs [122, 123, 125]. In contrast, 48 hrs of treatment with 5A-SM or 5A-DMPC caused a dose-dependent increase of cholesterol biosynthetic (*HMGCR, HMGCS1, SREBP*) and uptake genes (*LDLR*) in three independent lines of patient fibroblasts (Figure 2-4a, 2-5a, 2-5b). Additionally, expression of the cholesterol export gene *ABCA1* was significantly decreased (Figure 2-4a, 2-5a, 2-5b). Together, these data suggest that sHDLs efficiently extract cholesterol from target cells and act at different time scales than cyclodextrin.

Treatment with 5A-SM also significantly increased the expression of *NPC1* mRNA and protein (Figure 2-4a, 2-4b, 2-5c, 2-5d). This is notable since multiple groups have shown that a subset of NPC1 missense mutants are functional if they escape ER degradation and traffic to LE/Lys [126, 127]. To determine whether the induction of NPC1 contributed to rescue of lipid storage, we took advantage of the fact that the NPC1 protein is heavily glycosylated. These glycans are modified as the protein traffics through the medial Golgi, rendering them resistant to cleavage by endoglycosidase H (EndoH) but maintaining sensitivity to PNGaseF. As expected, wild type (WT) NPC1 protein expressed in control fibroblasts was resistant to EndoH cleavage, while mutant NPC1 protein from patient fibroblasts was sensitive to EndoH (Figure 2-4c). Treatment with 5A-SM did not alter the sensitivity of mutant NPC1 to digestion by EndoH, indicating that the accumulated protein did not traffic to LE/Lys (Figure 2-4c, 2-5e). We conclude that 5A-SM removes cholesterol from patient fibroblasts without correcting mutant NPC1 protein trafficking or function.

5A-SM enters cells through macropinocytosis and promotes cholesterol efflux

Cholesterol is loaded into nascent HDL particles when ApoA1 interacts with receptors such as ABCA1 at the plasma membrane. However, a prior report indicates that ApoA1 and ABCA1 may be endocytosed as a complex [128]. Studies have suggested that ApoA1/ABCA1 endocytosis is required for removal of accumulated LDL-derived cholesterol from LE/Lys [128, 129]. To determine if 5A-SM enters cells through endocytosis, we treated Niemann-Pick C patient fibroblasts with 5A-SM sHDLs containing the fluorescent lipophilic dye DiD (5A-SM-DiD). Confocal imaging revealed little 5A-SM-DiD signal on the plasma membrane, yet readily identified fluorescent signal in the cytoplasm, indicating uptake of the 5A-SM-DiD nanoparticles (Figure 2-6a). To define the mechanism of uptake, cells were pretreated with the macropinocytosis inhibitor amiloride [130] or the clathrin and caveolar inhibitor dynasore, then loaded with 5A-SM-DiD. Dynasore had little effect on 5A-SM-DiD uptake, while amiloride significantly reduced 5A-SM-DiD signal intensity, indicating that macropinocytosis is a major route of 5A-SM-DiD endocytosis (Figure 2-6a). Notably, the lipophilic tag DiD was not covalently conjugated to 5A-SM; therefore, the punctate cytoplasmic pattern of fluorescence could represent DiD dissociated from the nanoparticle. To rule out this possibility, we synthesized sHDLs containing 5A peptide covalently conjugated to Alexa647 (5A-Alexa647) and incorporated the lipophilic dye DiA into these particles (5A:Alexa647-SM:DiA). After 2 hrs incubation, the 5A and DiA signals strongly co-localized (Figure 2-6b) indicating that the internalized 5A-SM sHDL particles remained intact inside the cell.

Unesterified cholesterol that accumulates within Niemann-Pick C cells resides in LAMP1 positive LE/Lys [124]. To determine if 5A-SM traffics to this compartment, we conducted a time course and analyzed co-localization of 5A-SM-DiD with LAMP1 and filipin. We observed that a fraction of 5A-SM-DiD co-localized with LAMP1 and filipin positive lipid storage vesicles over a period of 2 hrs (Figure 2-6c). At this time point, 5A-SM-DiD did not co-localize with the recycling endosome/early endosome marker EEA1 (Figure 2-7), possibly because it had already traveled past this compartment. Whether lysosomal/filipin positive 5A-SM-DiD compartments represent the primary site of sHDL action requires further investigation, and it remains possible that sHDLs act at other intracellular sites. In either case, we sought to confirm that sHDL uptake was accompanied by efflux of stored cholesterol. To accomplish this, patient fibroblasts were loaded and then equilibrated with [3H]cholesteryl linoleate bound to LDL. We treated cells with 5A or 5A-SM for 24 hrs and then measured intracellular and extracellular [3H]cholesterol. Incubation with 5a peptide alone resulted in ~20% efflux of radiolabeled LDL-derived cholesterol to medium (Figure 2-6d). Notably, pre-formed 5A-SM sHDL particles were much more effective at effluxing LDL [3H]cholesterol than 5A alone, resulting in release of ~60% of labeled cholesterol into the media. In contrast, 24 hr treatment with 1 mM cyclodextrin resulted in a modest 6.2% ± 2.7 efflux of LDL-derived cholesterol at this early timepoint. This is in line with previous data showing that cyclodextrin extracts cholesterol from the plasma membrane and can mobilize it from intracellular stores [124, 125, 131].

5A-SM mobilizes cholesterol and ameliorates phenotypes in Niemann-Pick C mice

Based on the significant rescue of cholesterol storage observed *in vitro*, we sought to determine the extent to which administration of sHDLs benefit gene targeted mice homozygous for the *Npc1 I1061T* allele (Niemann-Pick C mice). These mice contain the most common Niemann-Pick C disease-causing mutation (I1061T). Starting at 7 weeks of age these mice develop robust, progressive phenotypes including cholesterol accumulation, Purkinje neuron loss, motor impairment and premature death by 13 weeks of age [110]. Niemann-Pick C mouse serum collected pre- and two hrs post-intraperitoneal (i.p.) injection of 5A-SM established that treatment significantly increased serum cholesterol content (Figure 2-8a). High-performance liquid chromatography (HPLC) was used to identify cholesterol-containing fractions (VLDL, LDL, or HDL). Serum cholesterol was distributed in all lipoprotein fractions 2 hrs post 5A-SM injection, with LDL and VLDL particles containing the most cholesterol (Figure 2-8b). This is a typical lipoprotein profile after sHDL administration, where immediate HDL-cholesterol elevation is followed by transient LDL/VLDL-cholesterol elevation while cholesterol is metabolized, returning to baseline 24 hrs post-treatment [101, 102, 106]. Consistent with data showing cholesterol mobilization into the serum, a single injection of 5A-SM significantly up-regulated the cholesterol biosynthetic gene *HMGCS* in the liver (Figure 2-8c), similar to our findings in patient fibroblasts (Fig. 2-4a). These data provide evidence of target engagement after *in vivo* administration of sHDL to Niemann-Pick C mice.

To determine whether Niemann-Pick C mice showed benefits from sHDL administration, we initially focused on peripheral disease manifestations that might be responsive to i.p. administration. Niemann-Pick C mice exhibit significantly elevated

serum bilirubin levels, diminished body weight, and liver macrophage activation. We analyzed total bilirubin levels in seven-week old WT and Niemann-Pick C mice 48 hrs after a single injection of vehicle or 5A-SM. sHDL administration rescued bilirubin levels in Niemann-Pick C mice without altering them in WT littermates (Figure 2-8d). Niemann-Pick C mice also exhibit progressive body weight loss as they age [110]. To determine effects on this disease manifestation, 5A-SM or vehicle was injected i.p. three times per week from 7-11 weeks of age, and the change in weight was calculated for each mouse for the duration of the treatment trial. WT mice treated with either vehicle or 5A-SM gained ~2g during the treatment period, whereas vehicle treated Niemann-Pick C mice failed to gain body weight. In contrast, Niemann-Pick C mice treated with 5A-SM exhibited a significant rescue of body weight, gaining as much weight as WT controls (Figure 2-8e). Administration of 5A-SM also significantly reduced liver macrophage size in Niemann-Pick C mice (Figure 2-8f). While i.p. administration of sHDL showed significant benefits for these peripheral phenotypes, it did not correct motor phenotypes (Figure 2-9a), suggesting poor blood brain barrier penetration.

The Niemann-Pick C mouse motor phenotypes are driven, in part, by loss of cholesterol-laden cerebellar Purkinje neurons [132, 133]. To determine whether sHDLs could rescue cholesterol storage in neurons, we treated cultured cerebellar slices from adult WT and Niemann-Pick C mice with vehicle or 5A-SM for four days. Slices were fixed and co-labeled for Purkinje neurons (calbindin) and cholesterol (filipin). Confocal imaging demonstrated that treatment of Niemann-Pick C brain slices significantly reduced cholesterol storage in Purkinje neurons (Figure 2-8g, 2-9b). This finding demonstrates that sHDLs are active on CNS target cells if they gain access to the brain.

To directly test CNS activity, we performed intraventricular injections in 6-7 week old Niemann-Pick C mice with vehicle or 5A-SM containing the fluorescent dye DiD (5A-SM-DiD), a manipulation that was well tolerated. One-week post injection 5A-SM-DiD signal localized to the cerebellum, brain stem, cortex, and hippocampus (Figure 2-10). In the cerebellum the fluorescent signal from DiD localized predominantly to astrocytes and, to a lesser extent, microglia at this time point (Figure 2-11b, 2-11c). We calculated Purkinje neuron soma size as a potential indicator of *in vivo* toxicity of 5A-SM one-week post injection. Suggesting little toxicity, Purkinje neuron soma size was unchanged with 5A-SM treatment (WT+Veh, 185±44; NPC+Veh, 207±57; and NPC+5A-SM, 206±61 pixels). One-week post-injection, we observed significant reduction of cholesterol accumulation in Purkinje neurons in Niemann-Pick C mice treated with sHDL (Figure 2-8h).

5A-SM reduces accumulated sphingomyelin in Niemann-Pick A fibroblasts

Both cholesterol and sphingomyelin utilize the ABCA1 transporter to efflux from cells into an HDL acceptor [134]. These two lipids physically interact and commonly traffic together [135]. This suggested that sHDL might be effective at rescuing aberrant storage of sphingomyelin as well as cholesterol. Sphingomyelin is normally metabolized by the lysosomal enzyme acid sphingomyelinase, and loss-of-function mutations in the encoding gene result in sphingomyelin accumulation, causing Niemann-Pick Disease types A and B [136].

To determine whether sHDL was capable of removing stored sphingomyelin from cells, Niemann-Pick A and control primary fibroblasts were loaded with

[3H]sphingomyelin for 24 hrs and then treated with 5A-SM. After 24 hrs, 5A-SM promoted the efflux of twice as much [3H]sphingomyelin from Niemann-Pick A cells than control cells (Figure 2-12a). To confirm this observation, Niemann-Pick A fibroblasts were loaded overnight with fluorescent NBD-sphingomyelin. Cells were then treated with vehicle, cyclodextrin or 5A-SM for 48 hrs (Figure 2-12b). As expected, control cells metabolized NBD-sphingomyelin and had little signal, while Niemann-Pick A cells showed marked cytoplasmic accumulation. Remarkably, 5A-SM significantly reduced NBD-sphingomyelin storage in mutant cells. In contrast, cyclodextrin treatment was ineffective, consistent with previous work in other sphingolipidoses [65].

The addition of exogenous sphingomyelin can alter membrane dynamics and impact downstream protein function [137, 138]. Therefore, we sought to determine effects of 5A-SM on endogenous lipids stored in Niemann-Pick A cells. To detect total lipids in a live, unfixed state, we utilized stimulated Raman scattering (SRS) microscopy. This SRS system generates virtual histology images that are useful for a variety of applications, including the clinical setting [139]. SRS utilizes an excitation and pump beam at the Raman wave number for CH2 bonds to rapidly image total lipids in biological samples. Since sphingomyelin contains extensive CH2 bonds, we developed SRS cell plating, imaging, and analysis procedures for Niemann-Pick A fibroblasts. SRS imaging demonstrated that Niemann-Pick A fibroblasts had double the lipid signal intensity compared to control cells (Figure 2-12c). Treatment of Niemann-Pick A fibroblasts with 5A-SM rescued this lipid storage, whereas treatment with cyclodextrin did not. Collectively, these data show that 5A-SM is effective at reducing sphingomyelin

storage in Niemann-Pick A cells and suggest that sHDL nanoparticles may be therapeutically beneficial for the family of Niemann-Pick diseases.

2.5 **Discussion**

We describe an innovative approach to ameliorating lipid storage in the Niemann-Pick family of diseases by harnessing the activity of the body's endogenous cholesterol scavenging particle, HDL. The sHDL particles characterized here potently remove stored cholesterol from Niemann-Pick C fibroblasts (Figure 2-2) and neurons (Figure 2-8f). The particles show evidence of cholesterol target engagement and rescue disease phenotypes when administered to Niemann-Pick C mice (Figure 2-8). The 10-12 nm sHDL nanodiscs are generated at high purity by assembling peptide-lipid nanoparticles by a co-lyophilization and thermocycling process (Figure 2-1). Notably, the degree of cholesterol removal was affected by altering the constituent ApoA1 mimetic peptide, lipid, and peptide:lipid ratio (Figure 2-2), demonstrating that sHDLs provide a flexible platform that can be tuned to adjust therapeutic potency. Moreover, our observation that the sHDL that rescues cholesterol storage in type C disease also rescues sphingolipid storage in type A disease (Figure 2-12) raises the possibility that alternative sHDL compositions may be beneficial for additional lipid storage disorders. The initial *in vivo* analyses presented here provide a proof-of-concept of activity for a single sHDL formulation, 5A-SM, at limited points. These data set the stage for additional analyses in Niemann-Pick animal models, including comparisons with other therapies currently administered to patients or in clinical trial.

Prior studies have established that Niemann-Pick type C cells have normal ApoA1 receptor binding, endocytosis and re-secretion [140, 141], yet Niemann-Pick patients have reduced serum HDL levels [140, 142-146] that likely worsen lipid storage. Previous reports have also demonstrated that Niemann-Pick type C cells are defective in loading cholesterol into ApoA1 [140, 141, 147]. Similarly, we noted that ApoA1 mimetic peptides are not sufficient for reducing Niemann-Pick C cholesterol storage (Figure 2-2a, b). Our strategy bypassed the HDL formation deficiencies in disease by utilizing an investigational new drug, 5A-SM sHDL, that exhibits no significant cellular toxicity. The activity of alternative sHDL formulations will be the subject of future research. Additionally, the extent to which incorporation of ApoE rather than ApoA1 mimetic peptides and the addition of brain targeting peptides enhance therapeutic efficacy in the CNS remain to be defined.

While the rescue of cholesterol storage from mutant fibroblasts required expression of ABCA1 (Figure 2-2e), fluorescently labeled sHDLs readily entered cells by macropinocytosis (Figure 2-6a). The lipid and peptide constituents of the nanoparticles remained tightly associated within cells (Figure 2-6b, c), with some trafficking to LAMP1 and filipin staining vesicles (Figure 2-6c). Other intracellular sHDLs remained outside these lipid storage vesicles, and the precise location of cholesterol loading remains to be determined. In contrast to LDL, there is still incomplete understanding of HDL endocytosis and subcellular trafficking [148]. Interestingly, multiple intracellar pools of HDL have been described. After endocytosis HDL can be re-secreted, sent to the lysosome, or trafficked to the Golgi before re-secretion [148-150]. The location of the subcellular pools of HDL are still being described and are likely cell

type dependent. Although we were not able to define where all of the 5A-SM localized within cells, treatment with sHDLs did trigger cholesterol efflux (Figure 2-6d), a finding that may reflect release of cholesterol-laden nanoparticles and/or enhanced lysosomal exocytosis.

The identification of therapeutic rescue of lipid storage in Niemann-Pick type A cells by sHDL was greatly facilitated by SRS microscopy (Figure 2-12c). This technique was used to circumvent challenges associated with labeling endogenous sphingolipids and shortcomings of applying exogenous sphingolipids to study intracellular trafficking. We were not able to identify the accumulated lipid species by current technology and cannot exclude the possibility that sphingomyelin correction is a consequence of cholesterol removal. However, this seems unlikely as treatment with the cholesterol-removing agent cyclodextrin did not alter sphingomyelin accumulation or lipid content in Niemann-Pick type A cells (Figure 2-12b, 2-12c). Notably, limited techniques allow live cell imaging of endogenous lipids. While SRS cannot currently delineate lipid subspecies, we anticipate that continued development of this technology will enable this process. Moreover, the robust rescue of lipid storage in Niemann-Pick type A cells, along with the amelioration of peripheral phenotypes in Niemann-Pick C mice following i.p. administration, are particularly encouraging in the context of Niemann-Pick type B. Niemann-Pick B is characterized by peripheral organ system phenotypes, but not CNS involvement. Even with the successful removal of sphingomyelin in Niemann-Pick A cells by 5A-SM, future research is needed to establish the optimal sHDL formulation for removing stored lipids in this disorder.

Our study demonstrates a proof of concept that sHDL significantly reduce lipid storage in both Niemann-Pick C and A. Future work will assess the long-term effects of sHDL in NPC and NPA/NPB mouse models. Considering the safety of sHDL in clinical trials, correction of peripheral phenotypes would justify testing large animals and perhaps in patients with these disorders. As such, our data suggest that 5A-SM or other sHDLs may be therapeutically beneficial for patients with Niemann-Pick Diseases and possibly other lysosomal storage disorders.

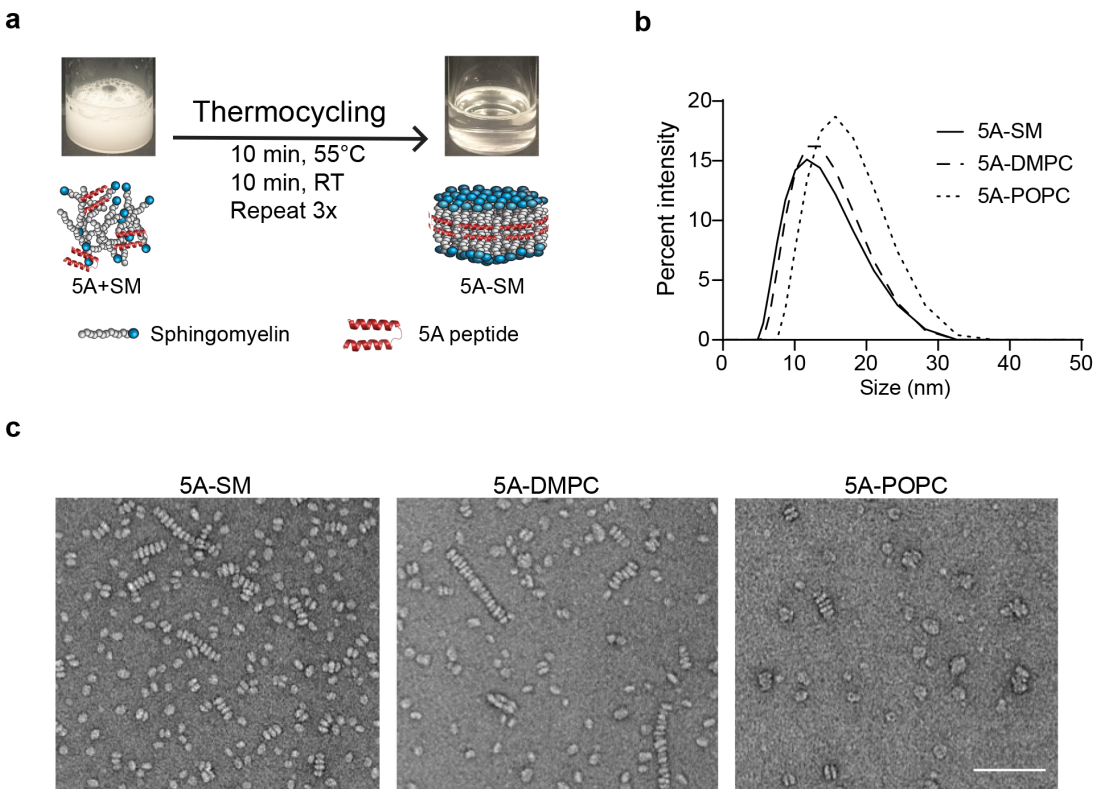

Figure 2-1 Synthesis and characterization of sHDL nanoparticles. *(a) A lyophilized mixture of 5A peptide and sphingomyelin (SM) was hydrated in PBS and thermocycled to assemble sHDL particles. (b, c) Particle size distribution was analyzed by (b) dynamic light scattering for 1 mg/mL of 5A-SM, 5A-DMPC or 5A-POPC sHDL or (c) transmission electron microscopy of 5A-SM, 5A-DMPC and 5A-POPC. Scale bar = 100 nm.*

Table 2-1 Expected and actual peptide: lipid ratios.

sHDL Formulation	Peptide Concentration (mg/mL)	Phospholipid Concentration (mg/mL)	Expected Peptide:Lipid Ratio	Actual Peptide:Lipid Ratio
5A-SM 1	11.96	6.12	1:0.5	1:0.51
5A-SM 2	10.13	8.91	1:1	1:1.14
5A-SM 3	10.84	15.26	1:1.5	1:1.41
5A-POPC	9.33	13.5	1:1.5	1:1.45
5A-DMPC	11.51	17.28	1:1.5	1:1.50

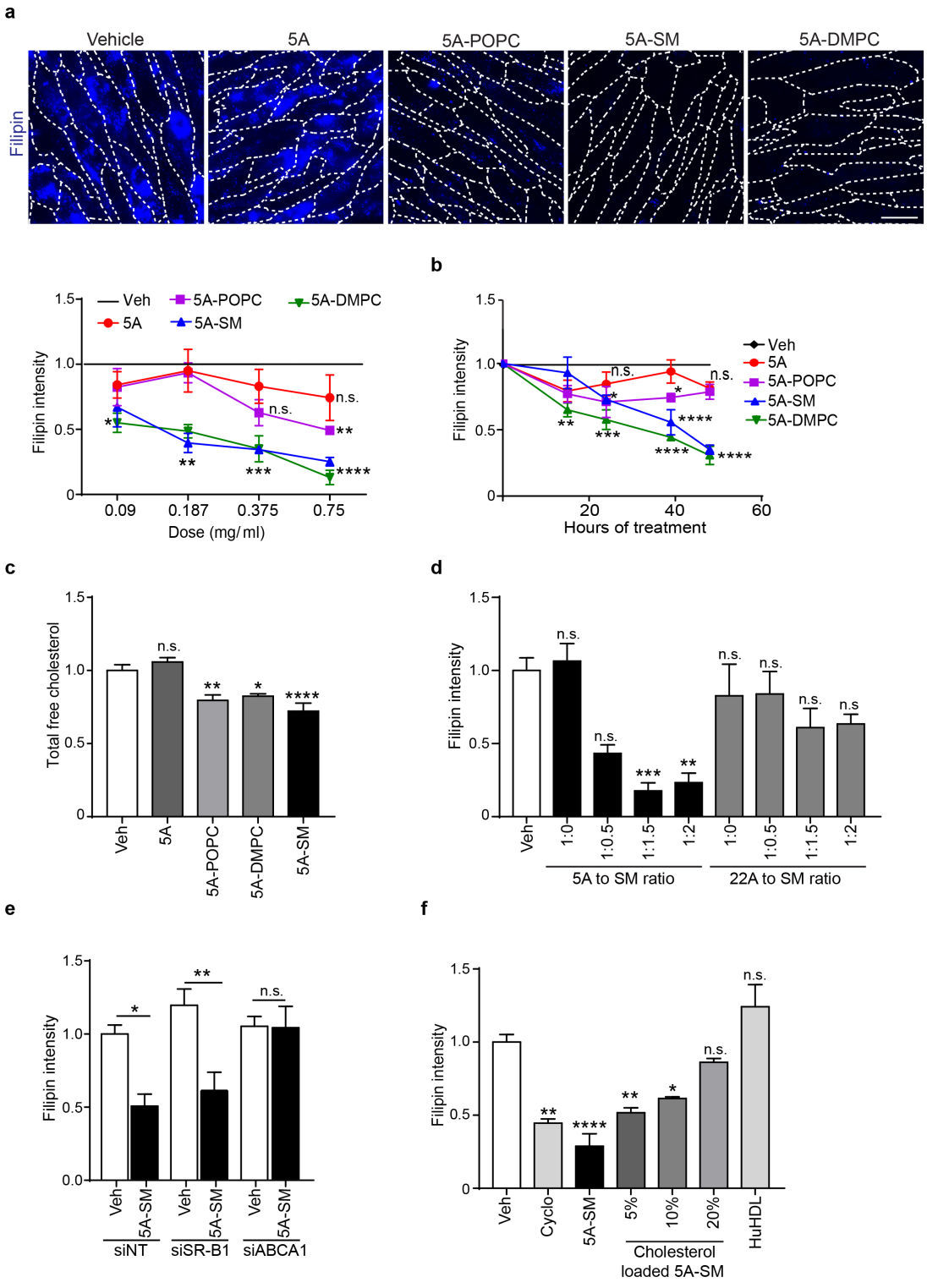

Figure 2-2 sHDLs require ABCA1 to remove accumulated cholesterol from Niemann-Pick C fibroblasts. *(a-f) Primary fibroblasts homozygous for NPC1 I1061T were treated with various sHDL formulations. Plasma membranes are outlined with dashed lines. (a, b) Accumulation of unesterified cholesterol was visualized by filipin staining (a) following 48 hr*

*treatment with increasing doses (representative images of 0.75 mg/ml) of vehicle (Veh), 5A peptide, 5A-POPC, 5A-SM, and 5A-DMPC (quantified below) or (b) with 0.75 mg/ml sHDL at various time points. (c) Effects of 48 hr treatment with sHDL (0.75 mg/ml), 5A peptide or vehicle (Veh) on total cellular cholesterol were measured using the Amplex Red assay. (d) The ratio of 5A or 22A peptide to sphingomyelin (SM) was altered during synthesis and the effect of peptide:SM ratio on cholesterol removal was determined by filipin staining (48 hr treatment). (e) Cells were treated for two consecutive days with the following siRNAs: non-targeting (NT), ABCA1, or SR-B1, and concurrently treated with vehicle (Veh) or 5A-SM. Cholesterol storage was determined by filipin staining. (f) Cells were treated with cyclodextrin (Cyclo), 5A-SM, or 5A-SM preloaded with increasing amount of cholesterol content (5%-20% total lipid weight), or human HDL (HuHDL). Cholesterol storage was assessed by filipin staining 48 hr after treatment. Data are mean ± s.e.m. from (a, b, e) three, (c) five, (d) 5-8, or (f) 4-6 independent experiments. n.s., not significant, *p≤.05, **p≤.01, ***p≤.001, ****p≤.0001 by (a, b) Two-way ANOVA with Bonferroni posthoc test (F, df=(a) 33.53, df=4; (b) 32.88, 4), (c-f) One-way ANOVA with Tukey posthoc test(F, df=(c) 13.98, 4; (d) 6.96, 8; (e) 22.5, 6; (f) 6.94, 5). (a) Dash lines indicate plasma membrane, scale bar = 20 μm.*

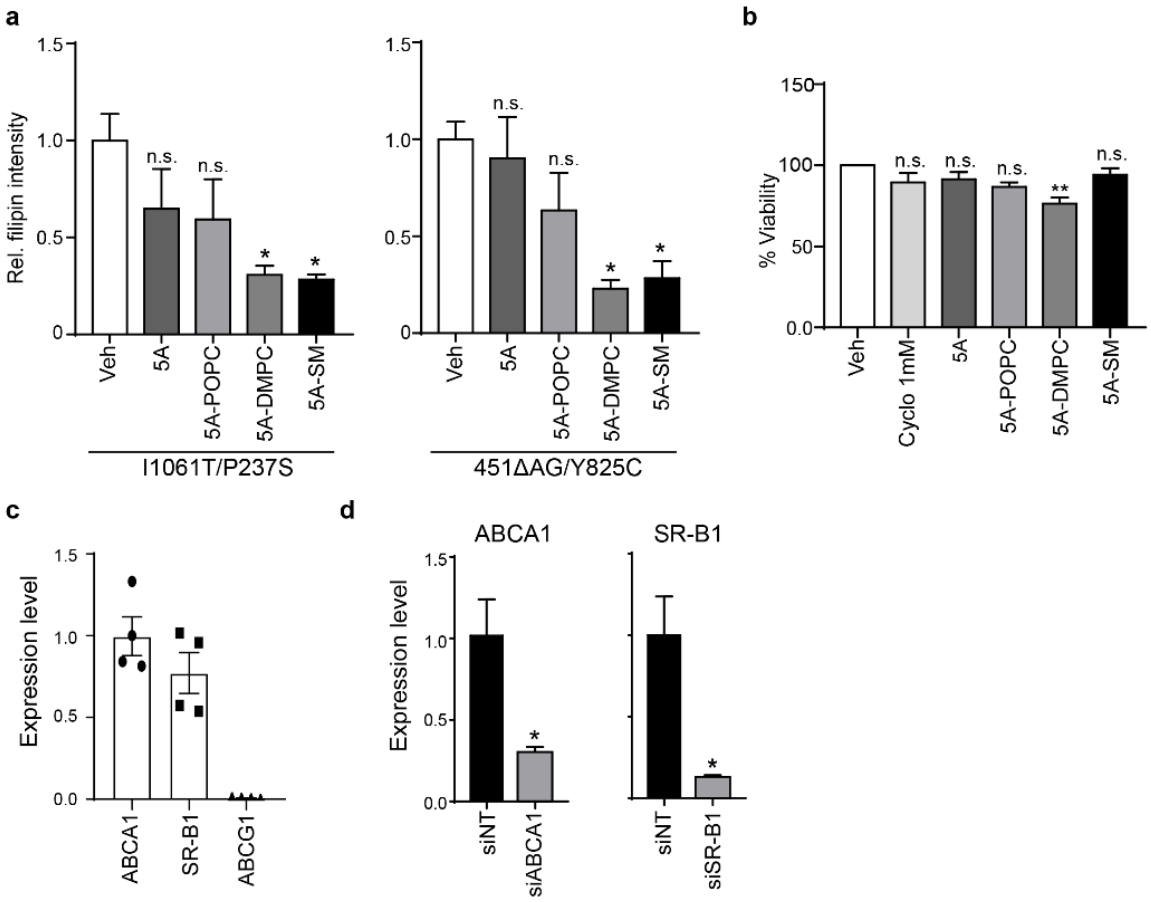

Figure 2-3 sHDLs rescue cholesterol storage in Niemann-Pick C patient fibroblasts. *(a) Primary human fibroblasts with compound heterozygous mutations in NPC1, encoding I1061T/P237S or 451ΔAG/Y825C, were treated with vehicle (Veh) or 0.75 mg/ml of 5A peptide, 5A-POPC, 5A-DMPC, or 5A-SM for 48 hrs. Unesterified cholesterol was labeled with filipin and quantified. (b) Viability of Niemann-Pick C patient (I1061T/I1061T) primary fibroblasts after 24-hour treatment with vehicle (Veh), 1 mM cyclodextrin (Cyclo), 0.75 mg/ml of 5A peptide, 5A-POPC, 5A-DMPC, or 5A-SM. (c) qPCR was used to assess expression level of ABCA1, SR-B1, and ABCG1 mRNAs in NPC1 I1061T primary fibroblasts. (d) NPC1 I1061T primary fibroblasts were treated with siRNAs against ABCA1 (siABCA1) or SR-B1 (siSR-B1), or with non-targeting (NT) siRNAs for 48 hrs. mRNA expression was analyzed by qPCR. Data are mean ± s.e.m. from (a, d) three, (c) four or (b) seven independent experiments. (a, b) One-way ANOVA with Tukey posthoc test (F, df=(a) (Left) 4.015, 4; (Right) 6.603, 3; (b) 4.171, 5). (d) Student's t-test (t=(ABCA1) 3.20, (SR-B1) 3.69). n.s., not significant, *p≤.0.05, **p≤.01.*

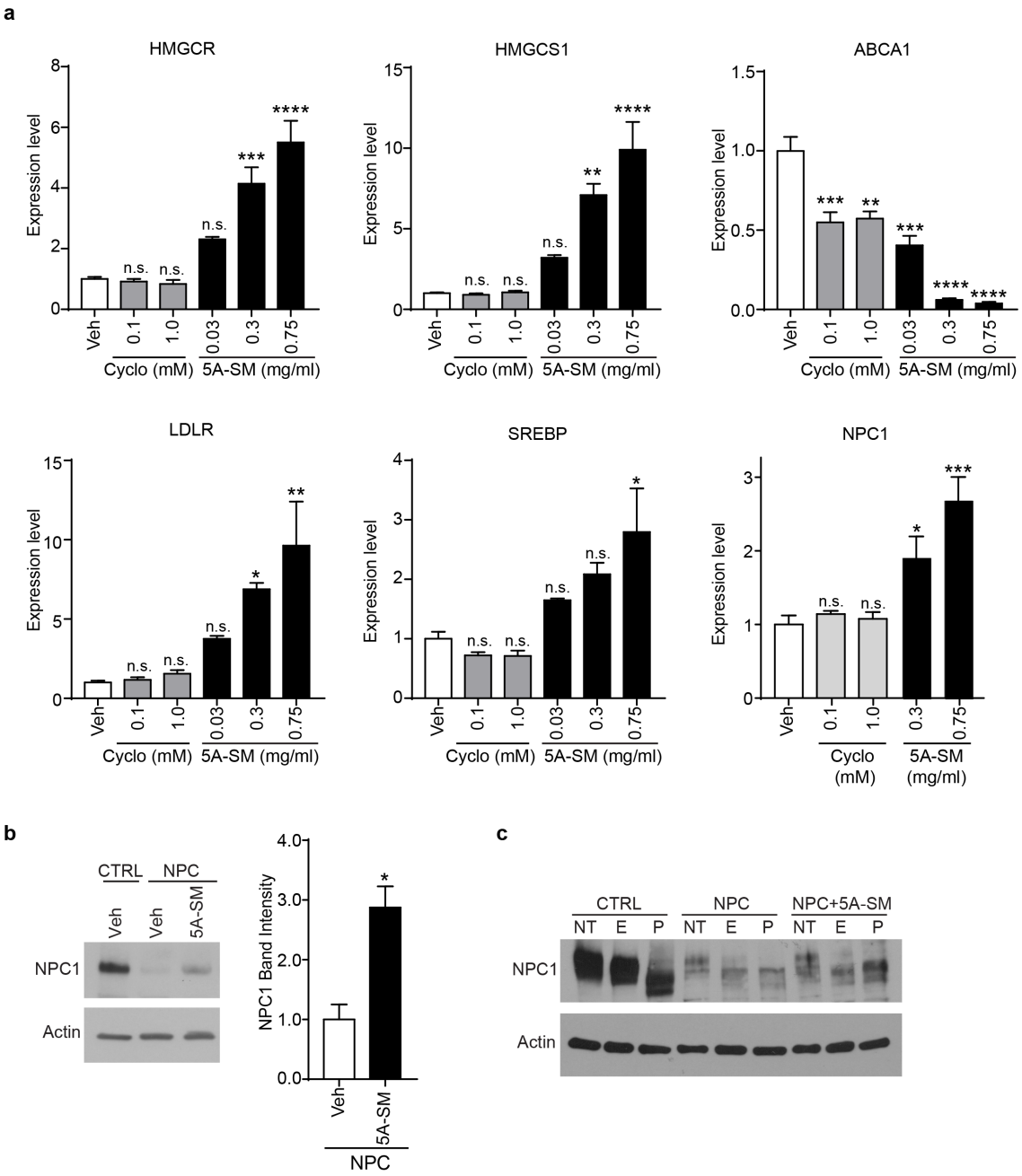

Figure 2-4 sHDLs modulate cholesterol regulatory genes. *(a) Primary fibroblasts homozygous for NPC1 I1061T were treated with vehicle (Veh), cyclodextrin (cyclo), or 5A-SM at the indicated concentrations for 48 hours. HMGCR, HMGCS1, ABCA1, LDLR, SREBP, or NPC1 mRNA expression was analyzed by qPCR. (b, c) NPC1 protein in control (CTRL) and NPC1 I1061T (NPC) fibroblasts was analyzed by (b) western blot (quantified at right) or (c) digested with endoglycosidase H (E), PNGase F (P), or not treated (NT) and analyzed by western blot. Data are mean ± s.e.m. from three independent experiments. n.s., not significant, *p≤.05, **p≤.01, ***p≤.001, ****p≤.0001 relative to Veh by (a) One-way ANOVA with Tukey posthoc test (F, df=(HMGCR) 27.43, df=5; (HMGCS1) 24.75, 5; (ABCA1) 43.54, 5; (LDLR) 9.4, 5; (SREBP) 7.0, 5; (NPC1) 12.41, 4. (b) student's t-test t=3.83, df=2.*

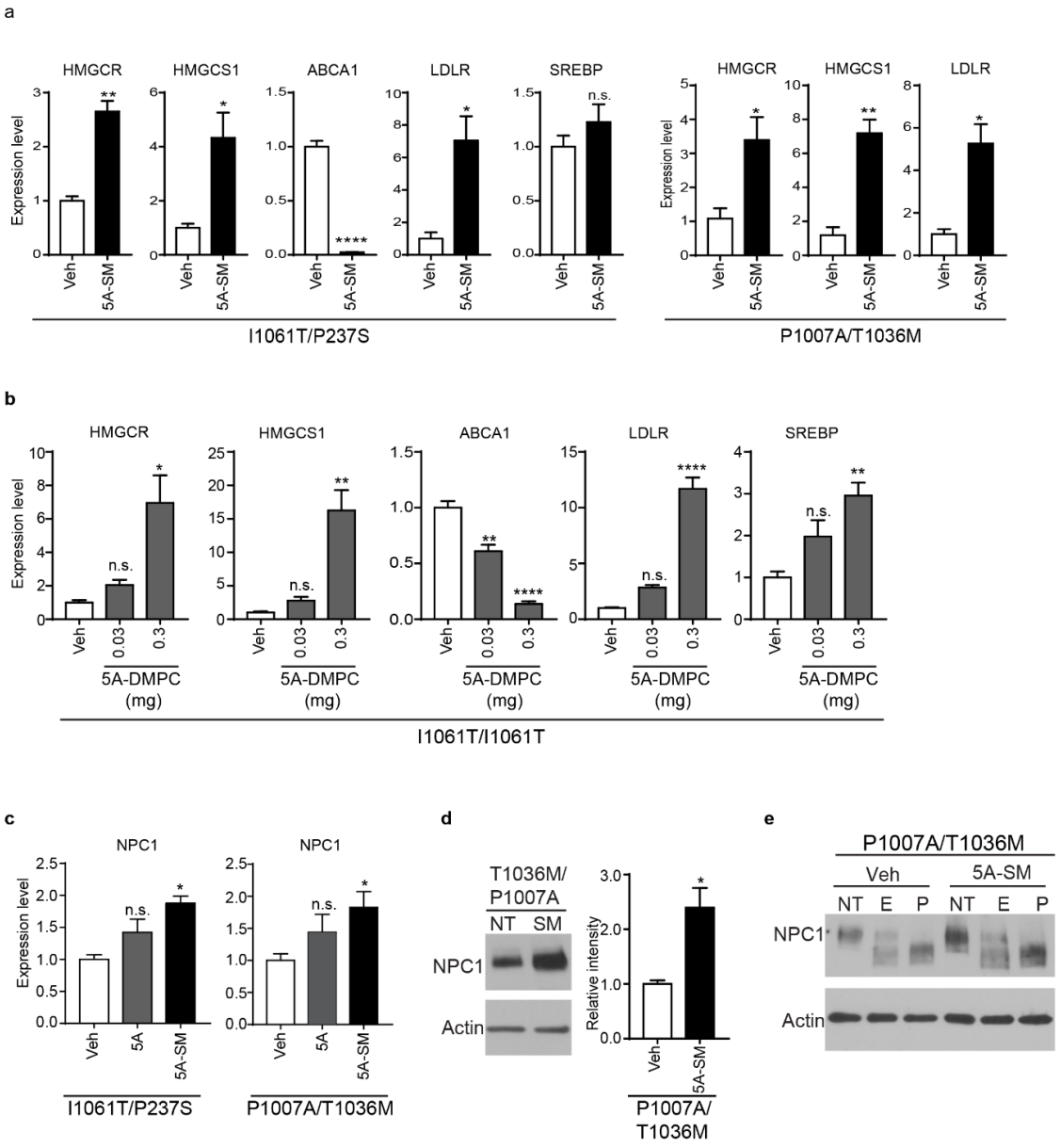

Figure 2-5 sHDLs induce the expression of cholesterol regulatory genes. *(a) Primary human fibroblasts with (a, c) I1061T/P237S, P1007A/T1036M, or (b) I1061T/I1061T NPC1 alleles were treated with vehicle (Veh), (a, c) 0.75 mg/ml 5A-SM, or (b) increasing concentrations of 5A-DMPC for 48 hrs. mRNA expression of cholesterol regulatory genes was analyzed by qPCR. (d, e) NPC1 protein levels from P1007A/T1036M fibroblasts treated with vehicle (Veh) or 5A-SM were analyzed by western blot for (d) total levels or (e) digested with endoglycosidase H (E), PNGaseF (P) or not treated (NT). Data are mean ± s.e.m. from three independent experiments. (a, d) Student's t-test (t=(a) I1061T/P237S (HMGCR) 5.71; (HMGCS1) 38.35; (ABCA1) 17.92; (LDLR) 3.91; (SREBP) 1.173; P1007A/T1036M (HMGCR) 3.31; (HMGCS1) 6.43; (LDLR) 4.53; (d) 4.329); (b, c) One-way ANOVA with Tukey posthoc test (F, df=(b) (HMGCR) 10.73, 2; (HMGCS1) 21.72, 2; (ABCA1) 75.05, 2; (LDLR) 89.24, 2; (SREBP) 10.7, 2; (c) (Left) 9.78, 2; (Right) 5.23, 2). n.s., not significant, *p≤.05, **p≤.01, ****p≤.0001.*

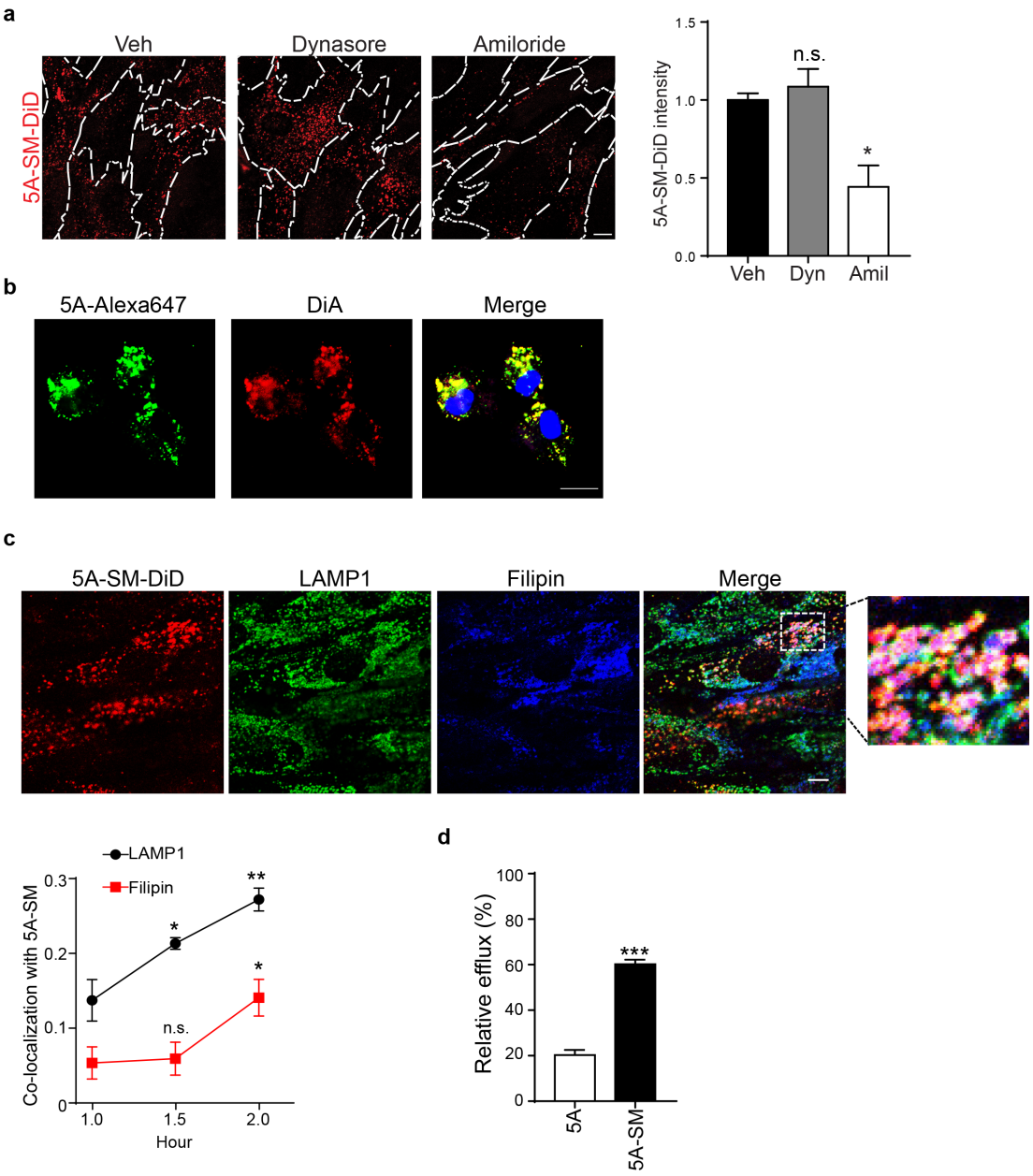

Figure 2-6 5A-SM is endocytosed and increases cholesterol efflux. *(a-d) NPC1 I1061T fibroblasts were treated with the indicated sHDL for (a-c) 2 or (d) 24 hours. (a) Cells were pre-treated with dynasore (80 μM), amiloride (1 mM) or vehicle (Veh) for 30 minutes, and then incubated with fresh media containing 5A-SM-DiD plus dynasore, amiloride or vehicle for two hours. Plasma membranes are outlined with dashed lines. 5A-SM-DiD (red) intensity is quantified at the right. (b) Cells were treated with sHDL composed of 5A-Alexa647 (green) and DiA (red) incorporated into the SM fraction. Following 2 hours incubation, cells were labeled with NucStain (blue) and imaged by confocal microscopy. Pearson co-localization coefficient = 0.75 ± 0.01. (c) Cells were incubated with 5A-SM-DiD (red) for 1, 1.5, and 2 hours, fixed, stained for LAMP1 (green) and filipin (blue), and imaged by confocal microscopy. Representative images from 2 hours post treatment. Pearson co-localization coefficient quantified below. (d) Cells were pre-treated for 24 hours with acetylated LDL containing [3H]cholesteryl linoleate to specifically*

*deliver cargo to the lysosomal compartment. Following 24 hour equilibration, cells were treated for 24 hour with 0.75 mg/ml 5A peptide or 5A-SM. Radioactivity in media and cell fractions was determined by liquid scintillation counting and values were normalized to vehicle treated group. Data are mean ± s.e.m. from three independent experiments. n.s., not significant, *p≤.05, **p≤.01, ****p≤.0001 by (a) One-way ANOVA with Tukey posthoc test relative to Veh or 5A (F=10.74, df=2); (c) Two-way ANOVA with Bonferroni posthoc test(F, df= 23.63, 2). (d) student's t-test t=13.09, df=4. Scale bar = (a) 12 μm, (b) 20 μm, (c) 10 μm.*

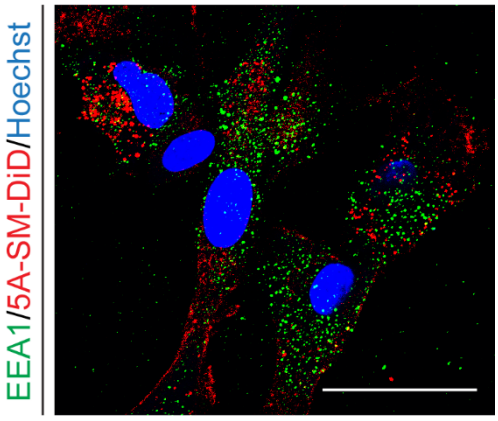

Figure 2-7 5A-SM does not co-localize with EEA1 at two hours post treatment. *NPC1 I1061T fibroblasts were treated with 0.75 mg/ml 5A-SM-DiD (red) for two hours. Cells were fixed and stained for EEA1 (green) and nuclei (blue). Representative images from 2 hours post treatment. Scale bar = 50 μm.*

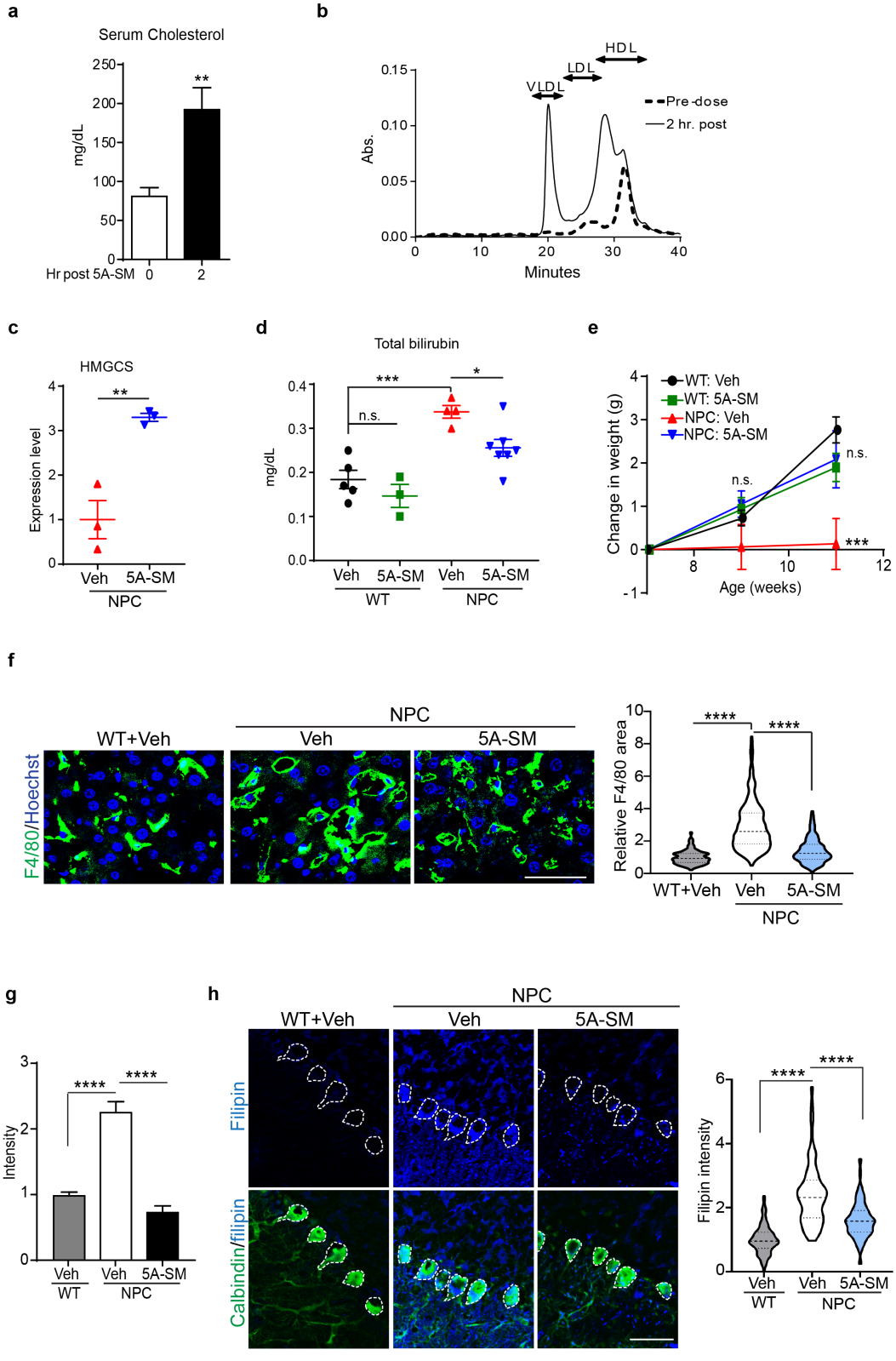

Figure 2-8 5A-SM mobilizes cholesterol in vivo and ameliorates disease phenotypes. *(a) Serum cholesterol from seven week old Npc1 I1061T homozygous mice pre- and 2 hr post-treatment with 100 mg/kg 5A-SM, i.p. (b) Pre- (dashed line) and 2 hr post-*

*treatment (solid line) serum was fractionated by HPLC and cholesterol was quantified by cholesterol oxidase assay. VLDL, LDL, and HDL fractions are indicated by arrows. (c, d) Seven week old wild type (WT) and Npc1 I1061T homozygous (NPC) mice were injected i.p. with vehicle (Veh) or 100 mg/kg 5A-SM. 48 hrs later (c) liver HMGCS transcript levels and (d) total serum bilirubin were analyzed. (e) WT and Npc1 I1061T mice were injected i.p. with vehicle (Veh) or 100 mg/kg 5A-SM three times per week from 7-11 weeks of age. The change in weight of each mouse from week 7 (t=0) to week 11 (t=4) was quantified. (f) Seven week old WT and NPC mice were injected with Veh or 100 mg/kg 5A-SM three times per week for two weeks. At nine weeks of age livers were stained for macrophages using F4/80 (green) and DNA Hoechst (blue). Macrophage area is quantified at right. Scale bar = 50 μm. Violin plot shows median (dashed line), 25% and 75% (dotted lines), and probability density (thickness). (g) Brain slices from 8 week old Npc1 I1061T mice were incubated with vehicle (Veh) or 5 mg/ml 5A-SM for four days and filipin levels in Purkinje neuron soma were quantified (see also Additional file 1: Fig. S4b). (h) Six to seven week old WT and Npc1 I1061T mice received intraventricular injections with vehicle (Veh) or 5A-SM-DiD. N: WT=4, NPC Veh=5, NPC 5A-SM=4 mice. One-week later cholesterol levels in Purkinje neuron soma (green) were analyzed by filipin (blue) staining. Dashed lines indicate Purkinje neuron soma (also see Additional file 1: Fig. S6a). Scale bar = 50 μm. Data quantified at right. Data are mean ± s.e.m. from (a, b, c) three; (d) genotype and treatment: number of mice, WT+Veh=5, WT + 5A-SM=3, NPC+Veh=4, NPC+5A-SM=7; (e) genotype and treatment: number of mice at 9 wks & 11 wks, WT+Veh: 13 & 8, WT + 5A-SM: 9 & 8, NPC+Veh: 6, NPC+5A-SM: 12 & 10 mice, (f) genotype and treatment: number of mice, cells, WT+Veh: 4, 301, NPC+Veh: 4, 514, NPC+5A-SM: 3, 373 (g) WT=93, NPC Veh=143, NPC+5A-SM= 116 cells. *p≤.05, **p≤.01, ***p≤.001, ****p≤.0001. (a, c) Student's t-test (t=(a) 6.375, (c) 5.23); (d, f, g, h) One-way ANOVA with Tukey posthoc test (F, df=(d) 13.28, 3; (f) 368.1, 2 (g) 38.89, 2; (h) 108.3, 2), (e) Two-way ANOVA with Bonferonni posthoc test (F, df= 7.12, 2).*

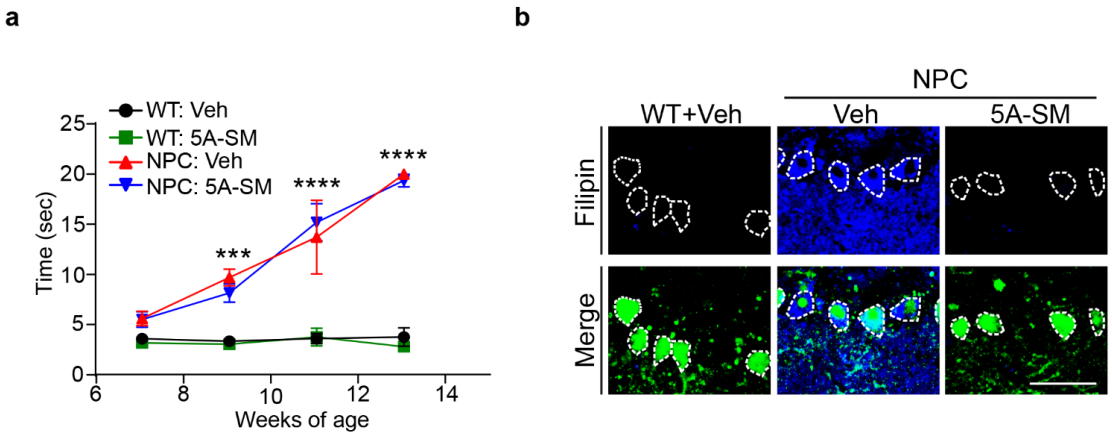

Figure 2-9 Effects of 5A-SM treatment. *(a) Mice were treated i.p. with vehicle (Veh) or 100 mg/kg 5A-SM three times per week from 7 days to 13 weeks of age. Motor function was tested every other week from 7-13 weeks of age by balance beam. Data are mean ± s.e.m. from WT+Veh (n=6-10), WT + 5A-SM (n=5-6), NPC+Veh (n=3-5), NPC+5A-SM (n=4) mice. Two-way ANOVA with Bonferonni posthoc test (F, df= (52.46, 3). n.s., not significant, *p≤.0.05, **p≤.01, ***p≤.001, ****p≤.0001. (b) Brain slices from 8 week old Npc1 WT or I1061T (NPC) mice were incubated with vehicle (Veh) or 5 mg/ml 5A-SM for four days. Purkinje cells were labeled with calbindin (green) and cholesterol with filipin (blue). Images were taken from lobules 3-6. Dashed lines outline Purkinje cell soma. Scale bar = 50 μm.*

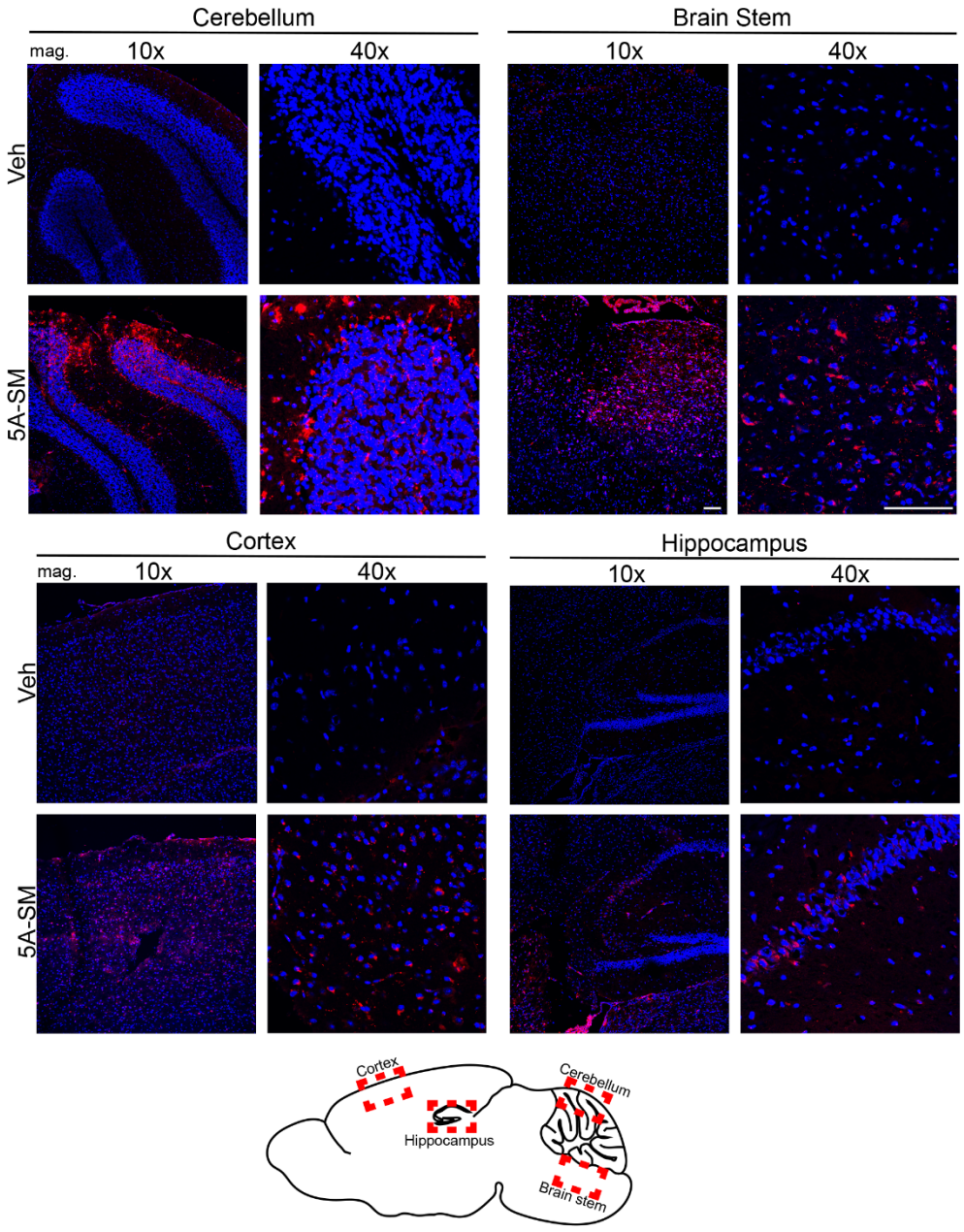

Figure 2-10 5A-SM distribution in the brain after ICV injection. *Seven week old Npc1 I1061T mice were injected ICV with vehicle (Veh) or 5A-SM-DiD. One-week post injection confocal microscopy was used to visualize distribution of DiD (red) and DNA (blue). Images of the cerebellum, brainstem, cortex, and hippocampus are shown (regions of images indicated below in the cartoon). Scale bars = 100 μm.*

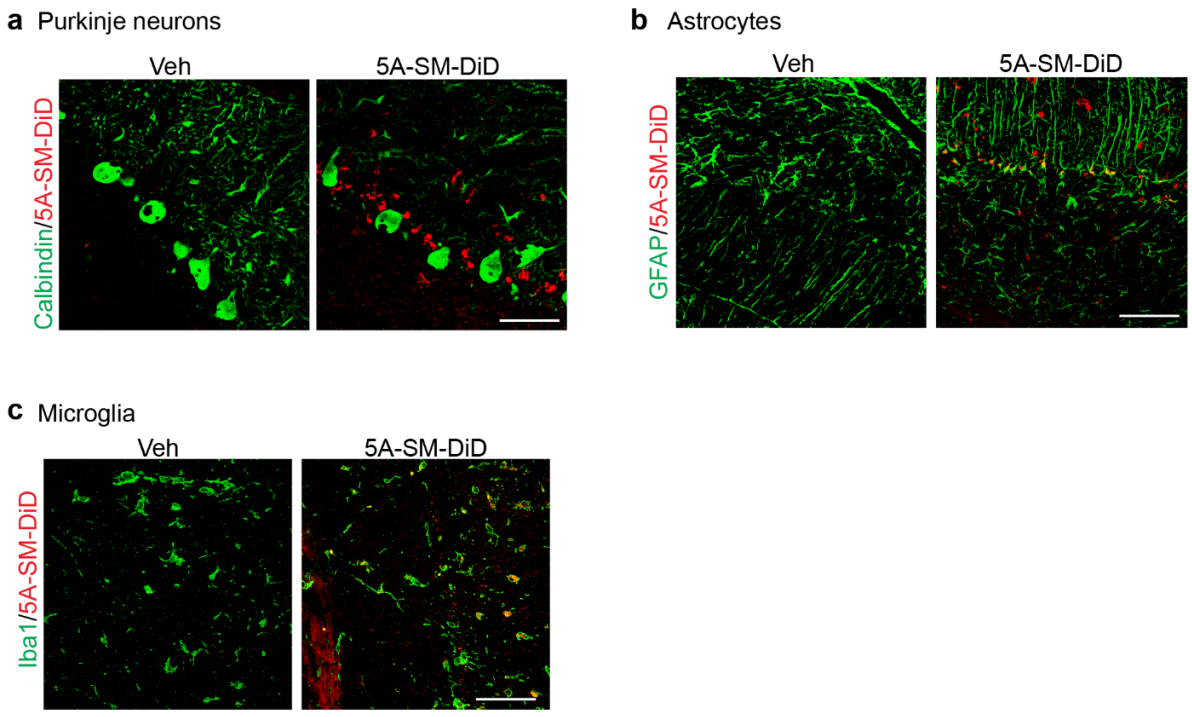

Figure 2-11 Cellular distribution of 5A-SM after ICV injection. *Npc1 I1061T mice received intraventricular injections with vehicle (Veh) or 5A-SM-DiD. Confocal microscopy was used to analyze co-localization of DiD (red) in cerebellum with (a) Purkinje neurons (calbindin), (b) astrocytes (GFAP), or (c) microglia (Iba1). Scale bar = 50 μm.*

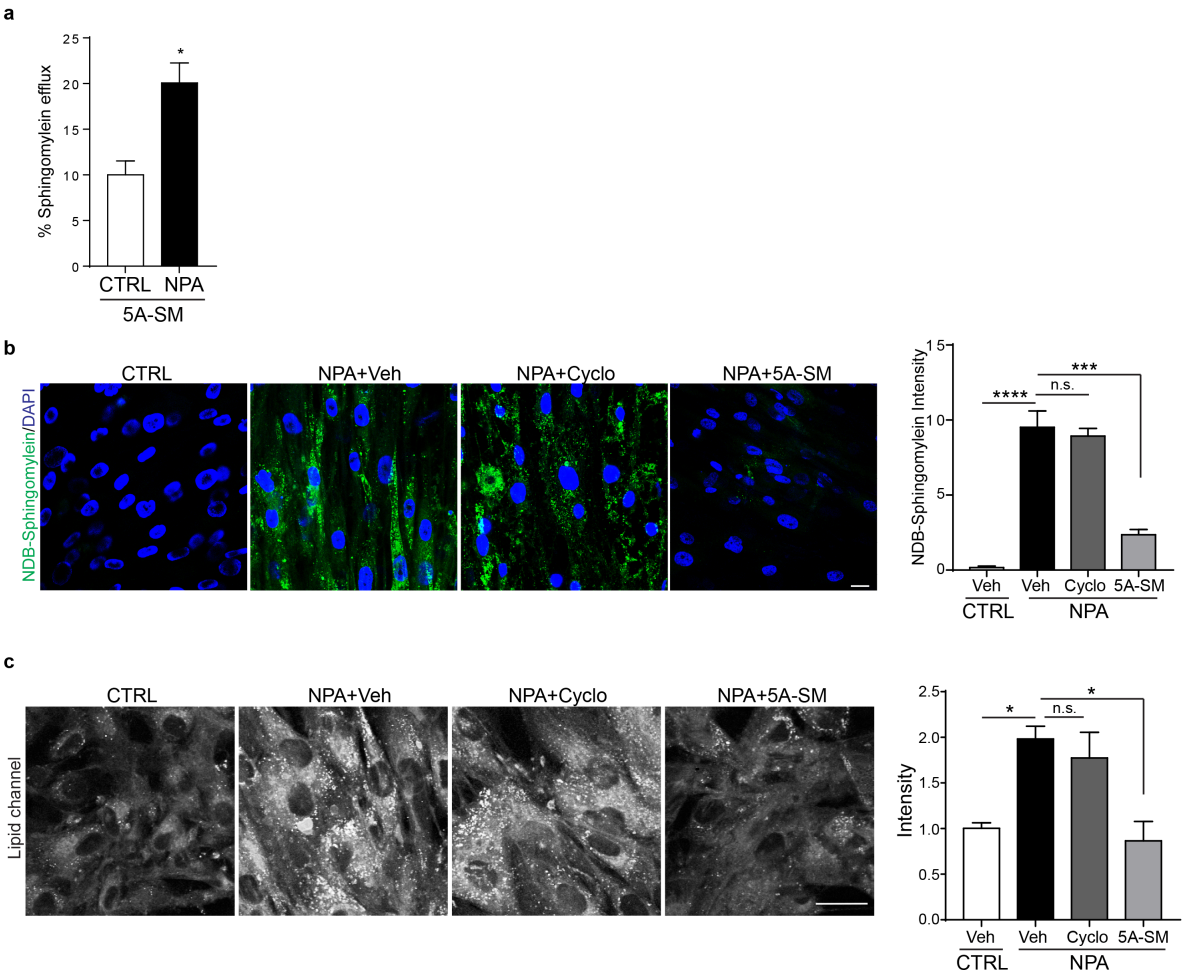

Figure 2-12 5A-SM removes sphingomyelin from Niemann-Pick type A fibroblasts. *(a) Control (CTRL) and Niemann-Pick A (NPA) primary fibroblasts were incubated with [3H]sphingomyelin for 24 h, followed by treatment with 0.75 mg/ml 5A-SM or vehicle (Veh). Radioactivity in media and cell fractions was determined by liquid scintillation counting. (b) CTRL and NPA primary fibroblasts were loaded with NBD-sphingomyelin, then treated for 48 hrs with vehicle (Veh), cyclodextrin (Cyclo), or 0.75 mg/ml 5A-SM. NBD-sphingomyelin intensity quantified at right. Scale bar = 20 μm. (c) SRS microscopy was used to image total endogenous lipids in CTRL and NPA cells with the indicated treatments. Quantified at right. Scale bar = 20 μm. Data are mean ± s.e.m. from (a, b, c) three; *p≤.05, ***p≤.001, ****p≤.0001. (a) Student's t-test (t=6.04); (b, c) One-way ANOVA with Tukey posthoc test (F, df=(b) 55.57, 3; (c) 8.285, 3).*

Chapter 3: Rescue of Sphingomyelin Storage in Niemann-Pick Disease Type A by Apolipoprotein A-I Mimetics

3.1 **Abstract**

Niemann-Pick Disease type A (NPA) is a severe lipid storage disorder caused by the deficient activity of the acid sphingomyelinase enzyme. NPA is characterized by the accumulation of sphingomyelin (SM) in late endosomes and lysosomes leading to progressive neurological dysfunction and hepatosplenomegaly. Our objective was to investigate the utility of synthetic Apolipoprotein A-I (ApoA-I) mimetics, peptides and synthetic high-density lipoproteins (sHDL), designed to act as lipid scavengers for the treatment of NPA. We identified a peptide (22A) and sHDL (22A-DMPC and 22A-DPPC) capable of reducing SM levels in human NPA fibroblast cells. Moreover, it was determined that the ATP-binding cassette A1 transporter, located on cellular membranes, was a key played in efflux of SM from NPA cells. Intravenous administration of 22A at 300 mg/kg to wild type mice rapidly mobilized SM from tissues into circulation. In addition to SM, 22A and 22A-sHDL could mobilize cholesterol, which was found to be elevated in NPA disease. Together, our data shows that ApoA-I mimetics might represent a novel therapeutic strategy for the treatment of Niemann-Pick Disease with acid sphingomyelinase deficiency.

3.2 **Background**

Niemann-Pick disease type A/B (NPA/B) is a rare genetic disorder caused by mutations in the acid sphingomelinase (ASM) enzyme leading to abnormal accumulation of sphingomyelin (SM) and other lipids in late endosomes and lysosomes (LE/Ls) [30, 82]. SM is an important signaling molecule, and it is an integral part of cellular membranes [151]. The inability of ASM to break down SM into ceramide and phosphocholine results in lipid trafficking defects in the periphery (NPA and NPB) and brain (NPA). Visceral manifestations such as hepatosplenomegaly and pulmonary insufficiency are commonly seen in both NPA and NPB patients, yet the type A is more severe due to extreme deficits (<5%) of ASM activity, leading to premature death by age 3 [152, 153]. Currently, there are no FDA-approved drugs for NPA and NPB, and thus there is a great unmet medical need.

NPA/B patients typically have decreased levels of high-density lipoproteins (HDL), which are responsible for cholesterol and phospholipid efflux from cells [83, 89]. Moreover, HDL from patients is highly enriched in SM compared to normal controls, suggesting the increased flux of SM to extracellular lipoprotein acceptors [88]. The body produces HDL as an 8-12 nm nanoparticle composed of a lipid membrane wrapped around by a belt of the 243 amino acid apolipoprotein A-I (ApoA-I) [99]. When ApoA-I is secreted by the liver and intestines, it interacts with the ATP-binding cassette transporter A1 (ABCA1) on the cell membranes to form nascent HDL particles mainly from phospholipids such as SM and phosphatidylcholine. Then, ApoA-I and phospholipid-rich nascent HDL particles circulate in the periphery to efflux excess cholesterol from cells for redistribution or elimination. Previous studies have shown that

ApoA-I isolated from NPB patients is able to form nascent HDL particles containing SM when incubated with human NPB cells, suggesting normal availability of lysosomally sequestered SM to its extracellular protein acceptors [88]. SM content of HDL is also sensitive to *ABCA1* gene modulation with 22 (*R*)-hydroxycholesterol and 9-cis-retionoic acid and thus ABCA1 transporter could be explored as a gate for SM flux. Based on this data, we decided to investigate the efficacy of ApoA-I mimetic peptides and synthetic HDL particles (sHDL) for their ability to scavenge SM from NPA/B primary human fibroblast cells.

Here, we examined three ApoA-I mimetic peptides (5A, 18A, and 22A) with different amino acid composition. One peptide, 22A, significantly reduced accumulated SM in human Niemann-Pick type A and B fibroblast cells in a dose and time-dependent manner. This peptide was originally developed by Esperion to mimic endogenous ApoA-I function and to be used for the treatment of atherosclerosis [27]. We showed that 22A was non-toxic *in vitro* and utilized the ATP-binding cassette transporter 1 (ABCA1) to efflux stored SM. Synthetic HDL nanoparticles composed of 22A and phosphatidylcholine (DMPC and DPPC) were also capable of scavenging SM *in vitro*. Furthermore, the 22A peptide and lipid-poor 22A-sHDL were administered into wild type mice to identify whether the dose and degree of lipidation was important for SM mobilization in animals. We found that only 22A peptide at 300 mg/kg rapidly mobilized SM into circulation. Higher concentrations of sHDL were still needed to be examined in vivo. Moreover, both 22A and sHDL could mobilize cholesterol, which has been previously shown to become accumulated in NPA cells [154]. Together, these studies provide the proof-of-concept data to support therapeutic potential of 22A for the

Niemann-Pick Disease characterized by ASM deficiency.

3.3 **Methods**

Materials and animals

22A peptide (PVLDLFRELLNELLEALKQKLK) was synthesized by Genscript while 5A (DWLKAFYDKVAEKLKEAF-P-DWAKAAYDKAAEKAKEAA) and 18A (Ac-DWLKAFYDKVAEKLKEAF-NH_2) were synthesized by Bachem Americas Inc. 1,2-dimyristoyl-*sn*-glycero-3-phosphocholine (DMPC), 1,2-dipalmitoyl-*sn*-glycero-3-phosphocholine (DPPC), sphingomyelin (SM) were purchased from NOF America Corporation (White Plains, NY); Sphingomyelin [choline methyl-3H] were from American Radiolabeled Chemicals (Saint Louis, MO). All other reagents were analytical grade and obtained from commercial suppliers.

All work performed on animals was in accordance with and approved by the Institutional Animal Care and Use Facility (IACUC) at the University of Michigan, Ann Arbor.

Preparation and analytical characterization of peptides and sHDL

Each peptide (5A, 18A, 22A) was diluted with PBS pH 7.4 to 10 mg/mL (accounted for the net peptide content) and pH adjusted to 7.4 with NaOH. Synthetic HDL (sHDL) compositions were prepared using a lyophilization and thermocycling method. Briefly, 22A and DMPC, DPPC (1:0.5, 1:1, 1:1.5, 1:2 weight ratio) were dissolved in glacial acetic acid and freeze-dried. The powder was rehydrated with PBS (pH 7.4) and then the suspension was cycled between 50°C (10 min) and room

temperature (10 min) until a clear sHDL solution was obtained. The pH of the sHDL solution was adjusted to 7.4 with NaOH. Synthetic HDL particles were analyzed at 1 mg/mL by gel permeation chromatography (GPC) for purity on Tosoh TSK gel G3000SWxl column (Tosoh Bioscience, King of Prussia, PA) with UV detection at 220 and 280 nm using PBS (pH 7.4) as a mobile phase with an isocratic flow rate of 1 mL/min. The hydrodynamic diameters at 1 mg/mL of sHDL particles were determined via dynamic light scattering (DLS) using Zetasizer Nano ZSP (Malvern Instruments, Westborough, MA).

Sphingomyelin efflux assays

Cell lines were obtained from the NIGMS Human Cell Repository at the Coriell Institute for Medical Research. The following cell lines were used: GM08399 - control (WT), GM03393 - and Niemann-Pick B (NPB), and GM00112 - Niemann-Pick A (NPA) cell line L302P/L302P mutation in the *SMPD1* gene. Cells were cultured in DMEM, penicillin-streptomycin, and FBS.

Radioactive sphingomyelin efflux: Cells (50,000 cells/well) were cultured for 24 hr in 24-well plates and then incubated with 1 μCi (80 Ci/mmol) sphingomyelin [choline methyl-3H] per 1 mL media. After 24 hr, cells were washed with PBS, pH 7.4, 3 X followed by the treatment with vehicle, peptide (5A, 18A, 22A) or 22A-sHDL (22A-DMPC or 22A-DPPC) in culture media. Radioactivity in media and cells was counted using a PerkinElmer scintillation counter. Percent [3H]sphingomyelin ([3H]SM) effluxed from cells was calculated by dividing media counts by the total sum of media and cell

counts and then multiplying this number by 100%. Non-specific [3H]SM efflux by vehicle was subtracted from all treatment data.

Non-radioactive sphingomyelin efflux: Cells (50,000 cells/well) were cultured for 24 hr in 24-well plates and then treated with vehicle, 22A or 22A-sHDL (22A-DMPC or 22A-DPPC) for 24 hr. Cells were trypsinized (0.25%) and separated for lipid and protein analysis. Protein concentration in each well was determined using BCA assay according to the manufacturer instructions. Lipids from cells and media were extracted in 2:1 v/v chloroform:methanol, placed in the sonicator bath for 1 min, centrifuged for 5 min at 500xg, and then chloroform layer was removed and dried under nitrogen. For LC-MS analysis, lipids were dissolved in acetonitrile. To quantify concentration of SM in each sample, Waters Acquity UPLC equipped with QDa System (Milford, MA) was used. Chromatographic separation was achieved on a BEH300 1.7µm HILIC column at 25 °C. The flow rate was set at 0.65 mL/min. A gradient elution was carried out with mobile phase A (water, 0.1% formic acid), mobile phase B (acetonitrile, 0.1% formic acid) and mobile phase C (100 mM ammonium formate) as follows: 0–0.7 min (5–17% A), (90–78% B), and (5-5% C); 0.7-0.71 min (17-5% A), (78-90% B) and (5-5% C); 0.71-3 min (17–17% A), (90–90% B), and (5-5% C). Mass spectra were acquired in the positive ion mode and SM was integrated at 704 m/z. SM standards were used in the range of 0.25-8 µg/mL and used for quantification of SM in the extracted samples. Data analysis was performed on Waters Empower software version 3, 2010 (Waters, Milford, MA).

RT-qPCR

Total RNA was purified using GeneJET RNA Purification Kit (Thermo Scientific) and converted to cDNA with the SuperScript III First-Strand Synthesis System. Taqman system was used to determine mRNA expression levels for human *ABCA1* (Hs 01059118) and normalized to *18S* (control) (Hs 03928990). Expression levels relative to control (non-treated) were calculated by the 2^ (-delta delta Ct) method.

siRNA transfection

Predesigned ON-TARGETplus SMARTpools containing 4 individual siRNAs per target sequence (Dharmacon Non-targeting SMARTpool D-001810-10-05, ABCA1 L-004128-00) were transfected using TransIT-X2® (Mirus) reagent at t=0 and t=24 hr. NPA cells were treated with 0.75 mg/mL 22A peptide after the second transfection (t=24 hr). RNA and SM analysis occurred 48 hr after the first transfection.

Cellular viability

Cell viability was assessed using Promega CellTiter 96 Aqueous One Solution cell proliferation colometric assay (G3580). Briefly, Niemann-Pick A cells were cultured in 96-well plates at 10,000 cells per well for 24 hr, washed three times with PBS, and treated with vehicle, peptides, and sHDL diluted in media for 24 hours. Cells were washed three times with PBS, and re-suspended in media supplemented with Promega CellTiter 96 reagent (20 µl reagent per 100 µl of media). After 45 min incubation at 37 °C, absorbance was read at 490 nm using a microplate reader. Each treatment was performed in triplicate and the average absorbance reading of non-treated (vehicle) cells was set to 100%. The

percent viability was determined by dividing the average absorbance of treated over non-treated cells and multiplying by 100.

In vivo PK/PD study

Healthy male C57BL/6J mice (8 weeks old) were purchased from Charles River Breeding Laboratories (Portage, MI) and were fed a standard rodent chow diet. To examine the impact of peptide concentration and lipid content on pharmacokinetic/ pharmacodynamics properties, animals were randomly assigned to four groups (n = 4/group) of 75 mg/kg, 150 mg/kg, and 300 mg/kg of 22A peptide or 75 mg/kg 22A-DMPC (1:1). All animals were fasted overnight before peptide dosing via tail vein injection. At each time point (pre-dose, 1, 6 and 24 hrs) blood samples (~0.1 mL) were collected from the jugular vein to Microvette® 500 Z-gel tube (Sarstedt Inc, German) and centrifuged at 10,000 rpm for 10 min at 4°C. The obtained serum samples were stored at -20°C for further analysis.

The levels of SM in serum samples (25x dilution) were determined using fluorometric assay according to manufacturer protocol (Cell Biolabs, Inc, CA, USA) and samples were analyzed using plate reader (SynergyTM NEO HTS Multi-Mode Microplate Reader, Bio-Tek). Fluorescence was read at 550 nm excitation and 595 nm emission. Background fluorescence value was subtracted from all standards and samples. Cholesterol levels in serum samples (10x dilution) were measured enzymatically (Wako Chemicals, Richmond, VA) as described in the manufacturer's instructions and samples were analyzed at 600 nm on the plate reader. A slope was calculated for each standard curve/plate and SM levels in samples were calculated

using the following formula: SM or cholesterol (mg/dL) = (Corrected sample fluorescence / Slope) × Sample dilution. The pharmacodynamic effect in each mouse was determined as the area under the total effect curve (*AUEC*) using trapezoidal rule.

Peptide (22A) concentration in serum was determined by LC-MS. The 10 µL serum aliquots were combined with 10 µL of 2.4 mg/mL of internal standard (5A peptide). Working standard solutions (0-100 µg/mL) of 22A were prepared using blank mouse serum. Serum proteins were precipitated by adding methanol. After 5 minutes, the mixture was centrifuged (12000 rpm × 10 min, 4°C) and supernatant was used for analysis. Samples were mixed (1:1 v/v) with LC-MS mobile phase (80:20 v/v H_2O:acetonitrile, 0.1% formic acid) and analyzed on Waters Acquity UPLC equipped with QDa System (Milford, MA) using Acquity UPLC BEH C18 1.7 µM column for separation. The mobile phase consisted of (A) water containing 0.1% v/v formic acid and (B) acetonitrile containing 0.1% v/v formic acid. The mobile phase was delivered at 0.3 mL/min using a gradient elution of 20% to 80% B during 0-1.5 min, and 80% to 20% B during 1.5-3.5 min. Mass spectra were acquired in the positive ion mode with the mass range set at m/z 150-1250. Data analysis was performed on Waters Empower software. The concentration of 22A peptide in each sample was determined from the standard curve. Pharmacokinetic parameters such as maximum serum concentration (C_{max}), the area under the serum concentration-time curve (*AUC*), elimination half-life ($T_{1/2}$) were obtained by non-compartmental analysis.

Statistical analysis

Significance of difference was determined by Student's *t*-test for comparing two groups or by one-way analysis of variance (ANOVA) for comparing multiple groups. All *in vitro* experiments were performed in triplicate and error bars were reported as a standard mean error (SEM) unless noted otherwise. $P < 0.05$ was considered statistically significant.

3.4 **Results**

Preparation of ApoA-I peptides and sHDL nanoparticles

In our studies, we utilized three ApoA-I peptides, 5A, 18A, and 22A, previously developed and well-characterized by others to mimic the properties of the full-length ApoA-I protein such as peptide helicity, lipid binding, and cholesterol efflux [27]. These peptides were readily available in large quantities compared to the ApoA-I protein, which required recombinant production. The amino acid composition for each peptide as shown in Figure 3-1a was distinctive from one another. Peptide 18A had strong lipid binding and good capacity to efflux phospholipids and cholesterol, 5A peptide was developed to promote ABCA1 receptor-mediated efflux of cholesterol, and 22A peptide could activate the lecithin:cholesterol acyltransferase (LCAT) enzyme involved in HDL particle maturation. Using phospholipids with differing chain length, we prepared a panel of sHDLs DMPC (1,2-dimyristoyl-sn-glycero-3-phosphocholine) or DPPC (1,2-dipalmitoyl-sn-glycero-3-phosphocholine) containing various peptide:lipid ratios. The reason for varying peptide to lipid ratios was to control the size of sHDL and its ability to bind SM. All sHDLs were prepared by co-lyophilization and thermocycling (Figure 3-1b) [101]. Particles with peptide:lipid of 1:0.5, 1:1, 1:1.5, and 1:2 w/w had an average

diameter of 6 nm, 7 nm, 8 nm, and 9-12 nm respectively as determined by dynamic light scattering and displayed >98% purity as measured by gel permeation chromatography (Figure 3-1c, 3-2).

ApoA-I mimetic peptides reduce lysosomal sphingomyelin in patient fibroblasts

To assess the activity of ApoA-I peptides on Niemann-Pick type A patient cells, we used [3H]SM and media supplemented with fetal bovine serum to load lysosomes in cells as previously described [155]. The analysis of [3H]SM effluxed from cells into media was performed by scintillation counting following the treatment with vehicle (media), 5A, 18A, or 22A peptides at 0.03, 0.3, and 0.75 mg/mL concentrations. The vehicle control value was subtracted from each peptide measurement. Treatment with 18A peptide (Figure 3-3a) displayed 70% of [3H]SM efflux at 0.75 mg/mL compared to 25% and 10% efflux for 22A and 5A peptides respectively. Additionally, the time-dependedent [3H]SM efflux at 0.75 mg/mL for each peptide was measured. Around 24 hr, the efflux for 5A and 22A saturated, but 18A efflux was not time sensitive (Figure 3-3b). It was noted that 18A caused significant cell death at all concentrations used. This possibly led to [3H]SM releasing into media and giving the false positive results. A cell toxicity assay confirmed that at 0.75 mg/mL only ~40% of cells were viable with 18A treatment while 5A and 22A did not result in cell death (Figure 3-4). Differences in 5A and 22A efflux of [3H]SM could be due to different lipid solubilization kinetics. Overall, the experimental data strongly suggested that 22A peptide was the most efficacious at [3H]SM efflux from NPA cells. Similar results were obtained with NPB fibroblasts (Figure 3-5). At this point, we chose 22A as the lead peptide to prepared sHDL particles.

Sphingomyelin efflux by sHDL

Both cholesterol and SM could be effluxed from cells by small nascent HDL via ABCA1 transporter [134]. These two lipids physically interact and commonly traffic together [135] suggesting that small sHDL might also be effective at reducing the SM load in cells. Here we chose two phospholipids, DMPC and DPPC, which have different chain length and degree of bilayer rigidity and prepared sHDL with 22A peptide via co-lyophilization and thermocycling [156]. In addition, we varied peptide to lipid ratio by weight (1:0.5, 1:1, 1:1.5, and 1:2) and made sHDL of 6-12 nm in size to closely mimic nascent HDL. To determine whether sHDL could remove stored SM, NPA and control fibroblasts were loaded with [3H]SM for 24 hrs then treated with vehicle (media), 0.75 mg/mL 22A-DMPC, and 22-DPPC at variable peptide:lipid weight ratio (1:0.5, 1:1, 1:1.5, and 1:2). The vehicle control value was subtracted from each sHDL measurement. After 24 hrs, 22A-DMPC and 22A-DPPC particles with lower lipid content (1:0.5) could efflux 17.1% and 12.4% [3H]SM respectively. Larger sHDL particles showed lower efflux (<12%) possibly due to lower ability to interact with specific efflux transporter such as ABCA1 and/or decreased capacity to bind SM (Figure 3-6). Efflux of [3H]SM from the wild type (WT) fibroblasts by peptides (5A, 22A) was higher than that of NPA cells, possibly due to higher concentration of easily accessible SM located on the plasma membranes of WT cells (Figure 3-7). The efflux of [3H]SM between WT and NPA cells when treated with sHDL was not significantly different, thus highlighting possibly distinctive efflux mechanisms between peptides and sHDL. To confirm [3H]SM efflux data, we set up a second non-radioactive assay without the use of externally added SM.

First, we confirmed that NPA cells had higher SM content than WT cells by measuring SM concentration using LC-MS (Figure 3-8a). It was found that NPA cells had ~1.5-fold higher SM concentration than WT cells. Next, NPA cells were treated with vehicle, 22A, 22A-DMPC (1:0.5) or 22A-DPPC (1:0.5) at the highest concentration of 0.75 mg/mL for 24 hrs. Lipids were extracted from cells and quantified by LC-MS. Results showed that the percent of SM efflux from cells into media was similar to [3H]SM assay, suggesting that 22A and 22A-sHDL were indeed the acceptors of SM (Figure 3-8b).

ABCA1 transporter is needed for 22A peptide efficacy

To examine whether ApoA-I mimetic peptides and sHDL effluxed SM via ABCA1-medicated mechanism and similar to that of endogenous ApoA-I protein and nascent HDL, we treated NPA cells with vehicle, peptide (5A, 22A) or sHDL (22A-DMPC or 22A-DPPC) at 0.75 mg/mL. According to Figure 3-9a, 22A increased the expression of *ABCA1* gene 1.5-fold and sHDL particles decreased its expression approximately 2-fold. Our results were partly in line with the endogenous mechanisms where newly secreted ApoA-I typically induced the expression of *ABCA1* to form nascent HDL particles and HDL downregulated the expression of *ABCA1* [157, 158]. To further confirm that ABCA1 was indeed important for 22A efficacy, we performed the siRNA knockdown of *ABCA1* gene in NPA fibroblasts. Figure 3-9b demonstrated the successful knockdown of *ABCA1* (siABCA1) expression compared to the treatment with non-targeting siRNAs (siNT). Next, we used LC-MS to measure differences in SM efflux by 22A in NPA cells treated with siNT or siABCA1. Our data indicated that ABCA1

knockdown resulted in a 2-fold decrease in SM efflux compared to siNT control (Figure 3-9c). This suggested that ABCA1 was indeed in part responsible for SM efflux by 22A.

To investigate other biological responses triggered by peptides and sHDLs, NPA fibroblasts were treated with vehicle, 5A, 22A, 22A-DMPC (1:0.5) or 22A-DPPC (1:0.5) at 0.75 mg/mL. Genes responsible for SM synthesis and breakdown (*SGMS1*, *SGMS2*, and *SMPD1*) were assessed (Figure 3-10). The expression of *SGMS1* and *SGMS2* (SM synthesis) was mostly unaffected. The expression of *SMPD1* (SM breakdown) was only slightly (~1.25-fold) upregulated by 5A, 22A, but not by sHDL.

In vivo pharmacokinetics and pharmacodynamics of 22A

Three doses of 22A peptide (75, 150, and 300 mg/kg) and one dose of 22A-DMPC 1:1 (75 mg/kg) were administered IV into healthy mice in order to evaluate the pharmacokinetics and pharmacodynamics of 22A peptide and 22A-sHDL with regards to SM mobilization. IV route of administration was selected based on the data previously published by our group where 22A peptide injected IP at 75 mg/kg was not effective at mobilizing phospholipids from healthy rats compared to IV route [159]. In this study, we evaluated the doses at and above 75 mg/kg to maximize the amount of SM efflux from tissues into circulation. Furthermore, 22A-DMPC was selected at 1:1 peptide to lipid ratio to investigate if some lipidation of 22A would enhance its *in vivo* circulation half-life and thus SM mobilization. The choice for DMPC lipid for PK/PD study was based on the degree of sHDL purity and homogeneity (size distribution). The lower concentration of 22A-DMPC at 75 mg/kg was evaluated to avoid possible liver toxicity due to strong cholesterol efflux capacity of sHDL compared to free peptide. The half-life of 22A in the

serum at 75 mg/kg and 150 mg/kg was 4.5 ± 1.1 hrs and 3.9 ± 1.2 hrs respectively (Figure 3-11a). However, the half-life of 22A at 300 mg/kg was 9.7 ± 2.0 hrs, which was 2-fold higher compared to two lower doses. This was most likely attributed to saturation of the elimination mechanisms in mice. The area under serum concentration curve (AUC) for 22A at 75, 150, and 300 mg/kg dose was 1571.9 ± 95.2, 4287.9 ± 529.3, and 9131.9 ± 368.0 mg*h/dL accordingly. At the 24 hrs time point, 22A peptide administered at 300 mg/kg was still present in circulation while the other two peptide concentrations were not detectable at 24 hrs. Compared to lipid-free 22A, peptide in sHDL (22A-DMPC) had similar half-life of 4.8 ± 0.7 hrs, but displayed 36% higher AUC (2469.1 ± 156.4 mg*h/dL), which could be attributed to differences in tissue distribution (Figure 3-11b).

To evaluate pharmacodynamics of 22A peptide and sHDL, cholesterol and SM concentrations were measured enzymatically, and the area under the effect curve (AUEC) for cholesterol was calculated. While SM is the main lipid that accumulates in LE/Ls, cholesterol levels have also been found to be elevated in NPA/B patients, so both lipids were analyzed. No differences were found in SM mobilization between 75 mg/kg of 22A, 150 mg/kg of 22A, and 75 mg/kg of 22A-DMPC treatments (Figure 3-12a, 3-12b). Only the 300 mg/kg dose of 22A could mobilize SM into serum. It was noted that SM concentration at pre-dose (t = 0 hrs) was higher compared to the level of SM at 1 hrs post-22A (75 and 150 mg/kg) and 22A-DMPC (75 mg/kg) treatments. This was observed because mice were fasted only 4 hrs at t=0 (blood collected 2 days before the treatment) compared to 8 hrs right before the treatment. Food was given to animals after the blood collection at 6 hrs time point. Finally, mice were fasted again for 4 hrs

before the final collection at t = 24 hrs post-treatment. Typically, fasting of animals is necessary to normalize their lipid profile before the treatment and our protocol only allows prolonged fasting of 8 hrs to be performed once per week.

The cholesterol trend was slightly different to that of SM, where cholesterol mobilization of lipid-free 22A steadily increased was steadily increasing (AEUC = 2550.5, 2939.2, 3194.4 mg*h/dL) with the increase of 22A dose (75, 150, 300 mg/kg) (Figure 3-12c). Differences were found in cholesterol mobilization between 22A (AUEC = 2550.5 mg*h/dL) and sHDL (AEUC = 3149.5 mg*h/dL) administered at the same dose of 75 mg/kg (Figure 3-12d). Taken together, these results suggest that at the same dose of 75 mg/kg, sHDL has greater ability to mobilize SM and cholesterol than naked 22A peptide. Yet, greater SM mobilization can be achieved with 300 mg/kg of lipid-free 22A without pulling substantial amount cholesterol that could cause liver toxicity.

3.5 **Discussion**

Here we present a novel strategy for the treatment of Niemann-Pick disease type A by utilizing the body's natural mechanism of SM transport from cells to ApoA-I extracellular acceptors. Lipid-free ApoA-I mimetic peptides or ApoA-I peptide-sHDL particles have the ability to remove SM from human NPA fibroblast cells as detected in two independent assays. The degree of SM removal in cells depends on the type of ApoA-I peptide used and the peptide to lipid ratio in sHDL. The PK/PD study of ApoA-I peptide and sHDL in healthy mice shows that the mobilization of SM from tissues into circulation can be achieved by modulating ApoA-I peptide concentration.

Previous studies by our group in Niemann-Pick disease type C showed that ApoA-I mimetic peptides were not sufficient for reducing Niemann-Pick C cholesterol storage, possibly due to defects in loading cholesterol into ApoA-I acceptors via ABCA1 transporter [160]. Our strategy in NPC bypassed the HDL formation deficiencies by utilizing ApoA-I mimetic peptide, 5A, complexed with SM for optimal cholesterol binding. In NPA, however, the expression of *ABCA1* gene and HDL formation are normal and SM can be mobilized from cells by ApoA-I protein [88]. Therefore, ApoA-I mimetics (peptide or sHDL) may serve as potential lipid acceptors in NPA.

In our studies, three ApoA-I mimetic peptides were explored for SM efflux from NPA cells. We chose these peptides (5A, 18A, and 22A) based on the differences in their functionality. The first ApoA-I mimetic peptide described in the literature was 18A, characterized by good capacity to efflux phospholipids and cholesterol [161]. Unfortunately, our results indicated that 18A was cytotoxic to NPA cells possibly due to disruption of cellular phospholipid bilayer. Another peptide, 5A, was a modified version of 18A containing two amphipathic helixes instead of one that were kinked by a proline residue to mimic the native ApoA-I structure [162]. These helixes in 5A had different lipid affinities to reduce potential cellular cytotoxicity. The third peptide, 22A, was developed by a biotechnology company (Esperion) as part of ETC-642 sHDL product to be an activator of LCAT enzyme responsible for HDL maturation [163]. Previous data from our laboratory showed excellent lipid solubilization properties of 22A, and, most importantly, it has been previously tested in humans [164, 165].

Nevertheless, peptides are not very stable *in vivo,* and thus the alternative delivery methods have been widely described in the literature, including the use of

phospholipids [166]. Endogenously, ApoA-I first interacts with ABCA1 transporter and binds lipids such as phosphatidylcholine and SM to form nascent HDL particles. These small HDL are very potent lipid acceptors [167]. Thus, our initial studies using NPA fibroblasts were focused on determining which peptide was the most efficacious. We found that 22A could efflux up to ~25% of SM from NPA cells and utilized ABCA1 transporter. Next, we prepared sHDL particles with 22A peptide via lyophilization and thermocycling. Phospholipids for sHDL formation were chosen based on their transition temperatures (T_m), with DMPC having a lower T_m than DPPC. The differences in T_m affect the fluidity of lipids and thus the structure of sHDL, possibly resulting in differences in SM binding. The peptide to lipid ratio in sHDL affects the size of sHDL and the capacity to incorporate phospholipids. Particles of 5-12 nm in size were prepared and tested in NPA cells. Smaller lipid-poor sHDL effluxed the most SM from cells regardless of phospholipid type.

Studies conducted in our laboratory have previously established that the physical state of 22A peptide (lipid-free or lipid-bound) and its route of administration (IV or IP) affect the PK and PD parameters [159]. Tang et al. has shown that 22A administered in rats at 75 mg/kg using IP route was not effective in mobilizing phospholipids and cholesterol regardless of its state of lipidation. However, the IV dose of 22A-sHDL at 75 mg/kg had much better pharmacological response. Here, we evaluated the lipid-free 22A peptide using IV administration route at three doses of 75, 150, and 300 mg/kg and lipid poor 22A-DMPC sHDL at one dose of 75 mg/kg in healthy mice. Our data showed that only 22A peptide at 300 mg/kg was able to mobilize SM into blood compartment. In terms of cholesterol mobilization, 150 and 300 mg/kg of 22A peptide and 75 mg/kg of

sHDL worked to the same extent while 22A at 75 mg/kg had lower efficacy. Interestingly, at 24 hrs post-administration of 22A at the 300 mg/kg dose, cholesterol and SM concentrations in serum did not return to baseline. This is most likely due to saturation of peptide elimination mechanisms supported by the peptide PK profile. Overall, this data suggested that 22A (300 mg/kg) could elicit the desired pharmacological response. Although we examined healthy mice that didn't accumulate SM and cholesterol, the information obtained from this work could still help guiding future experiments in NPA disease models. We learned that the concentration and degree of 22A lipidation could be customized to achieve the necessary SM binding, PK, and safety profile. Altogether, this data supports the concept of ApoA-I peptide mimetics as potential therapy for the Niemann-Pick diseases characterized by the insufficient activity of acid sphingomyelinase enzyme.

A

Name	Peptide Sequence
5A	D-W-L-K-A-F-Y-D-K-V-A-E-K-L-K-E-A-F-P-D-W-A-K-A-A-Y-D-K-A-A-E-K-A-K-E-A-A
18A	Ac-E-W-L-E-A-F-Y-K-K-V-L-E-K-L-K-E-L-F-NH_2
22A	P-V-L-D-L-F-R-E-L-L-N-E-L-L-E-A-L-K-Q-K-L-K

B

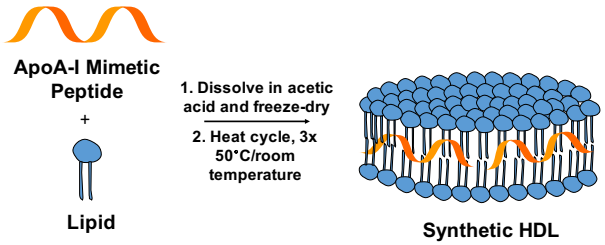

C

sHDL Formulation	Purity (%)	Particle Size (nm)
22A-DMPC 1:0.5	98.7	5.6 ± 1.5
22A-DMPC 1:1	97.4	7.3 ± 1.9
22A-DMPC 1:1.5	98.0	7.9 ± 2.3
22A-DMPC 1:2	98.1	9.4 ± 2.2
22A-DPPC 1:0.5	97.5	6.9 ± 2.0
22A-DPPC 1:1	90.5	7.6 ± 1.8
22A-DPPC 1:1.5	97.7	8.3 ± 2.0
22A-DPPC 1:2	95.1	12.5 ± 1.7

Figure 3-1 ApoA-I mimetic peptide structure, sHDL assembly and analytical characterization. *(a) Amino acid sequence for 5A, 18A and 22A peptide. (b) A lyophilized mixture of ApoA-I peptide and DMPC or DPPC at 1:0.5, 1:1, 1:1.5, and 1:2 peptide: lipid wt/wt ratio was hydrated in PBS and thermocycled at 50 °C to assemble sHDL particles. (c) The purity of sHDL particles was determined using gel permeation chromatography and particle size was assessed by dynamic light scattering.*

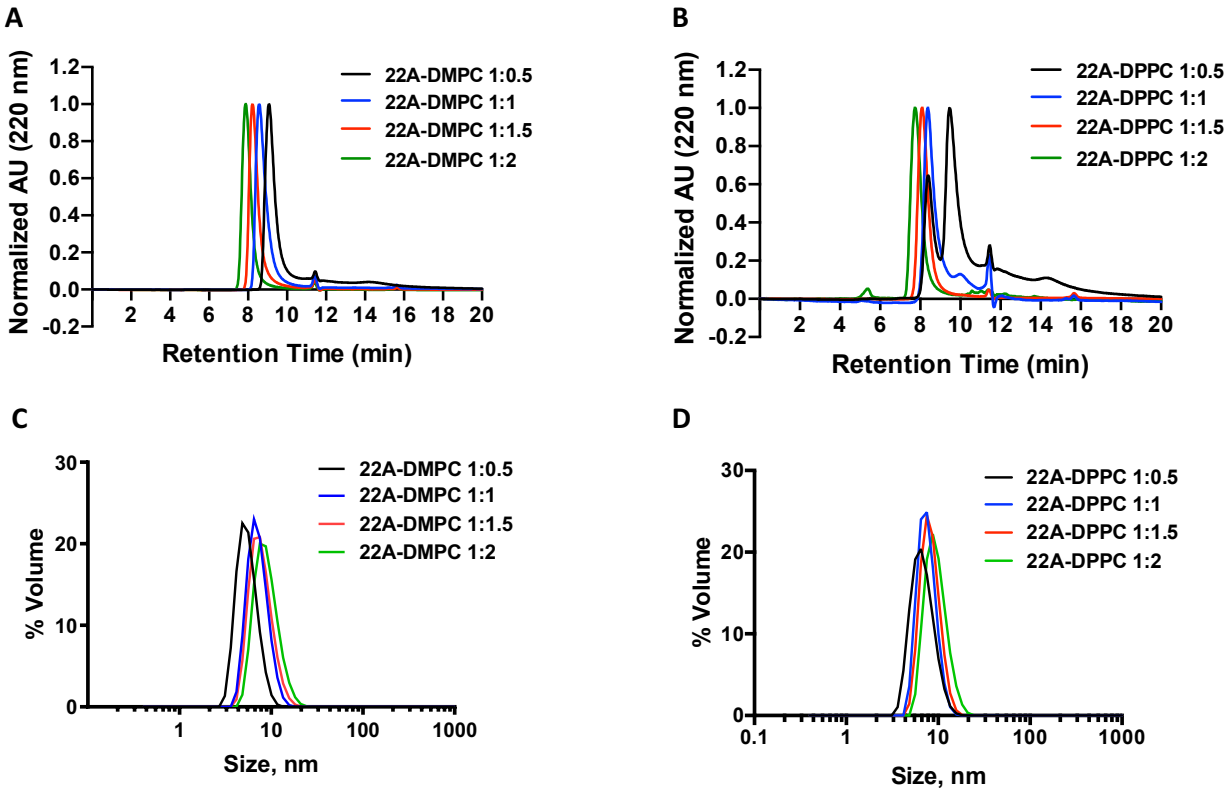

Figure 3-2 sHDL purity and size distribution. *The purity of sHDL particles was determined using gel permeation chromatography (a, b) and particle size was assessed by dynamic light scattering (c, d) at 1 mg/mL concentration.*

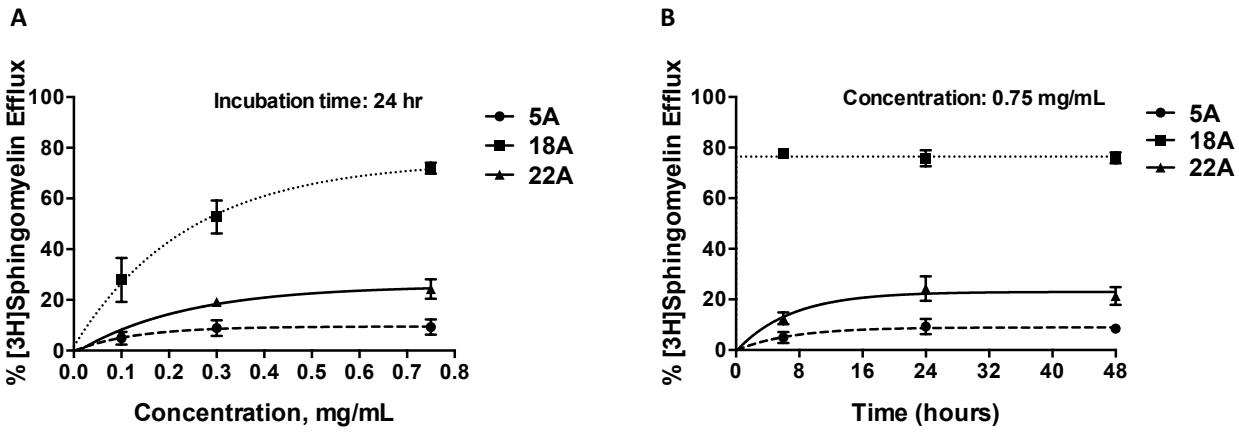

Figure 3-3 ApoA-1 mimetic peptides efflux [3H]Sphingomyelin from human NPA fibroblast cells in a dose and time-dependent manner. *NPA cells were loaded with 1 µCi/mL [3H]Sphingomyelin diluted into media containing fetal bovine serum for 24 h. Cells were washed with PBS and treated with (a) 0.03, 0.3 or 0.75 mg/mL of 5A, 18A, 22A, or vehicle (media) diluted in lipoprotein-deficient media for 24 hr; (b) 0.75 mg/mL of 5A, 18A, 22A or vehicle (media) diluted in lipoprotein-deficient media for 6, 24 or 48 hr. Radioactivity in media and cell fractions was counted and the % [3H]Sphingomyelin efflux was calculated by dividing the media counts by total media plus cell counts and multiplied by 100. Non-specific (vehicle) efflux was subtracted from each treatment group. Data are mean ± s.e.m, N=3.*

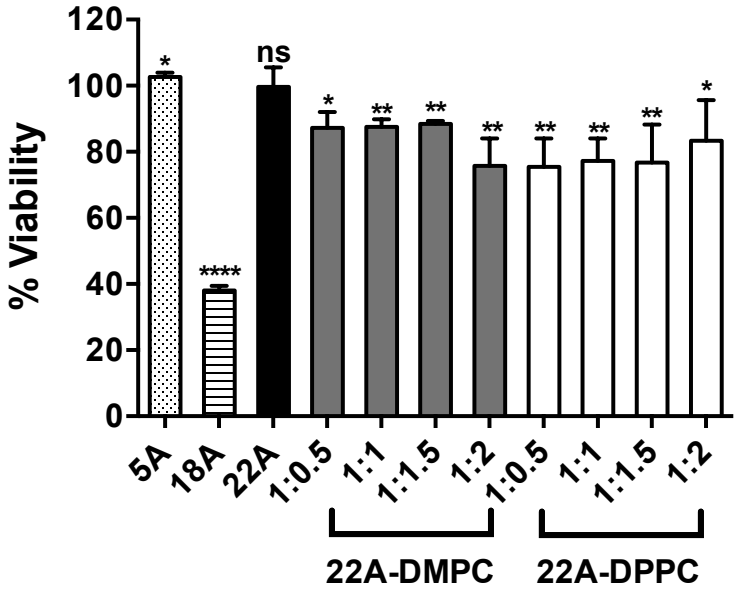

Figure 3-4 Cellular viability of NPA cells after the treatment with peptides or sHDL nanoparticles. *Viability of NPA primary fibroblasts after 24 hr treatment with vehicle (media), 5A, 18A, 22A, 22A-DMPC (1:0.5, 1:1, 1:1.5, 1:2) or 22A-DPPC (1:0.5, 1:1, 1:1.5, 1:2). Vehicle group viability was set to 100%. Data are mean ± s.e.m., N=3. Statistical differences between vehicle and other groups was calculated using unpaired Student's t-test; ns, not significant, *p≤.05, **p≤.01, ****p≤.0001.*

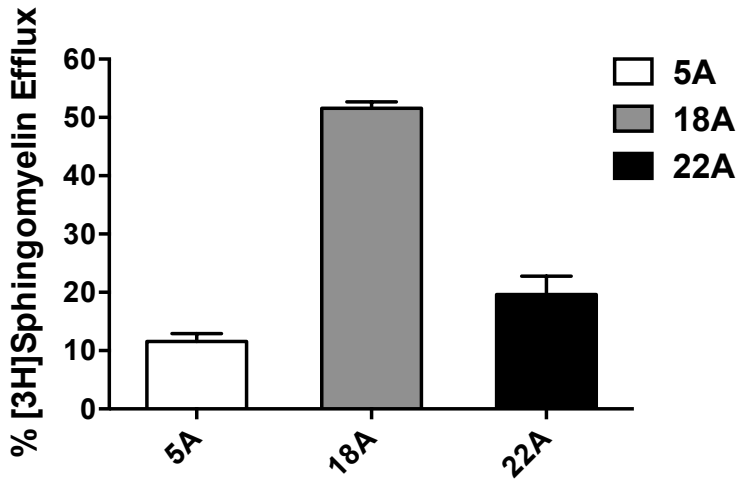

Figure 3-5 [3H]Sphingomyelin efflux by ApoA-I peptides from human NPB fibroblast cells. *NPB cells were loaded with [3H]Sphingomyelin as described in Fig. 3-3 and treated with 0.75 mg/mL of 5A, 18A, 22A or vehicle (media) diluted in lipoprotein-deficient media for 24 hr. Radioactivity in media and cell fractions was counted and the % [3H]Sphingomyelin efflux was calculated by dividing the media counts by total media plus cell counts and multiplied by 100. Non-specific (vehicle) efflux was subtracted from each treatment group. Data are mean ± s.e.m, N=3.*

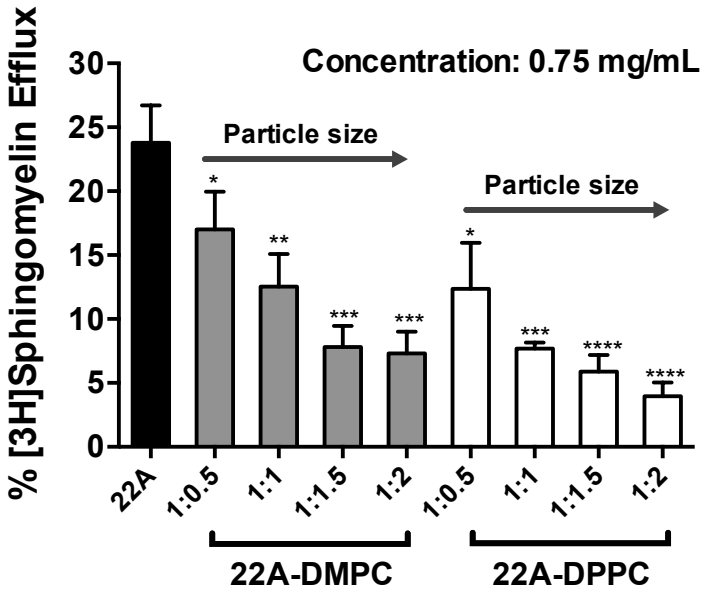

Figure 3-6 [3H]Sphingomyelin efflux in human NPA fibroblast cells by sHDL. *NPA cells were loaded with [3H]Sphingomyelin as described in Fig. 3-3 and treated with 0.75 mg/mL of 22A, 22A-DMPC (1:0.5, 1:1, 1:1.5, 1:2) or 22A-DPPC (1:0.5, 1:1, 1:1.5, 1:2) for 24 hr. Radioactivity in media and cell fractions was counted and the % [3H]Sphingomyelin efflux was calculated by dividing the media counts by total media plus cell counts and multiplied by 100. Non-specific (vehicle) efflux was subtracted from each treatment group. Data are mean ± s.e.m., N=3. Statistical differences between 22A peptide and each sHDL treatment were calculated using one-way ANOVA; *p≤.05, **p≤.01, ***p≤.001, ****p≤.0001.*

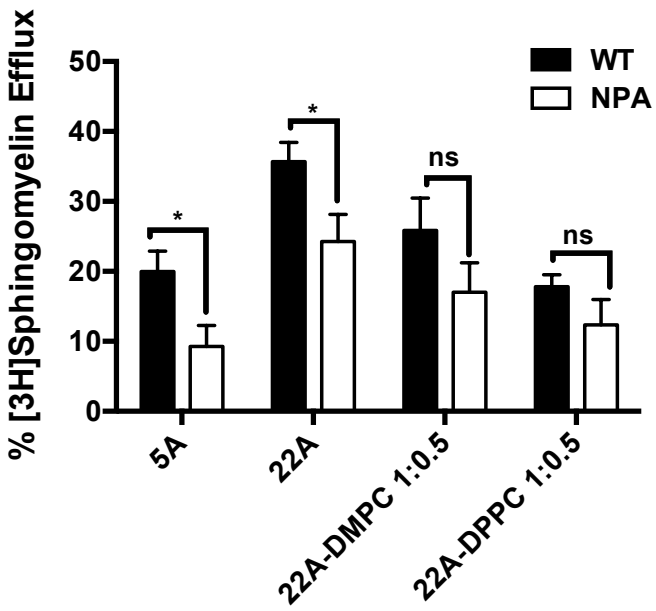

Figure 3-7 Differences in [3H]Sphingomyelin efflux between wild type (WT) and NPA cells. *WT and NPA cells were loaded with [3H]Sphingomyelin and treated with 0.75 mg/mL of 5A, 22A, 22A-DMPC (1:0.5) or 22A-DPPC (1:0.5) for 24 hr as described in Fig. 2. Data are mean ± s.e.m., N=3. Statistical differences between WT and NPA treatments in each group was calculated using Student's t-test; ns, not significant, *p≤.05.*

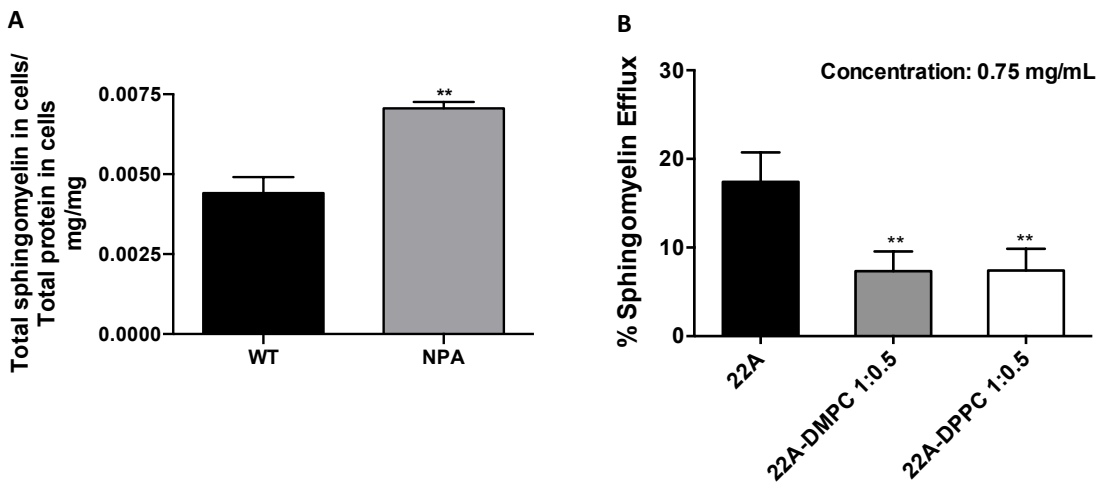

Figure 3-8 Sphingomyelin efflux from NPA cells using label-free LC-MS method.
*(a) NPA and WT cells were cultured without externally added sphingomyelin. The concentration of sphingomyelin (16:0) in WT and NPA cells was quantified using LC-MS and normalized to total protein concentration in cells. (b) NPA cells were treated with 0.75 mg/mL of 22A, 22A-DMPC (1:0.5), 22A-DPPC (1:0.5) or vehicle (media) control diluted in lipoprotein-deficient media for 24 hr. Sphingomyelin concentration in the media and cells was determined by LC-MS. Percent (%) sphingomyelin efflux was calculated by dividing the media sphingomyelin concentration by total media plus cell concentration and multiplied by 100. Non-specific (vehicle) efflux was subtracted from each treatment group. Data are mean ± s.e.m, N=3. Statistical differences between WT and NPA groups was calculated using Student's t-test (a) and between 22A versus sHDL groups (b) using one-way ANOVA; **p≤.01.*

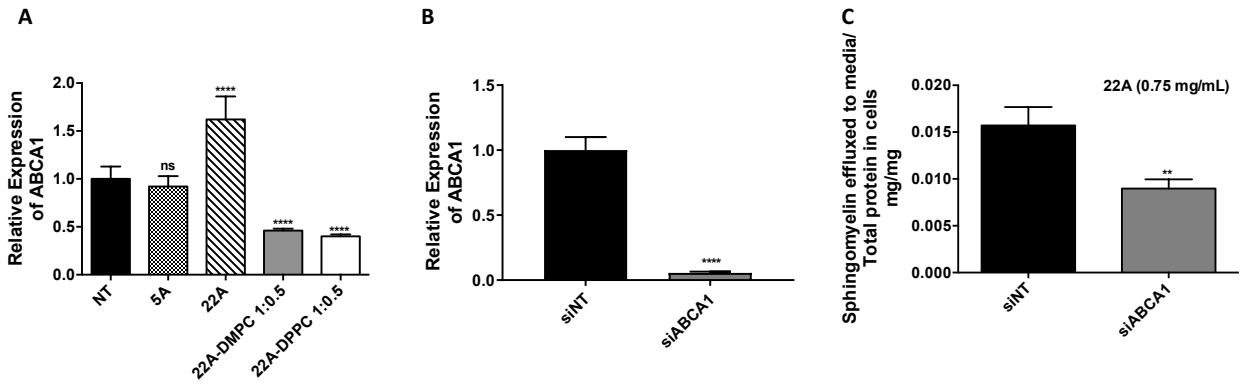

Figure 3-9 ABCA1 transporter expression in NPA cells is required for efficacy of 22A peptide. *(a) Primary NPA fibroblasts were treated with vehicle (NT), 5A, 22A, 22A-DMPC (1:0.5) or 22A-DPPC (1:0.5) at 0.75 mg/mL for 24 hr. ABCA1 mRNA expression was analyzed by qPCR. (b) NPA cells were treated for two consecutive days with the following siRNAs: non-targeting (NT) and ABCA1. ABCA1 mRNA expression was analyzed by qPCR. (c) Following siRNA knockdown, cells were treated with 0.75 mg/mL 22A for 24 hr. The concentration of sphingomyelin effluxed into media was quantified using LC-MS and normalized to total protein concentration in cells for each group. Data are mean ± s.e.m., N=3. Statistical differences between NT and other groups was calculated using one-way ANOVA (a) and Student's t-test (b, c); ns, not significant, **p≤.01, ****p≤.0001.*

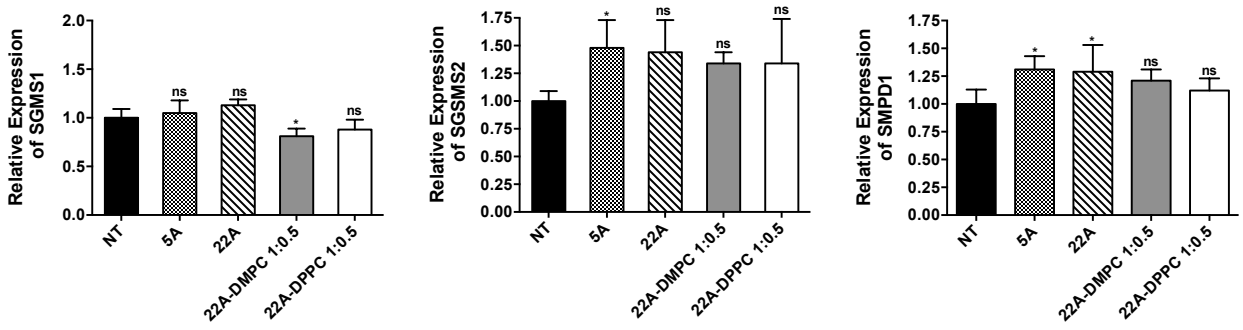

Figure 3-10 Relative expression of sphingomyelin metabolism genes SGMS1, SGMS2, and SMPD1. *Primary NPA fibroblasts were treated with vehicle (NT), 5A, 22A, 22A-DMPC (1:0.5) or 22A-DPPC (1:0.5) at 0.75 mg/mL for 24 hr. SGMS1, SGMS2, and SMPD1 mRNA expression was analyzed by qPCR. Data are mean ± s.e.m., N=3. Statistical differences between NT and other groups was calculated using one-way ANOVA; ns, not significant, *p≤.05, **p≤.01.*

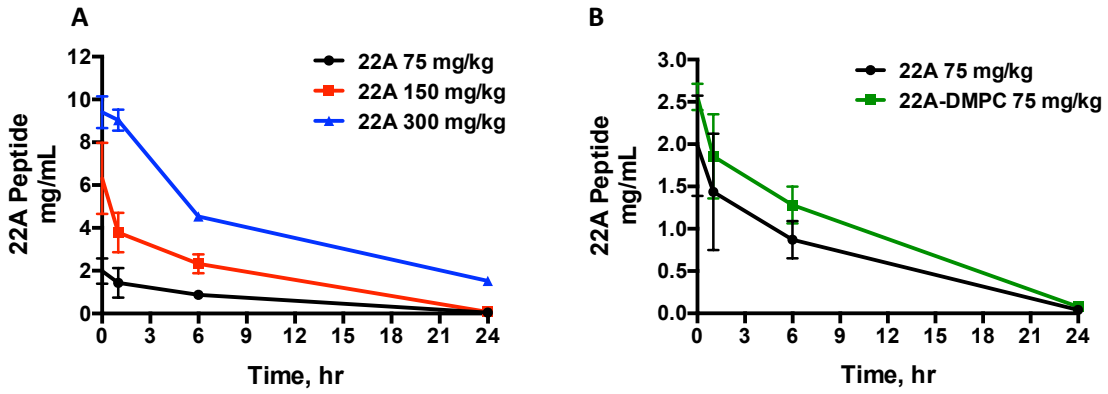

Figure 3-11 Pharmacokinetic analysis of 22A and 22A-DMPC in mouse serum. *Healthy male C57BL/6J mice were given a single tail vein injection of (a) 75, 150 or 300 mg/kg of 22A peptide or (b) 75 mg/kg (based on peptide) of 22A-DMPC at 1:1 peptide to lipid ratio by weight. Blood samples were collected at pre-dose and 1, 6, and 24 h after peptide or sHDL administration. Serum concentration of 22A was determined by LC-MS (N=3).*

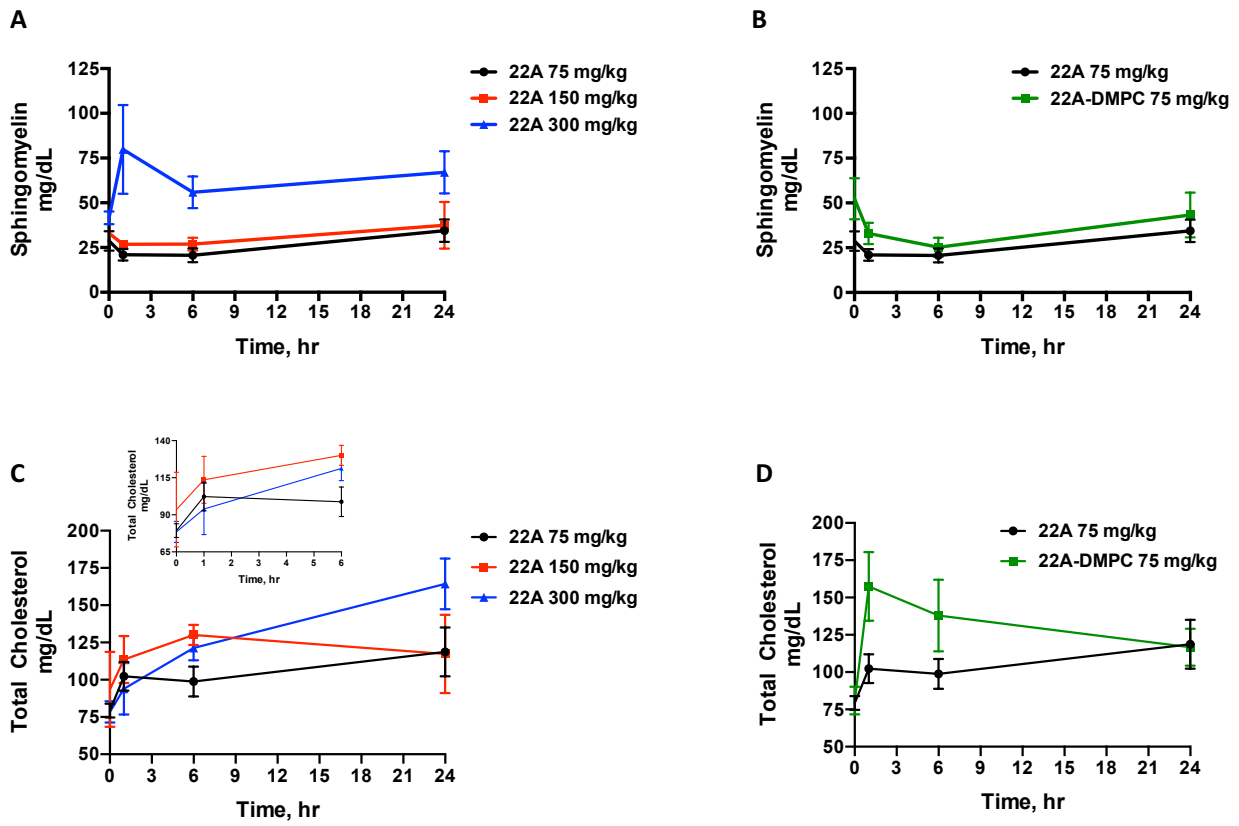

Figure 3-12 Pharmacodynamic analysis of (a, b) sphingomyelin and (c, d) cholesterol in mouse serum after 22A and 22A-DMPC administration. *Healthy male C57BL/6J mice were given a single tail vein injection of 75, 150 or 300 mg/kg of 22A peptide (a, c) or 75 mg/kg (based on peptide) of 22A-DMPC at 1:1 peptide to lipid ratio by weight (b, d). Blood samples were collected at pre-dose and 1, 6, and 24 h after peptide administration. Serum concentrations of sphingomyelin and total cholesterol concentration were measured ezymatically (N=3).*

Chapter 4: Phospholipid Component Defines Pharmacokinetic and Pharmacodynamic Properties of Synthetic High-Density Lipoproteins

4.1 Abstract

Synthetic high-density lipoprotein (sHDL) nanoparticles composed of apolipoprotein A-I (ApoA-I) mimetic peptide and phospholipids have been shown to reduce atherosclerosis in animal models. Cholesterol is mobilized from atheroma macrophages by sHDL into the blood compartment and delivered to the liver for elimination. Historically, sHDL drug discovery efforts were focused on optimizing peptide sequences for interaction with cholesterol cellular transporters rather than understanding how both sHDL components, peptide and lipid, influence its pharmacokinetics (PK) and pharmacodynamic (PD) profiles. We designed two sets of sHDL having either identical phospholipid but variable peptide sequences with different plasma stability, or identical peptide and phospholipids with variable fatty acid chain length and saturation. We found that sHDL prepared with proteolytically stable 22A-P peptide had 2-fold longer circulation half-time relative to the less stable 22A peptide. Yet, longer half-life did not translate into any improvement in cholesterol mobilization. In contrast, sHDL with variable phospholipid compositions showed significant differences in phospholipid PK, with distearoyl

phosphatidylcholine-based sHDL demonstrating the longest half-life of 6.0 h relative to 1.0 h for palmitoyl-oleoyl phosphatidylcholine-based sHDL. This increase in half-life corresponded to a ~6.5-fold increase in the area under the curve for the mobilized cholesterol. Therefore, the phospholipid component in sHDL plays a major role in cholesterol mobilization *in vivo* and should not be overlooked in the design of future sHDL.

4.2 **Introduction**

Reverse cholesterol transport (RCT) is a mechanism of cholesterol removal from the periphery to the liver for elimination. This transport starts when lipid-poor apolipoprotein A-I (ApoA-I) facilitates extracellular efflux of phospholipids and cholesterol through the transmembrane ATP-binding cassette transporter A1 (ABCA1) resulting in formation of pre-β high-density lipoprotein (HDL) particles. Then, pre-β HDLs interact with lecithin:cholesterol acyltransferase (LCAT), an enzyme responsible for cholesterol esterification, leading to formation of larger mature HDLs. Mature HDLs can either deliver esterified cholesterol (EC) cargo directly to the liver for elimination through scavenger receptor class B type I (SR-BI) or transfer EC to LDL by interaction with cholesterol ester transfer protein (CETP) for the elimination by the liver following LDL receptor-mediated uptake.

The idea of using reconstituted (rHDL) or synthetic (sHDL) HDL for the treatment of cardiovascular disease has been prominent in the past 20 years, with several therapies reaching clinical trials [19, 21, 25, 105]. While some clinical trials for rHDL products were successful [19, 21], others failed [168, 169]. A 17,400-patient Phase 3 trial (AEGIS-II) is currently ongoing for CSL-112 to show possible reduction of major adverse

cardiovascular events in subjects with acute coronary syndrome (clinicaltrials.gov, NCT03473223). The two most advanced sHDL products, CSL-112 and CER-001, both contain ApoA-I but differ in their lipid composition. CSL-112 is prepared from unsaturated soybean phosphatidylcholine while CER-001 is composed of primarily saturated sphingomyelin [168]. Recently, we have shown that the type of phospholipid used in sHDL preparation is critical for its anti-inflammatory and anti-atherosclerotic properties [101]. Several other studies had examined the effects of phospholipid composition on the ability of sHDL to efflux cholesterol and interact with LCAT *in vitro* [170-172], yet the impact of phospholipid chain length and saturation on sHDL pharmacodynamics *in vivo* has not been systematically examined.

In contrast, significant body of research had been performed to develop short peptides (2F (18A), D-4F, L-4F, 5A, 22A, and ATI-5261) as cost-efficient, safe and easily scalable alternatives to a full-length ApoA-I [26, 173-178]. These ApoA-I mimetic peptides have been optimized with the goal to improve several properties such as ABCA1 mediated cholesterol efflux, ability to activate LCAT and facilitate cholesterol esterification, enhance anti-oxidant properties, improve chemical stability and reduce hemolytic side-effects [27, 162, 173, 179]. Most ApoA-I mimetics were optimized as “naked” or lipid-free peptides *in vitro* and *in vivo* and only a few studies examined the pharmacological activity of peptide-based sHDL [159, 162].

Thus, we decided to systematically evaluate the effect of both peptide sequence and phospholipid composition of sHDL on nanoparticle’s ability to mobilize and esterify cholesterol *in vitro* and *in vivo*. For our studies, we used the first ApoA-I mimetic peptide (22A) that reached clinical trials as part of the sHDL product called ETC-642 [164, 180].

ETC-642 contained 22A ApoA-I mimetic peptide, which was optimized for its ability to bind phospholipids and activate LCAT [120, 173]. While ETC-642 successfully completed single and multiple dose trials in dyslipidemia patients, it was recently discovered by us that 22A peptide undergoes rapid hydrolysis in plasma to form the 21A peptide, which lacks the C-terminal lysine, a residue potentially important for LCAT activation [159, 175]. We hypothesized that the addition of a proline moiety after the labile lysine (22A-P) would be able to protect 22A from proteolysis and result in longer circulation time while retaining LCAT activity *in vivo*. Thus, we prepared a set of sHDL particles using 22A, 21A, and 22A-P peptides while keeping lipid composition constant.

The second set of sHDL was prepared by varying only the phospholipid component and keeping the peptide component, 22A, constant. We used phospholipids with different chain length and saturation including 1-palmitoyl-2-oleoyl-*sn*-glycero-3-phosphocholine (POPC), 1,2-dimyristoyl-*sn*-glycero-3-phosphocholine (DMPC), 1,2-dipalmitoyl-*sn*-glycero-3-phosphocholine (DPPC) or 1,2-distearoyl-*sn*-glycero-3-phosphocholine (DSPC) known for their differences in cholesterol binding affinity and LCAT interaction [119, 181, 182]. Phospholipids with longer, saturated fatty acid chains such as DPPC and DSPC have higher affinity for cholesterol binding and higher physical stability due to their high transition temperatures (T_m) of 41°C and 55°C, respectively [118, 119, 183]. In contrast, unsaturated phospholipids like POPC (T_m= -2°C) and those with shorter fatty acid chains like DMPC (T_m = 23°C) form fluid bilayers at physiological temperature facilitating LCAT-sHDL binding. The unsaturated fatty acids are superior substrates for LCAT esterification activity [181, 184]. By comparing two sets of sHDL with varying peptide and lipid components side by side, we expected to be able to elucidate the relative

contribution of both components to cholesterol efflux and engagement of LCAT *in vitro* as well as the overall pharmacokinetic and pharmacodynamic behavior of sHDL *in vivo*.

4.3 **Materials and Methods**

Materials

22A (PVLDLFRELLNELLEALKQKLK), 21A (PVLDLFRELLNELLEALKQKL), and 22AP (PVLDLFRELLNELLEALKQKLKP) were synthesized by Genscript (Piscataway, NJ), using solid-phase Fmoc (9-fluorenylmethyl carbamate) protection chemistry and purified with reverse phase chromatography (>95% pure). 5A peptide (DWLKAFYDKVAEKLKEAF-P-DWAKAAYDKAAEKAKEAA) was obtained from Bachem Americas Inc (Torrance, CA). Phospholipids including 1,2-dimyristoyl-*sn*-glycero-3-phosphocholine (DMPC), 1,2-dipalmitoyl-*sn*-glycero-3-phosphocholine (DPPC), 1,2-distearoyl-*sn*-glycero-3-phosphocholine (DSPC), and 1-palmitoyl-2-oleoyl-*sn*-glycero-3-phosphocholine (POPC) were purchased from NOF America Corporation. Ergosta-5,7,9(11), 22-tetraen-3β-ol (dehydroergosterol, DHE), cholesterol oxidase was obtained from Sigma-Aldrich (St. Louis, MO). Cholesterol (1,2-^{3}H(N)] was purchased from Perkin Elmer. Anti-human ApoA-I horseradish peroxidase-conjugated (HRP) antibody (1:1000 dilution) was purchased from Meridian Life Science (Memphis, TN). Recombinant human lecithin cholesterol acyl transferase (LCAT) was kindly provided by MedImmune (Gaithersburg, MD). All other materials were obtained from commercial sources.

Preparation and characterization of synthetic high-density lipoproteins

sHDL composed of a peptide (22A, 21A, or 22A-P) and phospholipid (DMPC, POPC, DPPC, or DSPC) were prepared by a co-lyophilization procedure [156]. Briefly,

peptide and phospholipids were dissolved in glacial acetic acid, mixed at 1:2 w/w ratio of peptide:lipid, and lyophilized overnight. The powder was hydrated with PBS pH 7.4 to make 10 mg/mL sHDL and cycled between 55°C (10 min) and room temperature (10 min) to facilitate sHDL formation. The resulting sHDL complexes were analyzed by gel permeation chromatography for purity at 1 mg/mL using a 7.8 mm x 30 cm Tosoh TSK gel G3000SWxl column (Tosoh Bioscience, King of Prussia, PA) with UV detection at 220 nm. The HDL hydrodynamic diameters were determined by dynamic light scattering (DLS) using a Zetasizer Nano ZSP, Malvern Instruments (Westborough, MA). The volume intensity average values were reported. The α-helical content of free and lipid-bound peptide was determined by Jasco J715 (Jasco, Easton, MD) circular dichroism (CD) spectropolarimeter. Samples at 0.1 mg/mL concentration in 10 mM phosphate buffer (pH 7.4) or buffer alone were loaded into a quartz cuvette (d = 0.2-cm path length), and CD spectra from 190 to 260 nm were recorded at 37°C. Buffer spectra were subtracted from each peptide or sHDL sample. Data analysis was conducted using CDPro analysis software and the percent helical content for each sample was calculated via CONTIN analysis method with the reference Soluble–Membrane Protein 56 Data Base [185].

Generation of helical wheel peptide models and calculation of lipid binding parameters

Helical wheel plots of 22A, 21A, and 22A-P peptides were created by Helixator (http://tcdb.org/progs/helical_wheel.php). This program displayed a peptide sequence looking down the axis of the alpha helix with aliphatic residues shown as blue circles. The hydrophobic momentum of 22A, 21A, and 22A-P peptides was calculated using the 3D Hydrophobic Moment Vector Calculator (http://www.ibg.kit.edu/HM/) [186]. The helix

stability (ΔG_{hel}), transfer energy from water to membrane (ΔG_{trans}), and parameters of spatial positions in membranes (tilt angle and membrane penetration depth) for each ApoA-I-mimetic peptide were calculated by the Folding of Membrane-Associated Peptide (FMAP) server [187] and the Positioning of Proteins in Membranes (PPM) server [188].

Cholesterol efflux assay in vitro

Cholesterol efflux studies were performed, as described by Remaley *et al*. [103]. Briefly, RAW 264.7, BHK-Mock and BHK stably transfected with human ABCA1 cDNA cell lines were labeled for 24 h with 1 μCi/mL of [^{3}H] cholesterol in minimum Dulbecco's modified Eagle's medium (DMEM), containing 0.2 mg/ml of fatty acid-free bovine serum albumin (BSA). Then, BHK-MOCK and BHK-ABCA1 cell lines were treated with 10 nM mifepristone for 18 h to selectively induce the expression of ABCA1 cholesterol transporter for BHK-ABCA1. ABCA1 transporter was not selectively induced in RAW 264.7 cell line. Following the radiolabeling or induction step, peptides (22A, 21A or 22A-P) or sHDL (21A-DMPC, 22A-P-DMPC, 22A-DMPC, 22A-POPC, 22A-DPPC or 22A-DSPC) were added at 0.01, 0.03 and 0.1 mg/mL concentration using DMEM-BSA media. After 18 h of incubation with cholesterol acceptors, media were collected and cells were lysed in 0.5 ml of 0.1% SDS and 0.1 N NaOH for 2 h. Radioactive counts in media and cell fractions were measured by liquid scintillation counting (Tri-Carb 2910 TR, PerkinElmer), and percent cholesterol efflux was calculated by dividing media counts by the sum of media and cell counts.

Phospholipid lipolysis by LCAT

The rate of phospholipid (POPC, DMPC, DPPC or DSPC) lipolysis was evaluated by incubating 15 μg/mL of rhLCAT with 0.1 mg/mL of sHDL (based on total lipid concentration) in 0.1 M sodium phosphate buffer pH 7.4 for 0, 5, 15, 30, 60, 90, and 120 min. The LCAT-sHDL reaction aliquots were collected into methanol (1:5 v/v) and vortexed to stop the lipolysis reaction at each time point. The amount of POPC, DMPC, DPPC or DSPC remaining at each time point was measured by Waters UPLC-MS equipped with QDa Mass Detector (Milford, MA). Chromatographic separation was achieved on Acquity BEH300 1.7 μm HILIC 2.1 x 50 mm column with gradient elution at 0.65 mL/min: mobile phase A (H_2O/0.1% formic acid), mobile phase B (acetonitrile/0.1% formic acid) and mobile phase C (100 mM ammonium formate) as follows: 0-0.7 min (5-17% A, 90-78% B, and 5-5% C), 0.7-0.71 min (17-5% A, 78-90% B, and 5-5% C), and 0.71-3 min (17-5% A, 78-90% B, and 5-5% C). Mass spectra were acquired in the positive ion mode with the mass range set at m/z 150-1250 and POPC was detected at 760.7 amu, DMPC at 678.7 amu, DPPC at 734.7 amu, and DSPC at 790.7 amu. Data analysis was performed with Waters Empower software. The plot of POPC, DMPC, DPPC or DSPC area under the curve over time was generated for each sHDL sample. The rate of LCAT lipolysis (k) was calculated from the linear slope of the log10 (concentration) versus time.

Cholesterol esterification by LCAT assay

Two different sets of sHDL containing dehydroergosterol (DHE) was prepared via the thin-film method**.** Briefly, the first set was made from POPC, DPPC and DHE combined at a 4.5:4.5:1 molar ratio in chloroform and then mixed with peptide (22A, 21A

or 22A-P) at 2:1 lipid:peptide weight ratio in methanol/water (4:3 v/v). The second set was prepared from POPC, DMPC, DPPC or DSPC and DHE at a 9:1 molar ratio then mixed with 22A peptide at 2:1 lipid:peptide weight ratio in methanol/water (4:3 v/v). The solvent was removed under nitrogen flow at room temperature and then in a vacuum oven overnight. The lipid film was hydrated with 20 mM phosphate buffer containing 1mM EDTA (pH 7.4) followed by 5 min water bath sonication at room temperature and probe sonication (2 min × 50 w) to obtain clear DHE-sHDL. The final DHE concentration in peptide-DHE-sHDL was 0.5 mM. The LCAT assay was adapted from Homan *et al.* [189] and performed in 384-well black polystyrene plates in triplicate. Briefly, 8 µL of different concentrations (0, 5, 10, 20, 40, 60, and 100 µM) of DHE-sHDL (substrates) in assay buffer (PBS containing 1 mM EDTA, 5 mM β-mercaptoethanol, and 60 µM albumin, pH 7.4) preheated to 37°C were incubated with 8 µL of 5 µg/mL LCAT in dilution buffer (PBS with 1 mM EDTA and 60 µM albumin, pH 7.4) preheated to 37°C in triplicates. The plates were incubated at 37°C with gentle shaking (80 rpm/min) for different lengths of time (0, 10, and 20 min). Reactions were stopped by adding 4 µL of stop solution (3.75 U/mL cholesterol oxidase) in PBS containing 1mM EDTA and 7% Triton X-100. Then, the plates were incubated at 37°C with shaking (80 rpm/min) for another 1 h to quench the fluorescence of unesterified DHE. The fluorescence was measured at an excitation wavelength of 325 nm and an emission wavelength of 425 nm using the plate-reader (SynergyTM NEO HTS Multi-Mode Microplate Reader, Bio-Tek). A standard curve was made by plotting the fluorescence of serially diluted DHE-containing sHDL mixed with LCAT and using stop solution without COx versus the concentration (µM) of DHE. To calculate the concentration (µM) of DHE ester for each reaction, the background

fluorescence (0 μM of DHE) was subtracted from all fluorescence measurements and then divided by the slope (fluorescence/μM) of the above standard curve. To calculate V_{max} and K_m, the concentrations (μM) of DHE ester at different time points were plotted against time (h), and the initial velocity (V_0, μM DHE-ester/h) was the slope of the linear range of DHE-ester concentration versus time. The V_{max} and K_m were obtained by plotting V_0 versus DHE concentration and then analyzed by GraphPad Prism 7 (nonlinear regression, Michaelis-Menten model).

Plasma peptide stability

The *in vitro* stability of 22A, 21A, and 22A-P peptides was assessed by the addition of 2.5 μL of 10 mg/mL of a peptide to 97.5 μL of fresh rat plasma (K2 EDTA, Innovative Research Inc). Immediately after the addition of peptide to plasma, 10 μL of serum was removed to serve as a baseline and stored at -20 °C. Samples were incubated at 37°C for 24 hours with shaking at 240 rpm. To determine peptide concentration at 0 and 24 h post plasma incubation, 10 μL of plasma containing a peptide or working standard (0-100 μg/mL) was mixed with 2 μL of 2.4 mg/mL internal standard (5A peptide) and 38 μL of H_2O. Methanol (200 μL) was added to precipitate plasma proteins. The mixture was vortexed for 10 s, centrifuged at 12,000 rpm for 10 min and the supernatant was collected for LC-MS analysis. Samples were mixed (1:1 v/v) with LC-MS mobile phase (80:20 v/v H_2O:acetonitrile, 0.1% formic acid) and analyzed on Waters Acquity UPLC equipped with QDa System (Milford, MA) using Acquity UPLC BEH C18 1.7 μM column for separation. The mobile phase consisted of (A) water containing 0.1% v/v formic acid and (B) methanol containing 0.1% v/v formic acid. The mobile phase was delivered at 0.3 mL/min using a

gradient elution of 20% to 80% B during 0-1.5 min, and 80% to 20% B during 1.5-3.5 min. Mass spectra were acquired in the positive ion mode with the mass range set at m/z 150-1250. Data analysis was performed on Waters Empower software. The concentration of 22A, 21A or 22A-P peptide in each sample was determined from the standard curve.

Peptide pharmacokinetics, cholesterol mobilization, and esterification in vivo

Healthy male Sprague-Dawley rats (8 weeks old) were purchased from Charles River Breeding Laboratories (Portage, MI) and were fed a standard rodent chow diet. To examine the impact of peptide composition on sHDL PK/PD properties, animals were randomly assigned to two groups (n = 4/group) for 22A-POPC/DPPC and 22A-P-POPC/DPPC administration. To examine the impact of lipid composition on sHDL PK/PD, animals were randomly assigned to four groups (n = 3/group) for 22A-POPC, 22A-DMPC, 22A-DPPC, and 22A-DSPC administration. All sHDL particle was prepared at 1:2 w/w peptide to phospholipid ratios, sterile filtered and characterized by DLS and gel permeation chromatography for size and purity prior to animal dosing. All animals were fasted overnight before sHDL dosing at 50 mg/kg (based on peptide concentration) via tail vein injection. At each time point (pre-dose, 0.25, 0.5, 1, 2, 4, 8, and 24 h) blood samples (~0.3 mL) were collected from the jugular vein to heparinized BD tubes (Franklin Lakes, NJ) and centrifuged at 10,000 rpm for 10 min at 4°C. The obtained serum samples were stored at -20°C for further analysis.

The levels of plasma phospholipids (PL), total cholesterol (TC) and free cholesterol (FC) were determined enzymatically (Wako Chemicals, Richmond, VA) using a plate reader (SynergyTM NEO HTS Multi-Mode Microplate Reader, Bio-Tek). Esterified

cholesterol levels (EC) were calculated as the difference between TC and FC levels at each time point. Briefly, serum samples were diluted with PBS for TC and FC detection, or with MilliQ water for PL detection. Defined amounts of standards or diluted samples were transferred to 96-well plates (50 µL, 60 µL and 20 µL for TC, FC and PL analyses, respectively), and assay reagents were added per manufacturer's instructions. The plates were gently shaken using an orbital shaker and incubated at 37˚C for 5 minutes. The UV absorbance at 600 nm was measured by a Molecular Devices SpectraMax M3 plate reader (Sunnyvale, CA). Pharmacokinetic parameters were also obtained by non-compartmental analysis. The pharmacodynamic effect in each rat was determined as the area under the total effect curve (*AUEC*) using trapezoidal rule. Secondary pharmacodynamic endpoints, maximal effect (E_{max}) and time to E_{max} ($T_{max,E}$) were also analyzed to compare pharmacodynamic effects.

Peptide (22A or 22A-P) concentration in serum was determined by LC-MS. The 10 µL serum aliquots were combined with 10 µL of 2.4 mg/mL of internal standard (5A peptide) and then mixed with 40 µL ddH_2O. Working standard solutions (0-100 µg/mL) of 22A and 22A-P were prepared as described above for plasma samples with the exception of using blank rat serum. Plasma proteins were precipitated by adding 180 µL of methanol. After 5 minutes, the mixture was centrifuged (12000 rpm × 10 min, 4°C) and 100 µL of the supernatant was used for analysis. Each sample was analyzed by LC-MS as described above in the plasma peptide stability section. Pharmacokinetic parameters such as maximum serum concentration (C_{max}), the area under the serum concentration-time curve (*AUC*), elimination rate constant (*K*), elimination half-life ($T_{1/2}$), total clearance (*CL*), and volume of distribution (V_d) were obtained by non-compartmental analysis.

Remodeling of endogenous lipoproteins by sHDL in human plasma

Remodeling of endogenous lipoproteins in human plasma by sHDL was assessed by one-dimensional native polyacrylamide gel electrophoresis (1-D native PAGE) following sHDL incubation in plasma. Various sHDL (22A-POPC, 22A-DMPC, 22A-DPPC, 22A-DSPC, 21A-sHDL, 22A-sHDL, and 22A-P-sHDL) at 1 mg/mL concentration were incubated at 37°C for 1 h with shaking at 300 rpm. The sub-classes of HDL were separated by size using 1-D native PAGE and visualized by Western Blot using the anti-ApoA-I antibody. Briefly, samples were subjected to electrophoresis using Tris-borate-EDTA (TBE) gradient (4 – 20%) acrylamide mini-gels. For each well, 10 µL of human plasma incubated with or without sHDL was mixed with 10 µL of 2X TBE sample buffer, and 6 µL of the resulting mixtures were loaded per well. Gels were run at 200V. Proteins were transferred to polyvinylidene difluoride membrane (PVDF) and incubated overnight with the anti-human ApoA-I-HRP conjugated antibody. Proteins were visualized with the enhanced chemiluminescent substrate on Protein Simple FluorChem M imaging system (San Jose, CA).

Statistical analysis

Significance of difference was determined by Student's *t*-test for comparing two groups or by one-way analysis of variance (ANOVA) with Dunnett's post-hoc test for comparing multiple groups with 22A peptide or 22A-DMPC as the control. All samples were performed in triplicate and error bars were reported as a standard mean error (SEM) unless noted otherwise. $P < 0.05$ was considered statistically significant.

4.4 **Results**

Design of ApoA-I peptides with improved plasma stability

Helical wheel plots for 22A, 22A-P, and 21A were generated to assess the amphipathic nature of each peptide. The hydrophobic amino acids clustered on one side of the helix suggested an amphipathic orientation of each peptide (Table 3-1). The 3D hydrophobic moment vector calculations were performed to predict and compare the interactions of each peptide with lipid membranes. It was determined that the hydrophobic moment vectors were almost identical with an average of 10.3 ± 0.7 A*kT/e. Additionally, we used an online server to determine the helix stability (ΔG_{hel}), transfer energy from water to membrane (ΔG_{trans}), and orientation of each peptide in the membrane (penetration depth, D). Again, we did not find large differences in any of the aforementioned parameters, suggesting that the absence of the terminal lysine in 21A or the addition of proline in 22A-P did not change the physical properties of these peptides compared to 22A. Next, we compared the plasma stability of 22A, 22A-P, and 21A as well as their abilities to bind lipid and form sHDL particles. We found that while 22A degrades in plasma with only 48% of intact peptide remaining after 24 h incubation at 37°C, both 22A-P and 21A are significantly more stable with 89 and 97% of intact peptide remaining, respectively. These results suggest that the plasma stability of 22A peptide can be greatly improved by the addition of a bulky proline, while computed lipid binding properties remained relatively unchanged.

Preparation and characterization of sHDL particles

We next evaluated the ability of 21A, 22A, and 22A-P peptide to form homogeneous sHDL particles. Synthetic HDL particles were prepared by combining 22A, 21A or 22A-P peptide with DMPC at 1:2 w/w peptide:lipid ratio, which was previously used in ETC-642 formulation resulting in the formation of homogeneous sHDL particles with approximately 10 nm size (Li *et al.*, 2015; Tang *et al.*, 2017). All three peptides formed homogeneous sHDL particles with average diameters of approximately 10 nm and a narrow polydispersity index of 0.17 ± 0.04 as determined by DLS (Figure 3-1a). Purity and homogeneity of sHDL size distribution were evaluated by gel permeation chromatography (Figure 3-1b). All three sHDL were over 98% pure, and negligible levels of the free peptide (<2%) were observed at the retention time of ~11 min (Table 3-2). The binding of a peptide to phospholipid was also confirmed by increased helicity of 22A, 21A and 22A-P in sHDL particles (94, 91 and 82%) relative to the free peptide (77, 79 and 77%) as measured by CD.

We also altered the phospholipid composition of 22A sHDL to study its impact *in vitro* and *in vivo*. We chose four lipids with different physical properties such as transition temperature (T_m) and affinity for cholesterol (DSPC>DPPC>DMPC>POPC) (Small, 1986; Ramstedt and Slotte, 1999; Ohvo-Rekilä *et al.*, 2002). The sHDL complexes were formed by combining 22A peptide with individual lipids at 1:2 w/w ratio using the co-lyophilization method. All were highly homogeneous with an average hydrodynamic diameter ranging between 8.3 to 10.5 nm, low polydispersity index and gel permeation chromatography purity greater than 95% (Figure 3-1c, 3-1d). The purity, size, and polydispersity levels of sHDL are summarized in Supplemental Table 1. The DMPC, DPPC and DSPC-based sHDL had smaller hydrodynamic diameters, higher GPC purities, and sharper GPC peaks

relative to 22A-POPC. The presence of free peptide (<1%, retention time ~11.3 min) and liposome impurities (<2%, retention time ~5.5 min) were observed for 22A-POPC, which also had the largest average particle size and broadest size distribution. Because POPC has the lowest T_m of -2 °C, it exists in a fluid gel state at room temperature, which likely impacts 22A-POPC stability.

Lipid composition of sHDL impacts macrophage cholesterol efflux

We next examined how the C-terminal modifications in 22A-P and 21A impact cholesterol efflux abilities relative to 22A, either as free peptides or reconstituted into sHDL. Radioactive cholesterol was loaded into BHK cell line stably transfected with human ABCA1 transporter and peptides were incubated with the cells at 0, 0.01, 0.03, and 0.1 mg/mL. The same experiment was repeated using the control BHK-Mock cell line to assess cholesterol efflux by passive diffusion. Then, the non-specific cholesterol efflux values were subtracted from the data obtained for each peptide with ABCA1 transfected cells to reveal receptor specific cholesterol efflux (Figure 3-2a). All three peptides exhibited concentration-depended cholesterol efflux with only minor differences (< 5%) observed, indicating that modifications at the C terminal end of 22A did not affect lipid binding and ABCA1 transporter interaction. Then, the three peptide sequences were assembled into sHDL and their abilities to efflux cholesterol from macrophages were examined in RAW 264.7 cell line (Figure 3-2b). Similar to free peptide, we observed concentration-dependent cholesterol efflux with only minor differences (< 5%) at concentrations tested.

To explore the impact of the phospholipid component of sHDL on macrophage cholesterol efflux, 22A-POPC, 22A-DMPC, 22A-DPPC, and 22-DSPC were incubated with RAW 264.7 cells. Saturated long chain length phospholipids such as DPPC and DSPC have higher physical binding affinity to cholesterol relative to POPC and DMPC (Ramstedt and Slotte, 1999; Ohvo-Rekilä *et al.*, 2002). However, the transition temperature of POPC and DMPC is below 37°C, thus the phospholipid bilayer is in liquid crystal state at physiological temperature facilitating cholesterol partitioning in these sHDL particles at the cell culture conditions (Davidson *et al.*, 1995). As expected, we observed greater cholesterol efflux to POPC and DMPC-based sHDL relative to DPPC and DSPC-based sHDL likely due to differences in lipid fluidity at 37°C (Figure 3-2c). Whereas 22A-DPPC and 22A-DSPC did not have any significant differences in cholesterol efflux as concentration increased, 22A-POPC and 22A-DMPC show sHDL concentration-dependent increase in cholesterol efflux. Interestingly, 22A-DMPC showed the most effective cholesterol efflux capability from as low as 36% at 0.01 mg/mL to as high as 61.8% at 0.1 mg/mL concentration. Membrane transporters such as ABCG1/G4 and SR-BI are known to play a major role in cholesterol efflux to HDL rather than lipid-free protein and may contribute to the differences seen between sHDL in our study [190, 191]. Taken together, the phospholipid composition of sHDL appears to play a significant role in cholesterol efflux from macrophages in cell culture.

Peptide and lipid composition both impact sHDL interaction with LCAT

Following cholesterol efflux from macrophages, sHDL particles interact in plasma with LCAT [192]. It is expected that both lipid and peptide composition of sHDL will have

an effect on LCAT interaction. The fluidity of HDL lipid membrane determines the ease of LCAT binding to HDL particles [193]. It has been shown that LCAT interaction with ApoA-I is critical for LCAT activation, especially for the facilitation of acyltransferase activity [194]. Whereas some ApoA-I mimetic peptides have similar LCAT activation ability to full-length ApoA-I, others fail to facilitate EC formation [173, 195, 196]. The presence of positively charged clusters on the C-terminus and presence of hydrophobic amino acids at positions 3, 6, 9 and 10, and net peptide charge of zero are believed to be critical to the high LCAT activation ability of 22A [164, 173]. To examine how modification of 22A and lipid composition of sHDL impact phospholipase A2 activity of LCAT, sHDL were co-incubated with enzyme and the kinetics of reduction of phospholipid concentration was monitored by LC-MS. We found that small changes in 22A sequence had only limited impact on phospholipase A2 activity (lipolysis) activity (Figure 3-3a), indicating that LCAT activation by a C-terminal positive cluster on the peptide might not be critical for lipase activity. In contrast, the sHDL lipid composition had profound effect on LCAT-catalyzed phospholipid lipolysis (Figure 3-3b) with the rates of 0.08, 0.08, 0.01, and 0.0 h^{-1} for 22A-POPC, 22A-DMPC, 2A-DPPC and 22A-DSPC, respectively. DSPC and DPPC, phospholipids with T_m values above 37°C, had minimal lipolysis likely due to poor LCAT binding to sHDL and, thus, presumably difficulty in the accessibility of substrate for the enzymatic reaction.

Next, we assessed the impact of peptide and lipid composition of sHDL on LCAT acyltransferase activity by incorporating a fluorescent cholesterol analog called dehydroergosterol and measuring the rate of sterol esterification by LCAT. Changes in C-terminus of 22A peptide had a significant effect on the acyltransferase activity with a 2.6-

fold decrease in k_{cat} upon the loss of lysine for 21A (Figure 3-3c). The rate was only decreased by 30% for 22A-P-HDL. When 22A-sHDL was complexed with different compositions of phospholipids, acyltransferase activity of LCAT was the highest for 22A-POPC sHDL (Figure 3-3d). Sterol esterification was only limited for 22A-DMPC sHDL, while no activity was detected for 22A-DPPC and 22A-DSPC. This trend was similar to the differences in phospholipase A2 activity observed for sHDL prepared with different lipids (POPC ≥ DMPC > DPPC > DSPC), following their general trends in T_m and membrane fluidity. The Michaelis-Menten parameter estimates for the LCAT assay and goodness of fit are provided in Table 3-3. The assay has significant run-to-run variability, however, the samples analyzed within a single experiment (either in Figure 3-3c or 3-3d) can be compared between each other.

Increase in peptide plasma half-life has no impact on cholesterol mobilization in vivo

To evaluate whether *in vitro* peptide stability data correlates with *in vivo* peptide pharmacokinetics and cholesterol mobilization, we injected healthy Sprague Dawley rats with 22A-POPC-DPPC or 22A-P-POPC-DPPC sHDL at 50 mg/kg based on peptide concentration in sHDL. Animal blood samples were collected before sHDL administration and at 0.25, 0.5, 1, 2, 4, 8, and 24 h post-dose. The peptide concentrations in rat serum were determined using LC-MS (Figure 3-4a). The noted stability of 22A-P when incubated with rat plasma translated well to *in vivo* settings with an increase in peptide circulation half-life and exposure ($T_{1/2}$ = 4.2 h and *AUC* = 17.2 mg*h/dL) compared to 22A ($T_{1/2}$ = 2.1 h and *AUC* = 5.5 mg*h/dL) (Table 3-4). We expected that these significant PK differences between two peptides would translate into increased cholesterol mobilization by sHDL *in*

vivo. Additionally, we anticipated that levels of esterified cholesterol would be different between two formulations *in vivo* based on clear differences in LCAT-catalyzed esterification between 22A-sHDL and 22A-P-sHDL *in vitro*. However, we saw no differences in cholesterol mobilization and esterification profiles between 22A-sHDL and 22A-P-sHDL *in vivo* as quantified by enzymatic assay of rat serum samples (Figure 3-4c, 3-4d, Table 3-4). Finally, if sHDL particle stayed intact upon *in vivo* administration, we would expect to see longer circulation half-life for total phospholipids with 22A-P-sHDL relative to 22A-sHDL. To test this hypothesis, we determined phospholipid concentrations in plasma pre- and post-sHDL administration by an enzymatic assay. We observed no differences in phospholipid PK parameters between 22A-sHDL and 22A-P-sHDL except for $T_{1/2}$ in which 22A-P-sHDL (1.3 h) showed significantly decreased $T_{1/2}$ compared to 22A-sHDL (1.8 h) (Figure 3-4b, Table 3-4). Altogether, these results suggest that the apparent differences in 22A-P and 22A stabilities in plasma and LCAT activation abilities had not resulted in measurable differences in cholesterol mobilization and esterification *in vivo*.

Lipid composition of sHDL impacts cholesterol mobilization in vivo

To investigate the contribution of phospholipid composition of sHDL on cholesterol mobilization and esterification profiles *in vivo*, we administered 22A-POPC, 22A-DMPC, 22A-DPPC, and 22A-DSPC sHDL to healthy Sprague Dawley rats. Based on cholesterol efflux from RAW 264.7 cells and LCAT-catalyzed esterification results *in vitro* we were expecting to see higher cholesterol mobilization and esterification for POPC and DMPC-based sHDL *in vivo*. However, the results of *in vivo* administration of 50 mg/kg of sHDL

were reversed with 22A-DSPC showed significantly higher free cholesterol mobilization to the plasma compartment represented by the area under the effect curve (*AUEC*) $AUEC_{22A\text{-}DSPC}$ = 540 mg*h/dL compared to three other sHDL formulations with lower $AUEC_{22A\text{-}POPC}$ = 80 mg*h/dL, $AUEC_{22A\text{-}DMPC}$ = 130 mg*h/dL, and $AUEC_{22A\text{-}DPPC}$ = 220 mg*h/dL (Figure 3-5, Table 3-5). Although the C_{max} of plasma EC was higher for DMPC-based sHDL, DSPC-based sHDL administration resulted in higher EC concentration at later time points and 3.5-fold greater *AUEC* values relative to DMPC-based sHDL (Figure 3-5d, Table 3-5). The differences between *in vitro* and *in vivo* results could be attributed to differences in lipid T_m affecting the *in vivo* circulation time. Our *in vivo* data supports this hypothesis where phospholipids with higher transition temperatures such as DSPC (T_m = 55°C) showed greater half-life and slower clearance than other phospholipids (Figure 3-5b). Interestingly, the 22A peptide kinetics such as plasma half-life after administration of sHDL in rats did not follow phospholipid kinetics similar to the differences in PK parameters between lipid and peptide obtained with 22A- and 22A-P-sHDL. The half-life of 22A after 22A-DSPC infusion was nearly identical to 22A-DMPC, 22A-POPC, and 22A-DPPC formulations (3.3 h, 3.0 h, 3.3 h, and 3.3 h, respectively) (Table 3-5). Taken together, these results suggest that the ability of sHDL to mobilize cholesterol is strongly dependent on phospholipid composition and pharmacokinetics.

Remodeling of endogenous HDL in human plasma

To assess how different compositions of sHDL facilitate the remodeling of endogenous lipoproteins, all sHDL particles were incubated with human plasma for 1 hour at 1 mg/mL peptide concentration. The HDL sub-fractions were separated by size using

1D native PAGE electrophoresis and visualized by Western Blot using anti-ApoA-I antibody (Figure 3-6). We have confirmed that anti-ApoA-I antibody does not recognize 22A, 21A or 22A-P, thus, we examined the impact of sHDL incubation on the remodeling of endogenous ApoA-I containing proteins. Compared to human plasma control incubated with PBS, incubation of plasma with 22A-sHDL, 21A-sHDL, and 22A-P-sHDL resulted in the remodeling of endogenous HDL indicated by a diminished signal for the large α-HDL and increased levels of lipid-poor ApoA-I. The effect of the phospholipid composition of sHDL on endogenous HDL remodeling was more prominent. Incubation of plasma with 22A-POPC resulted in a shift of HDL size from large α-HDL to smaller pre-β HDL. Incubation with 22A-DMPC showed the formation of even smaller pre-β HDL particles with a band of lipid-free ApoA-I. In contrast, plasma incubation with 22A-DSPC displayed very limited HDL remodeling, likely due to the rigidity of the DSPC lipid membrane and thus reduced the insertion of endogenous ApoA-I. The 22A-DPPC incubation with plasma resulted in some reduction of α-HDL levels and formation of a predominant band of lipid-free ApoA-I. Overall, the extent of HDL remodeling was significantly affected by the phospholipid composition of sHDL. The sHDL prepared with high T_m phospholipids (22A-DPPC and 22A-DSPC) exhibited higher plasma stability and less remodeling.

4.5 **Discussion**

Our previous studies have shown that upon intravenous administration of sHDL, 22A peptide becomes rapidly hydrolyzed into 21A due to loss of terminal lysine [159]. The addition of C-terminal proline after the labile lysine in 22A afforded a resistant to proteolysis peptide as shown by incubation of 22A-P with rat plasma. The new peptide

was successfully formulated into sHDL and dosed into rats. We expected to see longer circulation time and corresponding greater *in vivo* cholesterol mobilization for 22A-P-sHDL. As predicted *in vitro*, the half-life of 22A-P in animals was extended from 2.1 to 4.2 hours and AUC for 22A-P is nearly 3-fold higher. However, the longer circulation time of 22A-P *in vivo* did not translate into a higher cholesterol mobilization profile by 22A-P-sHDL compared to 22A-sHDL. Furthermore, the AUC of the phospholipid component of 22A-P-sHDL and 22A-sHDL were also not affected by the extension of the peptide half-life. When sHDL particles prepared with the same peptide 22A and different phospholipids (POPC, DMPC, DPPC, or DSPC) were administered to rats the peptide half-life was similar for all four formulations (3.2 $\pm$ 0.1 h). However, the phospholipid half-life varied dramatically with DSPC circulating for 6.0 h compared to 1.0 - 3.3 h for other lipids. The trend of phospholipid circulation time for each sHDL formulation in animal serum was similar to that of cholesterol mobilization (22A-DSPC> 22A-DPPC, 22A-DMPC> 22A-POPC). Moreover, these findings are further supported by our HDL remodeling results, showing only limited interaction of 22A-DSPC with endogenous HDL, which could extend circulation half-life. The limited interaction between sHDL and endogenous lipoproteins is likely due to the difficulty of protein insertion in the gel membrane of DSPC (T_m of 55 °C, above physiological temperature) as was observed *in vitro* for 22A-DSPC interaction with LCAT. Altogether, the data suggest that the pharmacokinetics of peptide and lipid components in sHDL are not interdependent and original infused sHDL particles may dissociate or become remodeled upon administration *in vivo*. In addition, the phospholipid rather than peptide component in sHDL has a major impact on the ability to mobilize cholesterol *in vivo*. However, it is important to note that the peptide sequence

modifications performed by us were rather minor. It has been shown that different sequences of ApoA-I mimetic peptides have measurable differences in cholesterol efflux *in vitro* and variable *in vivo* performance [162, 176, 177, 179].

Several other groups reported on the discordance between the PK of protein and phospholipid components of HDL *in vivo*. Xu *et al.* investigated the fate of ApoA-I protein and phospholipid after *in vivo* administration of HDL in an attempt to interrogate the validity of the reverse cholesterol transport pathway [197] (Xu *et al.*, 2017). The investigators used ABCA1-derived ApoA-I-HDL with radiolabeled components and reported that phospholipids and ApoA-I enter different pathways for clearance in mice. The authors suggested that after the administration of radiolabeled ApoA-I-HDL, phospholipids were rapidly cleared by the liver and also transferred to LDL while ApoA-I fused with endogenous HDL and circulated longer. CSL-112, the ApoA-I-soybean phosphatidylcholine sHDL product undergoing phase III clinical trial, is believed to undergo remodeling in human plasma with the generation of lipid-poor ApoA-I that is important for cholesterol efflux [198]. Another sHDL product in clinical development, CER-001, composed from ApoA-I and primarily sphingomyelin, have shown differences, specifically longer half-life for phospholipid (~46 h) relatively to ApoA-I (~10 h) [22, 158]. We also found that incorporation of polyethylene glycol-modified lipids in ApoA-I peptide-based sHDL extended circulation time for lipids and prolonged the duration of mobilized cholesterol circulation but had not altered ApoA-I peptide PK [199]. Therefore, peptide and lipid components of sHDL may both contribute to cholesterol mobilization, however not as intact nanoparticles, but rather as separate entities via different mechanisms.

The phospholipid composition also impacted the ease of sHDL preparation, purity, and size of the resulting nanoparticles and their stability *in vitro* and *in vivo*. The sHDL prepared with DSPC, DPPC, and DMPC showed relatively similar narrow size distributions and high purities while sHDL prepared with POPC appeared to be more heterogeneous with larger average particle sizes and a presence of liposomal impurities. This relative difficulty of forming pure POPC-based sHDL particles has been reported previously and was attributed to the fluidity and instability of the POPC membrane at room temperature, which was well above the phospholipid's T_m [165]. The sHDL prepared with saturated lipids appeared to be more homogeneous and pure but required heating particles above lipid T_m during preparation to facilitate ApoA-I peptide-lipid binding. In addition, the presence of unsaturated double bonds in lipids such as POPC could result in phospholipid oxidation, although this phenomenon was not investigated in this study.

Interestingly, we also observed a discordance between *in vitro* and *in vivo* results for sHDL prepared with different phospholipids and peptides. The *in vitro* trends for higher cholesterol efflux and superior ability to activate LCAT for 22A-POPC and 22A-DMPC did not translate into higher cholesterol mobilization and esterification *in vivo*. The free cholesterol mobilization and circulation time appear to be closely following the circulation time of phospholipids, with the longer circulating saturated DSPC exhibiting higher C_{max} for FC mobilization and *AUEC*. Thus, the ease of cholesterol incorporation in unsaturated 22A-POPC becomes of limited significance *in vivo* due to rapid elimination of POPC. The esterification seems to follow the same trend, as faster LCAT-catalyzed lipolysis and sterol esterification did not translate to greater C_{max} and *AUEC* for EC *in vivo*. However, it is important to point out that the actual rate of EC formation and LCAT activation *in vivo*

was not directly measured in this study and will require additional experiments as described by Turner *et a*l. (Turner *et al.*, 2012). The stability of 22A-P is greatly improved *in vivo* relative to 22A, however phospholipid PK appeared to be unchanged and cholesterol mobilization follows phospholipid PK. One of the explanations for this may be that both 22A and 22A-P are capable of forming sHDL *in vitro* and maintaining sHDL stability *in vivo*, as the structures of all three peptides used by us are very similar. It is also important to point out that other groups had seen discordance between showing some structure-activity relationship for ApoA-I peptides *in vitro* and seeing no statistical differences in their pharmacological effects *in vivo* [200].

Table 3-1 *Biophysical characterization of peptides. [a]Helical wheel plots were generated using the online tool called Helixator where hydrophobic amino acids were highlighted in blue. [b]Hydrophobic moments were calculated by the 3D Hydrophobic Moment Vector Calculator. [c]Helix stability (ΔG_{hel}), transfer energy from water to membrane (ΔG_{tran}), and tilt angle in membranes were predicted by FMAP server for 22A, 21A, and 22A-P peptide sequences; [d]Helical content of lipid-free and lipid-bound peptides was determined by circular dichroism; [e]Peptide stability in rat plasma was determined by LC-MS shown as percent remaining peptide following 24 h incubation at 37°C (n=3, mean ± standard deviation).*

Peptide name	**22A**	**21A**	**22A-P**
Sequence	PVLDLFRELLNELLEALK QKLK	PVLDLFRELLNELLEAL KQKL	PVLDLFRELLNELLEAL KQKLKP
Helical wheel plot[a]	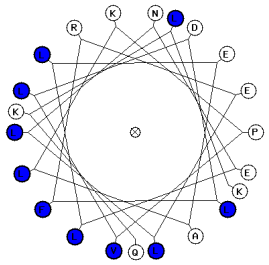	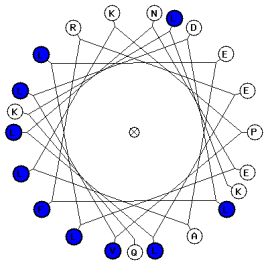	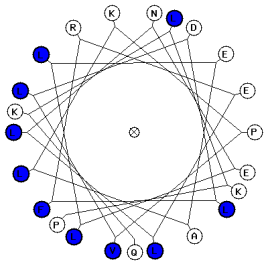
Hydrophobic moment vector (A*kT/e)[b]	11.1	10.0	9.9
ΔG_{hel} (kcal/mol)[c]	-19.8	-19.4	-19.8
ΔG_{tran} (kcal/mol)[c]	-14.7	-13.4	-14.7
D (Å)[c]	11.8 ± 3.6	8.1 ± 4.6	11.8 ± 3.6
Helical content of lipid-free peptide (%)[d]	76.6	79.0	76.5
Helical content of lipid-bound peptide (%)[d]	93.9	90.9	81.6
Peptide plasma stability (%)[e]	48.4 ± 10.6	96.8 ± 5.4	89.3 ± 12.5

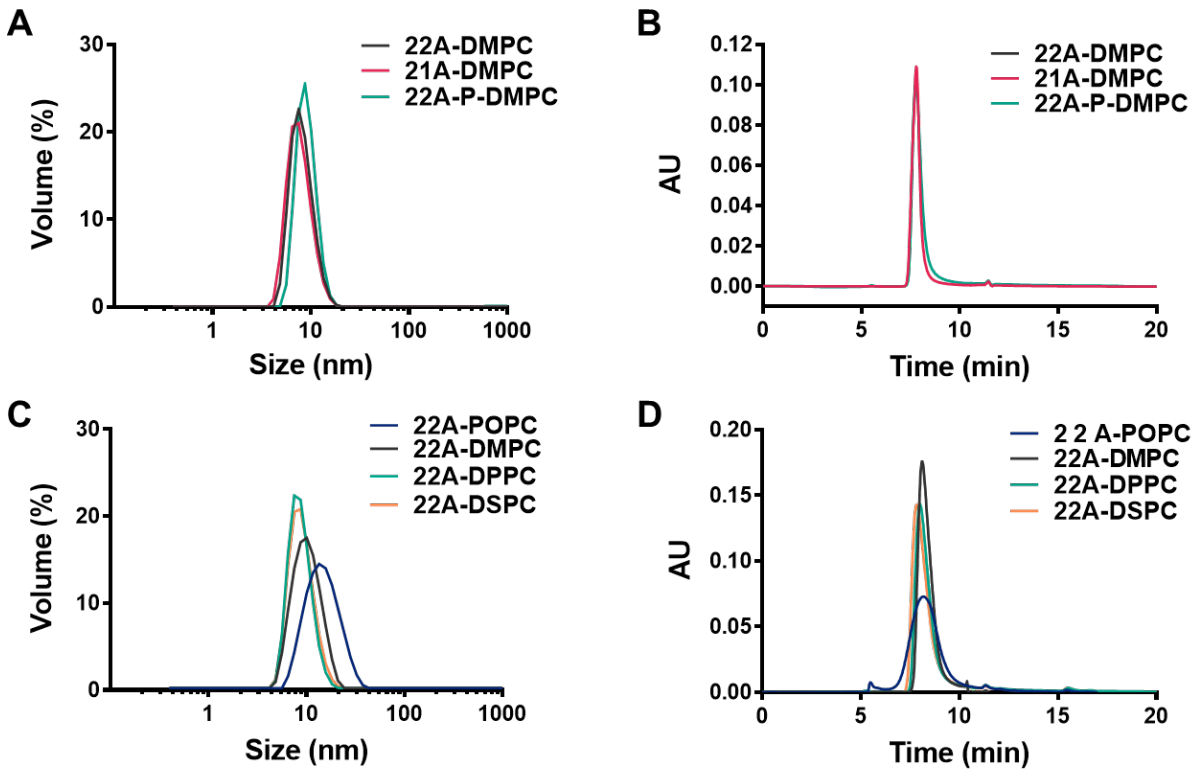

Figure 4-1 *Size distribution and purity of sHDL prepared with various peptide (A, B) and phospholipid (C, D) compositions. The size was determined by dynamic light scattering (DLS) (A, C) and purity was determined by gel permeation chromatography (GPC) (B, D).*

Table 4-2 *Characterization of sHDL particles prepared with different peptides and phospholipids. [a]Particle size of sHDL measured by DLS; [b]Retention time of sHDL particle measured bby GPC; [c]Purity and impurity of sHDL determined by area under the curve from GPC.*

Name	Particle Size (nm)[a]	Retention Time (min)[b]	Purity (%)[c]	Impurity (%)[c]	
				Free Peptide	Liposome
22A-DMPC	10.1 ± 3.3	8.0	98.5	1.1	0.4
21A-DMPC	9.9 ± 3.4	7.8	99.4	0.6	0.0
22A-P-DMPC	10.5 ± 3.6	7.6	98.2	1.8	0.0
22A-POPC	10.4 ± 3.9	8.2	98.0	0.9	1.1
22A-DMPC	8.3 ± 1.9	8.1	99.1	0.9	0.0
22A-DPPC	9.2 ± 2.3	8.0	98.8	0.9	0.3
22A-DSPC	9.9 ± 2.5	7.8	99.2	0.8	0.0

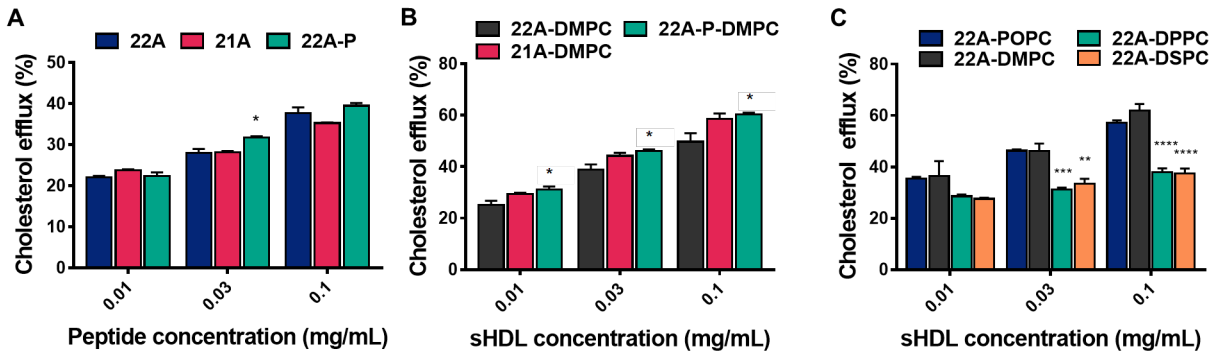

Figure 4-2 *Effect of peptides and sHDL on cholesterol efflux. Free peptides (22A, 21A, 22A-P) were used to efflux cholesterol from BHK cells stably transfected with ABCA1 transporter (a) and sHDL (22A-DMPC, 21A-DMPC, 22A-P-DMPC and 22A-POPC, 22A-DMPC, 22A-DPPC, 22A-DSPC) were utilized to efflux cholesterol from RAW 264.7 macrophage cells (b, c) at 0.01, 0.03, and 0.1 mg/mL for 18 hrs. The contribution of ABCA1 transporter was determined by subtracting efflux values of Mock-transfected cell line from ABCA1-transfected cell line (n=3, mean ± SEM). Statistical differences were compared to 22A peptide or 22A-DMPC with one-way ANOVA analysis with Dunnett's post-hoc test. $P < 0.05$ was considered statistically significant $^{*}P < 0.05$, $^{**}P < 0.01$, $^{***}P < 0.001$.*

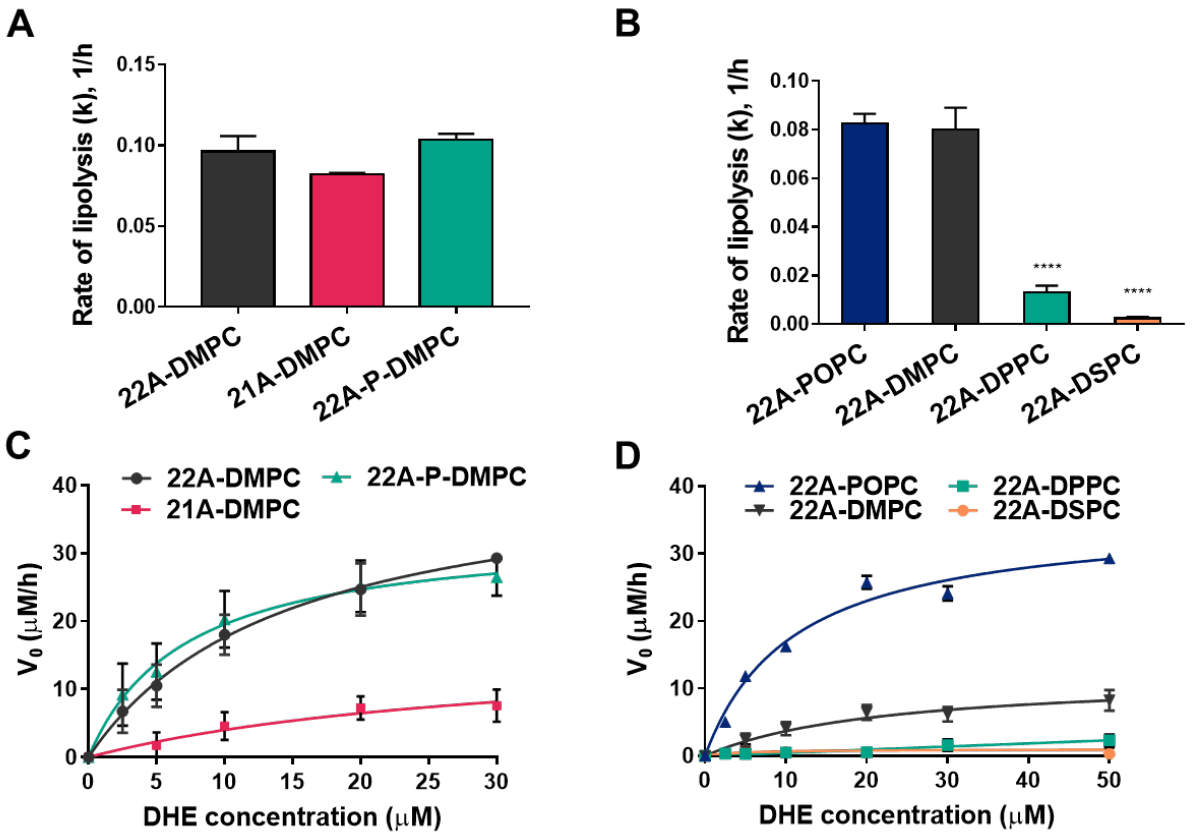

Figure 4-3 *Effect of peptide and phospholipid composition in sHDL on LCAT lipolysis and esterification rates. (a, b) The rate of sHDL lipolysis was determined by incubating sHDL (0.1 mg/mL) prepared with variable peptide composition (22A-DMPC, 21A-DMPC, 22A-P-DMPC) or variable phospholipid composition (22A-POPC, 22A-DMPC, 22A-DPPC, 22A-DSPC) with human rhLCAT (15 μg/mL) at 37 °C for 0, 5, 15, 30, 60, 90, and 120 min. The concentration of phospholipid at each time point was determined by LC-MS and the rate of lipolysis calculated from the slope of the concentration of the starting material versus time. LCAT esterification activity was measured for sHDL containing fluorescent cholesterol analog, dehydroergosterol (DHE) (c, d). The initial reaction rates (V_0) are plotted as a function of DHE concentration and the data were fitted into the Michaelis-Menten kinetic equation to calculate V_{max} and Km (n=3, mean ± SEM). Statistical differences were compared to 22A peptide or 22A-DMPC with one-way ANOVA analysis with Dunnett's post-hoc test. $P < 0.05$ was considered statistically significant $^{*}P < 0.05$, $^{**}P < 0.01$, $^{***}P < 0.001$.*

Table 4-3 *Michaelis-Menten paramenters of sHDL particles prepared with different peptides and phospholipids.*

Name	V_{max} (μM/h)	K_m (μM)	R square
22A-DMPC	43.2 ± 4.9	14.5 ± 3.6	0.97
21A-DMPC	16.8 ± 10.1	32.0 ± 31.8	0.80
22A-P-DMPC	33.4 ± 3.6	7.1 ± 2.2	0.93
22A-POPC	35.7 ± 1.7	11.0 ± 1.5	0.97
22A-DMPC	11.9 ± 3.0	22.2 ± 12.1	0.84
22A-DPPC	Ambiguous	Ambiguous	Ambiguous
22A-DSPC	Ambiguous	Ambiguous	Ambiguous

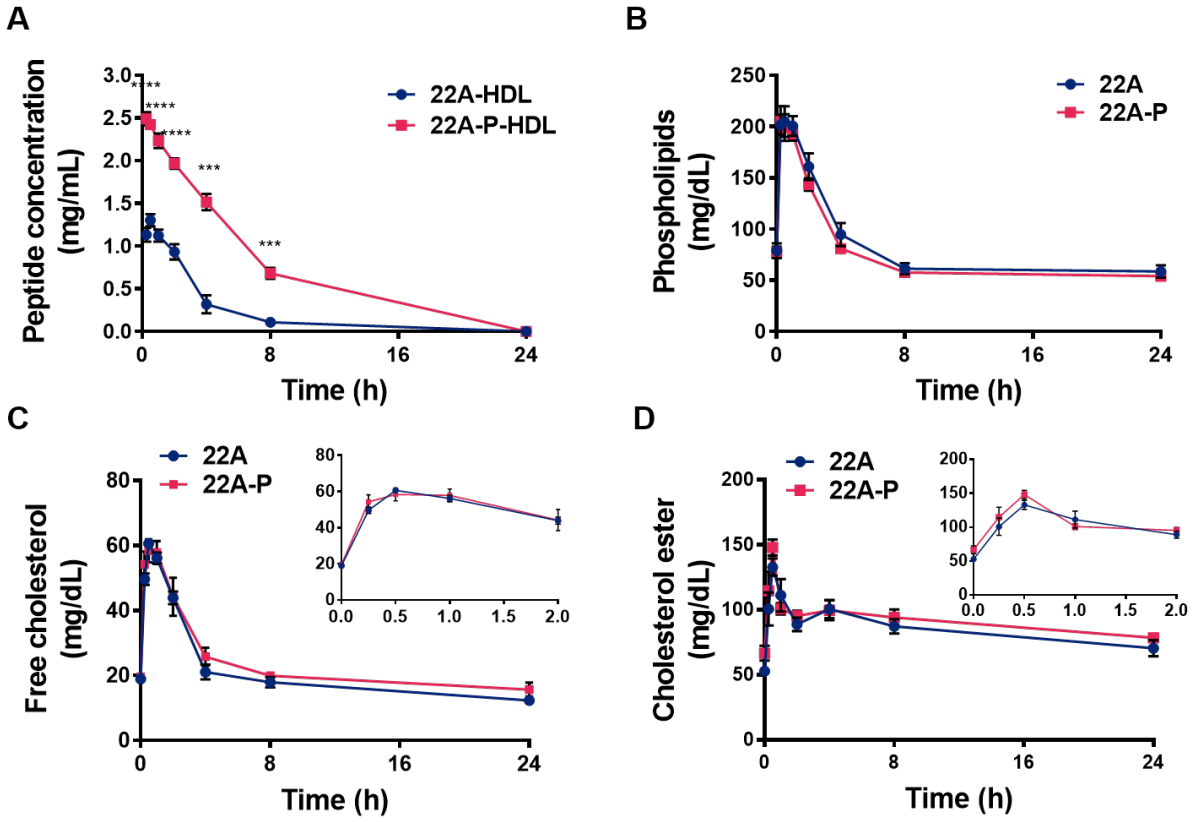

Figure 4-4 *Pharmacokinetic analysis of 22A and 22A-P peptides (a) or total phospholipids (b) in rat serum. Pharmacodynamic assessment of free cholesterol (c) and esterified cholesterol (d) mobilization in rat serum. Healthy male Sprague-Dawley rats were given a single tail vein injection of 50 mg/kg (based on peptide) of 22A-POPC-DPPC or 22A-P-POPC-DPPC and blood samples were collected at pre-dose and 0.25, 0.5, 1, 2, 4, 8, and 24 h after sHDL administration. Serum concentrations of peptides were determined by LC-MS while concentrations of phospholipids, free cholesterol, and esterified cholesterol were measured enzymatically (n=3). Statistical difference was compared with two-tailed Student's t-test. P < 0.05 was considered statistically significant* $^{*}P < 0.05$, $^{**}P < 0.01$, $^{***}P < 0.001$.

Table 4-4 *Pharmacokinetic and pharmacodynamic parameters (%CV) of peptide, total phospholipids (PL), free cholesterol (FC), and esterified cholesterol (EC) after 50 mg/kg doses of 22A-sHDL and 22A-P-sHDL treatments. Data were shown as mean with CV%. $^{*}P<0.05$, $^{**}P < 0.01$, $^{***}P < 0.001$. AUC: the area under the curve. K: elimination rate constant. $T_{1/2}$: the half-life of elimination. CL: total clearance. V_d: volume of distribution. $T_{max,E}$: time at which the E_{max} is observed. E_{max}: the maximum plasma concentration of different cholesterol species. AUEC: the area under the effect curve.*

	Parameters	Groups	
		22A-sHDL	22A-P-sHDL
Peptide	AUC (mg*h/dL)	5.5 (22.0)	17.2 (10.6)***
	K (h^{-1})	0.3 (25.8)	0.2 (12.0)
	$T_{½}$ (h)	2.1 (22.4)	4.2 (10.8)**
	CL (dL/h)	2.3 (21.8)	0.7 (10.9)**
	V_d (dL)	6.9 (7.7)	4.4 (6.2)**
PL	AUC (mg*h/dL)	424.4 (15.7)	371.8 (23.5)
	K (h^{-1})	0.4 (23.8)	0.5 (16.0)
	$T_{½}$ (h)	1.8 (18.8)	1.3 (11.4)*
	CL (dL/h)	0.1 (7.7)	0.1 (7.0)
	V_d (dL)	0.1 (21.4)	0.1 (2.1)
FC	$T_{max,E}$ (h)	0.5 (0.0)	0.8 (33.3)
	E_{max} (mg/dL)	46.7 (5.8)	44.4 (13.0)
	AUEC (mg*h/dL)	158.0 (19.1)	175.3 (28.5)
EC	$T_{max,E}$ (h)	0.42 (24.5)	0.4 (33.3)
	E_{max} (mg/dL)	51.3 (31.8)	42.2 (37.3)
	AUEC (mg*h/dL)	166.8 (12.8)	164.4 (31.8)

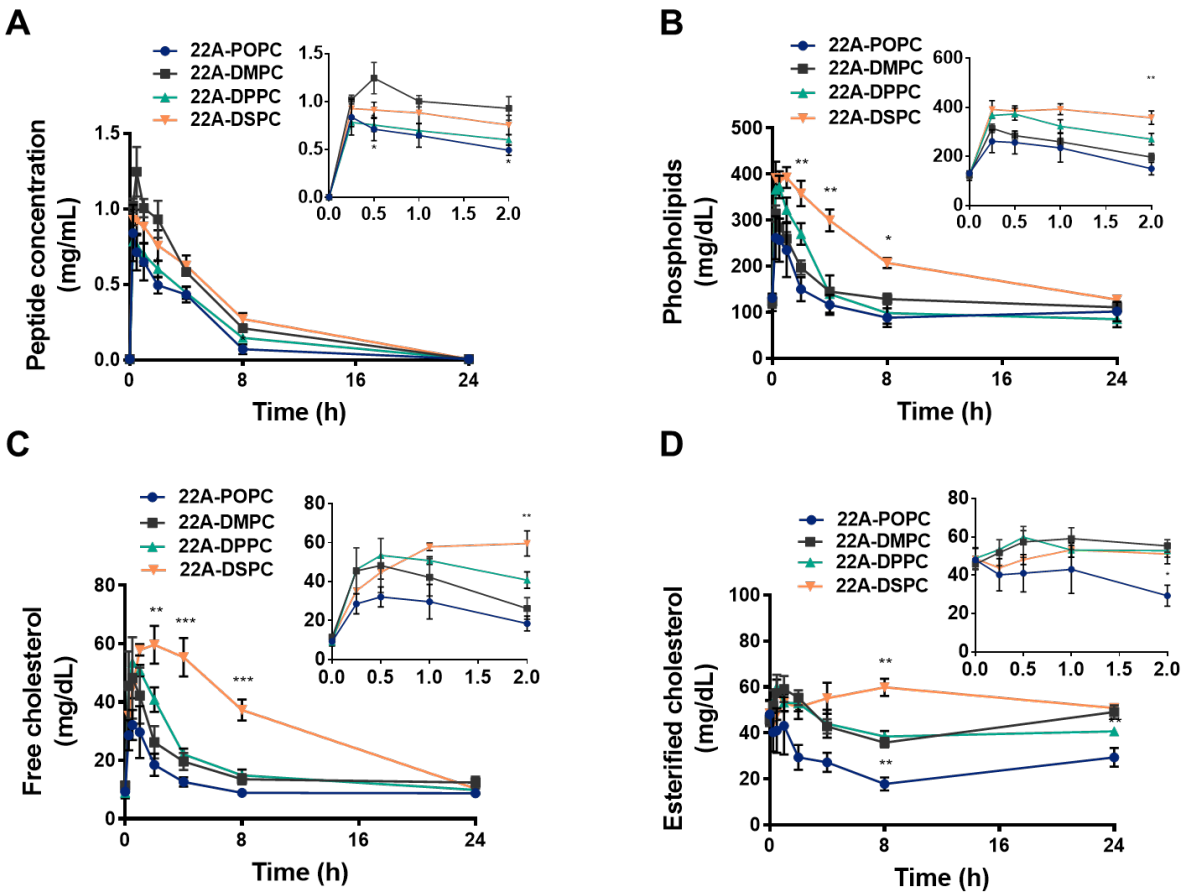

Figure 4-5 *Pharmacokinetic analysis of 22A (a) and total phospholipids (b) in rat serum. Pharmacodynamic assessment of free cholesterol (c) and esterified cholesterol (d) mobilization in rat serum. Healthy male Sprague-Dawley rats were given a single tail vein injection of 50 mg/kg (based on peptide) of 22A-POPC, 22A-DMPC, 22A-DPPC, or 22A-DSPC and blood samples were collected at pre-dose and 0.25, 0.5, 1, 2, 4, 8, and 24 h after sHDL administration. Serum concentrations of peptides were determined by LC-MS while concentrations of phospholipids, free cholesterol, and esterified cholesterol were measured enzymatically (n=3). Statistical differences for 22A-phospholipid were compared to 22A-DMPC with one-way ANOVA analysis with Dunnett's post-hoc test. $P < 0.05$ was considered statistically significant. $P < 0.05$, $^{**}P < 0.01$, $^{***}P < 0.001$.*

Table 4-5 *Pharmacokinetic and pharmacodynamic parameters (%CV) of 22A peptide, total phospholipids (PL), free cholesterol (FC), and esterified cholesterol (EC) after 50 mg/kg doses of 22A-POPC, 22A-DMPC, 22A-DPPC, and 22A-DSPC sHDL treatments. Data were shown as mean with CV%. $^{*}P<0.05$, $^{**}P < 0.01$, $^{***}P < 0.001$. AUC: the area under the curve. K: elimination rate constant. $T_{1/2}$: the half-life of elimination. CL: total clearance. V_d: volume of distribution. $T_{max,E}$: time at which the E_{max} is observed. E_{max}: the maximum plasma concentration of different cholesterol species. AUEC: the area under the effect curve.*

	Parameters	Groups			
		22A-POPC	22A-DMPC	22A-DPPC	22A-DSPC
Peptide	AUC (mg*h/dL)	3.6 (8.6)**	6.6 (10.0)	4.6 (15.2)*	6.9 (17.7)
	K (h^{-1})	0.2 (6.0)	0.2 (1.7)	0.2 (2.4)	0.2 (4.0)
	$T_{½}$ (h)	3.3 (6.2)	3.0 (1.8)	3.3 (2.4)	3.3 (4.2)
	CL (dL/h)	5.6 (11.8)**	3.2 (13.9)	4.6 (17.4)	2.9 (25.2)
	V_d (dL)	27.1 (16.7)**	14.0 (15.5)	21.9 (19.0)	13.7 (29.1)
PL	AUC (mg*h/dL)	371.6 (29.0)	703.2 (23.2)	934.9 (22.8)	2396 (21.1)***
	K (h^{-1})	0.7 (10.6)***	0.2 (4.4)	0.3 (16.8)	0.0 (12.6)**
	$T_{½}$ (h)	1.0 (9.8)***	3.3 (4.4)	2.2 (18.6)*	6.0 (12.4)***
	CL (dL/h)	0.1 (22.2)	0.1 (23.3)	0.0 (27.7)***	0.0 (27.3)***
	V_d (dL)	0.2 (29.8)	0.3 (23.3)	0.2 (45.9)	0.1 (16.0)*
FC	$T_{max,E}$ (h)	0.7 (35.4)	0.4 (28.3)	0.7 (35.4)	1.3 (35.4)*
	E_{max} (mg/dL)	25.8 (36.8)	37.6 (19.8)	44.8 (5.1)	51.5 (15.3)
	AUEC (mg*h/dL)	79.4 (33.9)	126.5 (10.0)	215.0 (20.9)	536.4 (19.1)***
EC	$T_{max,E}$ (h)	0.5 (70.7)	0.8 (28.3)	0.9 (84.3)	6.7 (28.3)**
	E_{max} (mg/dL)	7.7 (65.2)	28.2 (30.3)	24.9 (13.7)	20.6 (24.7)
	AUEC (mg*h/dL)	84.8 (65.3)	93.3 (41.9)	98.9 (31.6)	334.7 (18.0)**

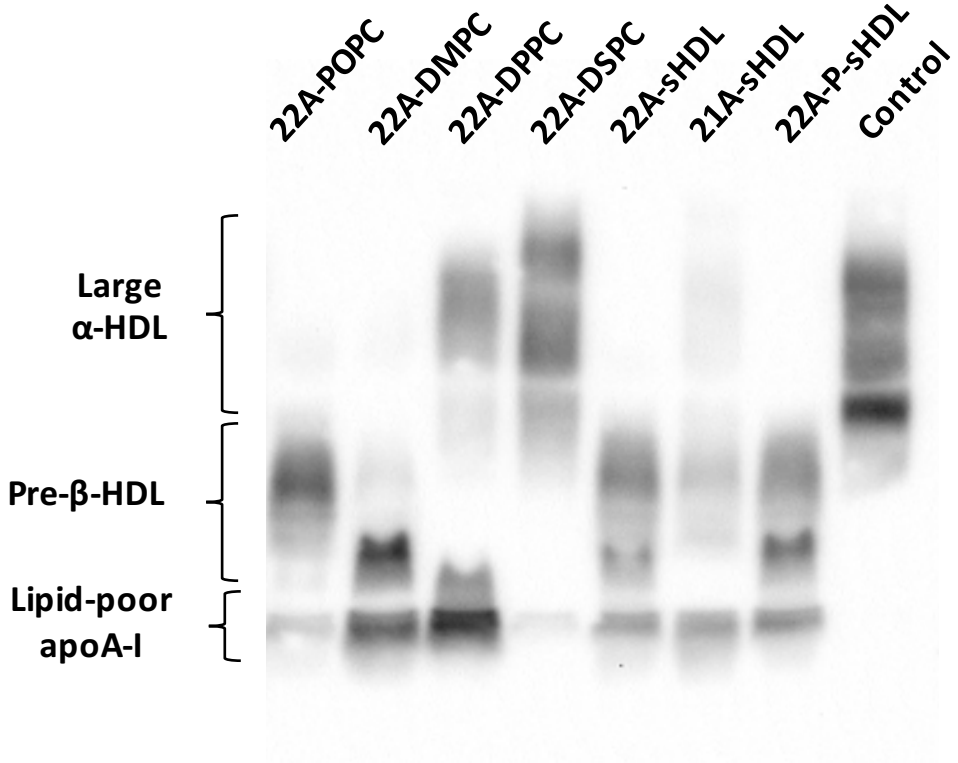

Figure 4-6 *Effect of sHDL incubation with human plasma on endogenous HDL remodeling. Various compositions of sHDL were incubated in human plasma at 1 mg/mL for 1 h at 37°C. Lipoproteins were separated by 1-D native page electrophoresis and visualized by western blot using anti-apoA-I antibody.*

Chapter 5: Conclusions and Future Direction

The work presented in this thesis describes innovative approaches to ameliorate lipid storage in the Niemann-Pick family of diseases by harnessing the activity of the body's endogenous cholesterol and sphingomyelin scavenging system, which includes ApoA-I and HDL.

Synthetic HDL (sHDL) has been previously tested in patients with atherosclerosis to reduce cholesterol accumulations in the hardened arteries. In Chapter 2, applying the same strategy to Niemann-Pick disease type C (NPC), we prepared sHDLs made from ApoA-I mimetic peptide 5A complexed with phospholipids such as SM, POPC, or DMPC at various ratios. The mimetic peptide 5A was selected based on its specific interaction with the ATP-binding cassette transporter A1 (ABCA1), which played a pivotal role in mediating cellular efflux of cholesterol and phospholipids to lipid-free ApoA-I and small HDL. Different sHDL formulations and 5A alone were tested in several NPC primary patient fibroblast cell lines, and it was found that 5A-SM was capable of reducing accumulated cholesterol while lipid-free 5A peptide was not a good cholesterol acceptor. Additionally, we observed dose and time-dependent reductions in cholesterol from endolysosomal compartments after the treatment with 5A-SM. While the rescue of cholesterol storage from mutant fibroblasts required expression of ABCA1, fluorescently labeled sHDLs readily entered cells by macropinocytosis. The lipid and peptide constituents of the nanoparticles remained tightly associated within cells, with some

trafficking to LAMP1 and filipin-stained vesicles. The particles showed evidence of cholesterol target engagement and rescue of disease phenotypes when administered to NPC mice via intraperitoneal injection. The amelioration of only peripheral, but not neurological phenotypes in NPC mice was observed. Thus, future studies will be focused on direct brain (intracranial) administration route of sHDL to determine its potential to prevent the loss of Purkinje neurons and rescue of motor phenotype.

Chapter 3 was focused on exploring ApoA-I mimetics for the treatment of acid sphingomyelinase deficiency in Niemann-Pick disease type A (NPA) and B (NPB). NPA/B patients had marked decrease in plasma HDL-cholesterol levels. Several groups showed that small pre-β HDL in patients with acid sphingomyelinase deficiency was highly enriched in sphingomyelin. Interestingly, the expression of the *ABCA1* gene as well as sphingomyelin efflux to lipid-free ApoA-I protein in fibroblast cells of NPB patients was normal. Taken together, these results suggested that lipid-free ApoA-I mimetic peptides or lipid-poor sHDL may be capable of binding sphingomyelin similar to native ApoA-I and nascent HDL. Here, we identified one ApoA-I mimetic peptide (22A) and 22A-sHDL (22A-DMPC and 22A-DPPC), which significantly reduced the amount of accumulated sphingomyelin in Niemann-Pick type A cells. We showed that peptide and sHDL were non-toxic *in vitro* and required the ABCA1 to efflux some stored sphingomyelin. Furthermore, we administered 22A and 22A-DMPC into wild type adult mice via intravenous route. It was found that 22A at 300 mg/kg rapidly mobilized sphingomyelin into circulation while sHDL was not effective at the dose tested (75 mg/kg). Together, these studies provide the proof-of-concept data to support the therapeutic potential of

ApoA-I mimetics for the Niemann-Pick Disease type A. Future studies of 22A safety and efficacy will be explored in the mouse model of NPA disease.

In Chapter 4, we examined the contribution of ApoA-I mimetic peptide and phospholipid type in sHDL on the ability of sHDL to mobilize cholesterol *in vivo*. Conventionally, the composition of ApoA-I mimetics was developed *in vitro* using a radioactive cholesterol efflux assay to predict its relative efficacy *in vivo*. Then, ApoA-I peptides were complexed with phospholipids to produce sHDL. The choice for phospholipids was mostly random and also not supported by *in vivo* studies. In this chapter, we systematically changed either ApoA-I peptide (22A, 21A, 22A-P) or phospholipid (DMPC, POPC, DPPC, DSPC) composition in sHDL and studied the ability of different sHDL formulations to efflux cholesterol *in vitro* and *in vivo*. We observed the discordance between *in vitro* and *in vivo* results for sHDL prepared with different phospholipids and peptides. The *in vitro* trends for higher cholesterol efflux for 22A-POPC and 22A-DMPC did not translate into higher cholesterol mobilization *in vivo*. The cholesterol mobilization and circulation time appeared to be closely following circulation time of phospholipids. The stability of 22A-P was greatly improved *in vivo* relative to 22A, however phospholipid pharmacokinetics appeared to be unchanged and cholesterol mobilization followed phospholipid. This data suggested that the pharmacokinetics of peptide and lipid components in sHDL were not interdependent and original infused sHDL particles may dissociate or become remodeled upon administration *in vivo*. In addition, the phospholipid, rather than peptide component in sHDL had a major impact on the ability to mobilize cholesterol *in vivo*. Further examination is needed to determine if higher

cholesterol mobilization for sHDL composed of saturated lipids will lead to a greater anti-atherosclerosis effect in a murine model of the disease is needed.

Although sHDL particles presented in this dissertation mimic endogenous lipoproteins, they have a short circulation half-life and may not cross the blood-brain barrier. *In vivo* stability of non-lipidated ApoA-I mimetic peptides is even less promising. Future research should be focused on extending the half-life of ApoA-I peptides and sHDL with the goal of decreasing the dose required to achieve efficacy and thus reducing the risk of toxic side effects. One way to increase the circulation time of ApoA-I peptides is to protect the vulnerable sites from *in vivo* proteolysis using unnatural or less labile amino acids or conjugation of peptides to poly (ethylene glycol), PEG. In terms of sHDL, few strategies have been already explored including PEGylation or addition of phospholipids with higher transition temperatures (e.g., di-steroyl-phosphatidylcholine, DSPC) [199]. The more complicated issue is a low brain uptake of sHDL particles, especially important for Niemann-Pick type C and A patients. In the brain, HDL is composed primarily from ApoE protein. Studies from other investigators revealed several successful approaches to improve brain targeting of sHDL by utilizing ApoE rather than ApoA-I mimetic peptide sequences or by incorporating brain endothelium targeting peptides [201-203]. The surface of sHDL could be modified by covalently attaching ligands targeting vascular cell adhesion molecule, integrin, LDL receptor-related protein, and LDL receptor.

The work presented in this dissertation serves as the foundation for future research in the area of Niemann-Pick disease and HDL field.

Bibliography

1. Davidson, W.S. and T.B. Thompson, The structure of apolipoprotein AI in high density lipoproteins. Journal of Biological Chemistry, 2007. **282**(31): p. 22249-22253.

2. Brouillette, C.G. and G. Anantharamaiah, Structural models of human apolipoprotein AI. Biochimica et Biophysica Acta (BBA)-Lipids and Lipid Metabolism, 1995. **1256**(2): p. 103-129.

3. Brouillette, C.G., et al., Structural models of human apolipoprotein AI: a critical analysis and review. Biochimica et Biophysica Acta (BBA)-Molecular and Cell Biology of Lipids, 2001. **1531**(1-2): p. 4-46.

4. Brooks-Wilson, A., et al., Mutations in ABC1 in Tangier disease and familial high-density lipoprotein deficiency. Nature genetics, 1999. **22**(4): p. 336.

5. Silva, R.G.D., et al., Structure of apolipoprotein AI in spherical high density lipoproteins of different sizes. Proceedings of the National Academy of Sciences, 2008. **105**(34): p. 12176-12181.

6. Linsel-Nitschke, P. and A.R. Tall, HDL as a target in the treatment of atherosclerotic cardiovascular disease. Nature reviews Drug discovery, 2005. **4**(3): p. 193.

7. Hasselwander, O., et al., HDL composition and HDL antioxidant capacity in patients on regular haemodialysis. Atherosclerosis, 1999. **143**(1): p. 125-133.

8. Mineo, C., et al., Endothelial and antithrombotic actions of HDL. Circulation research, 2006. **98**(11): p. 1352-1364.

9. Haase, C.L., et al., HDL cholesterol and risk of type 2 diabetes: a Mendelian randomization study. Diabetes, 2015. **64**(9): p. 3328-3333.

10. Davidson, W.S., et al., Proteomic analysis of defined HDL subpopulations reveals particle-specific protein clusters: relevance to antioxidative function. Arteriosclerosis, thrombosis, and vascular biology, 2009. **29**(6): p. 870-876.

11. Azuma, Y., et al., Retroendocytosis pathway of ABCA1/apoA-I contributes to HDL formation. Genes to Cells, 2009. **14**(2): p. 191-204.

12. Takahashi, Y. and J.D. Smith, Cholesterol efflux to apolipoprotein AI involves endocytosis and resecretion in a calcium-dependent pathway. Proceedings of the National Academy of Sciences, 1999. **96**(20): p. 11358-11363.

13. Ahsan, L., et al., Role of lecithin: cholesterol acyltransferase in HDL metabolism and atherosclerosis, in The HDL Handbook. 2014, Elsevier. p. 159-194.

14. Gordon, D.J., et al., High-density lipoprotein cholesterol and cardiovascular disease. Four prospective American studies. Circulation, 1989. **79**(1): p. 8-15.

15. Ding, Y., et al., Direct cytosolic siRNA delivery by reconstituted high density lipoprotein for target-specific therapy of tumor angiogenesis. Biomaterials, 2014. **35**(25): p. 7214-7227.

16. Spieker, L.E., et al., High-density lipoprotein restores endothelial function in hypercholesterolemic men. Circulation, 2002. **105**(12): p. 1399-1402.

17. Bisoendial, R.J., et al., Restoration of endothelial function by increasing high-density lipoprotein in subjects with isolated low high-density lipoprotein. Circulation, 2003. **107**(23): p. 2944-2948.

18. Shaw, J.A., et al., Infusion of reconstituted high-density lipoprotein leads to acute changes in human atherosclerotic plaque. Circulation research, 2008. **103**(10): p. 1084-1091.

19. Tardif, J.-C., et al., Effects of reconstituted high-density lipoprotein infusions on coronary atherosclerosis: a randomized controlled trial. Jama, 2007. **297**(15): p. 1675-1682.

20. Easton, R., et al., A multiple ascending dose study of CSL112, an infused formulation of ApoA-I. The Journal of Clinical Pharmacology, 2014. **54**(3): p. 301-310.

21. Nissen, S.E., et al., Effect of recombinant ApoA-I Milano on coronary atherosclerosis in patients with acute coronary syndromes: a randomized controlled trial. Jama, 2003. **290**(17): p. 2292-2300.

22. Keyserling, C.H., et al., CER-001, a synthetic HDL-mimetic, safely mobilizes cholesterol in healthy dyslipidemic volunteers. 2011, Am Heart Assoc.

23. Tardif, J.-C., et al., Effects of the high-density lipoprotein mimetic agent CER-001 on coronary atherosclerosis in patients with acute coronary syndromes: a randomized trial. European heart journal, 2014. **35**(46): p. 3277-3286.

24. Anantharamaiah, G., et al., Studies of synthetic peptide analogs of the amphipathic helix. Structure of complexes with dimyristoyl phosphatidylcholine. Journal of Biological Chemistry, 1985. **260**(18): p. 10248-10255.

25. Bloedon, L.T., et al., Safety, pharmacokinetics, and pharmacodynamics of oral apoA-I mimetic peptide D-4F in high-risk cardiovascular patients. Journal of lipid research, 2008. **49**(6): p. 1344-1352.

26. Miles, J., et al., P105 Single-Dose Tolerability, Pharmacokinetics, and Cholesterol Mobilization in HDL-C Fraction Following Intravenous Administration of ETC-642, a 22-mer ApoA-I Analogue and Phospholipids Complex, in Atherosclerosis Patients. Arteriosclerosis, Thrombosis, and Vascular Biology: Journal of the American Heart Association, 2004. **24**(5).

27. Li, D., et al., Apolipoprotein mimetic peptides for stimulating cholesterol efflux, in Apolipoprotein Mimetics in the Management of Human Disease. 2015, Springer. p. 29-42.

28. Shen, D., et al., Lipid storage disorders block lysosomal trafficking by inhibiting a TRP channel and lysosomal calcium release. Nature communications, 2012. **3**: p. 731.

29. Desnick, J.P., et al., Identification and characterization of eight novel SMPD1 mutations causing types A and B Niemann-Pick disease. Molecular Medicine, 2010. **16**(7-8): p. 316-321.

30. McGovern, M., et al., Natural history of Type A Niemann-Pick disease: possible endpoints for therapeutic trials. Neurology, 2006. **66**(2): p. 228-232.

31. Carstea, E.D., et al., Niemann-Pick C1 disease gene: homology to mediators of cholesterol homeostasis. Science, 1997. **277**(5323): p. 228-231.

32. Newton, J., et al., FTY720/fingolimod increases NPC1 and NPC2 expression and reduces cholesterol and sphingolipid accumulation in Niemann-Pick type C mutant fibroblasts. The FASEB Journal, 2017. **31**(4): p. 1719-1730.

33. Liscum, L., R.M. Ruggiero, and J.R. Faust, The intracellular transport of low density lipoprotein-derived cholesterol is defective in Niemann-Pick type C fibroblasts. The Journal of Cell Biology, 1989. **108**(5): p. 1625-1636.

34. Horton, J.D., J.L. Goldstein, and M.S. Brown, SREBPs: activators of the complete program of cholesterol and fatty acid synthesis in the liver. The Journal of clinical investigation, 2002. **109**(9): p. 1125-1131.

35. Repa, J.J. and D.J. Mangelsdorf, The liver X receptor gene team: potential new players in atherosclerosis. Nature medicine, 2002. **8**(11): p. 1243.

36. Leidl, K., et al., Mass spectrometric analysis of lipid species of human circulating blood cells. Biochimica et Biophysica Acta (BBA)-Molecular and Cell Biology of Lipids, 2008. **1781**(10): p. 655-664.

37. Demel, R. and J. Jansen, The preferential interaction of cholesterol with different classes of phospholipids. Biochimica et biophysica acta, 1977. **465**(1): p. 1-10.

38. Lin, Q. and E. London, Ordered raft domains induced by outer leaflet sphingomyelin in cholesterol-rich asymmetric vesicles. Biophysical journal, 2015. **108**(9): p. 2212-2222.

39. Oram, J.F. and A.M. Vaughan, ABCA1-mediated transport of cellular cholesterol and phospholipids to HDL apolipoproteins. Current opinion in lipidology, 2000. **11**(3): p. 253-260.

40. Neufeld, E.B., et al., Cellular localization and trafficking of the human ABCA1 transporter. Journal of Biological Chemistry, 2001. **276**(29): p. 27584-27590.

41. Neufeld, E.B., et al., The ABCA1 Transporter Modulates Late Endocytic Trafficking insights from the correction of the genetic defect in tangier disease. Journal of Biological Chemistry, 2004. **279**(15): p. 15571-15578.

42. Chen, W., et al., Preferential ATP-binding cassette transporter A1-mediated cholesterol efflux from late endosomes/lysosomes. Journal of Biological Chemistry, 2001. **276**(47): p. 43564-43569.

43. Boadu, E., R.C. Nelson, and G.A. Francis, ABCA1-dependent mobilization of lysosomal cholesterol requires functional Niemann–Pick C2 but not Niemann–Pick C1 protein. Biochimica et Biophysica Acta (BBA)-Molecular and Cell Biology of Lipids, 2012. **1821**(3): p. 396-404.

44. Newton, J., S. Milstien, and S. Spiegel, Niemann-Pick type C disease: the atypical sphingolipidosis. Advances in biological regulation, 2018. **70**: p. 82-88.

45. Brady, R.O., et al., The metabolism of sphingomyelin. II. Evidence of an enzymatic deficiency in Niemann-Pick diseae. Proceedings of the National Academy of Sciences of the United States of America, 1966. **55**(2): p. 366.

46. Pentchev, P., et al., Type C Niemann-Pick disease. A parallel loss of regulatory responses in both the uptake and esterification of low density lipoprotein-derived cholesterol in cultured fibroblasts. Journal of Biological Chemistry, 1986. **261**(35): p. 16775-16780.

47. Jahnova, H., et al., Observational, retrospective study of a large cohort of patients with Niemann-Pick disease type C in the Czech Republic: a surprisingly stable diagnostic rate spanning almost 40 years. Orphanet journal of rare diseases, 2014. **9**(1): p. 140.

48. Davidson, C.D. and S.U. Walkley, Niemann-Pick Type C Disease-pathophysiology and future perspectives for treatment. US Neurology, 2010. **8**: p. 88-94.

49. Patterson, M.C., et al., Recommendations for the diagnosis and management of Niemann–Pick disease type C: an update. Molecular genetics and metabolism, 2012. **106**(3): p. 330-344.

50. Garver, W.S., et al., The National Niemann–Pick C1 disease database: report of clinical features and health problems. American Journal of Medical Genetics Part A, 2007. **143**(11): p. 1204-1211.

51. Park, W.D., et al., Identification of 58 novel mutations in Niemann-Pick disease type C: Correlation with biochemical phenotype and importance of PTC1-like domains in NPC1. Human mutation, 2003. **22**(4): p. 313-325.

52. Li, X., et al., 3.3 Å structure of Niemann–Pick C1 protein reveals insights into the function of the C-terminal luminal domain in cholesterol transport. Proceedings of the National Academy of Sciences, 2017. **114**(34): p. 9116-9121.

53. Millat, G., et al., Niemann-Pick C1 disease: the I1061T substitution is a frequent mutant allele in patients of Western European descent and correlates with a classic juvenile phenotype. The American Journal of Human Genetics, 1999. **65**(5): p. 1321-1329.

54. Gelsthorpe, M.E., et al., Niemann-Pick type C1 I1061T mutant encodes a functional protein that is selected for endoplasmic reticulum-associated degradation due to protein misfolding. Journal of Biological Chemistry, 2008. **283**(13): p. 8229-8236.

55. Friedland, N., et al., Structure of a cholesterol-binding protein deficient in Niemann–Pick type C2 disease. Proceedings of the National Academy of Sciences, 2003. **100**(5): p. 2512-2517.

56. Li, X., et al., Clues to the mechanism of cholesterol transfer from the structure of NPC1 middle lumenal domain bound to NPC2. Proceedings of the National Academy of Sciences, 2016. **113**(36): p. 10079-10084.

57. Lachmann, R.H., et al., Treatment with miglustat reverses the lipid-trafficking defect in Niemann–Pick disease type C. Neurobiology of disease, 2004. **16**(3): p. 654-658.

58. Rosenbaum, A.I. and F.R. Maxfield, Niemann-Pick type C disease: molecular mechanisms and potential therapeutic approaches. Journal of neurochemistry, 2011. **116**(5): p. 789-795.

59. Lloyd-Evans, E., et al., Niemann-Pick disease type C1 is a sphingosine storage disease that causes deregulation of lysosomal calcium. Nature medicine, 2008. **14**(11): p. 1247.

60. Patterson, M.C., et al., Stable or improved neurological manifestations during miglustat therapy in patients from the international disease registry for Niemann-

Pick disease type C: an observational cohort study. Orphanet journal of rare diseases, 2015. **10**(1): p. 65.

61. Vance, J.E. and B. Karten, Niemann-Pick C disease and mobilization of lysosomal cholesterol by cyclodextrin. Journal of lipid research, 2014. **55**(8): p. 1609-1621.

62. Rosenbaum, A.I., et al., Endocytosis of beta-cyclodextrins is responsible for cholesterol reduction in Niemann-Pick type C mutant cells. Proceedings of the National Academy of Sciences, 2010. **107**(12): p. 5477-5482.

63. Liu, B., et al., Reversal of defective lysosomal transport in NPC disease ameliorates liver dysfunction and neurodegeneration in the npc1−/− mouse. Proceedings of the National Academy of Sciences, 2009. **106**(7): p. 2377-2382.

64. Liu, B., et al., Genetic variations and treatments that affect the lifespan of the NPC1 mouse. Journal of lipid research, 2008. **49**(3): p. 663-669.

65. Davidson, C.D., et al., Chronic cyclodextrin treatment of murine Niemann-Pick C disease ameliorates neuronal cholesterol and glycosphingolipid storage and disease progression. PLoS One, 2009. **4**(9): p. e6951.

66. Vite, C.H., et al., Intracisternal cyclodextrin prevents cerebellar dysfunction and Purkinje cell death in feline Niemann-Pick type C1 disease. Science translational medicine, 2015. **7**(276): p. 276ra26-276ra26.

67. Pontikis, C.C., et al., Cyclodextrin alleviates neuronal storage of cholesterol in Niemann-Pick C disease without evidence of detectable blood–brain barrier permeability. Journal of inherited metabolic disease, 2013. **36**(3): p. 491-498.

68. Ward, S., et al., 2-hydroxypropyl-β-cyclodextrin raises hearing threshold in normal cats and in cats with Niemann-Pick type C disease. Pediatric research, 2010. **68**(1): p. 52.

69. Ory, D.S., et al., Intrathecal 2-hydroxypropyl-β-cyclodextrin decreases neurological disease progression in Niemann-Pick disease, type C1: a non-randomised, open-label, phase 1–2 trial. The Lancet, 2017. **390**(10104): p. 1758-1768.

70. Chien, Y.-H., et al., Lung toxicity of hydroxypropyl-β-cyclodextrin infusion. Molecular genetics and metabolism, 2013. **109**(2): p. 231-232.

71. Matsuo, M., et al., Effects of cyclodextrin in two patients with Niemann–Pick type C disease. Molecular genetics and metabolism, 2013. **108**(1): p. 76-81.

72. Levade, T., et al., Evidence for both endogenous and exogenous sources of the sphingomyelin storage in lymphoid cell lines from patients with Niemann-Pick

disease types A and B. Journal of inherited metabolic disease, 1988. **11**(2): p. 151-157.

73. Thurberg, B., et al., Hepatic pathology of acid sphingomyelinase deficiency: Clearance of sphingomyelin with recombinant human acid sphingomyelinase administration is associated with improvement in pro-atherogenic lipid profiles. Molecular Genetics and Metabolism, 2015. **114**(2): p. S114.

74. Passini, M.A., et al., AAV vector-mediated correction of brain pathology in a mouse model of Niemann–Pick A disease. Molecular Therapy, 2005. **11**(5): p. 754-762.

75. Jones, I., et al., Characterization of common SMPD1 mutations causing types A and B Niemann-Pick disease and generation of mutation-specific mouse models. Molecular genetics and metabolism, 2008. **95**(3): p. 152-162.

76. Dhami, R., et al., Analysis of the lung pathology and alveolar macrophage function in the acid sphingomyelinase–deficient mouse model of Niemann-Pick disease. Laboratory investigation, 2001. **81**(7): p. 987.

77. Marathe, S., et al., Creation of a mouse model for non-neurological (type B) Niemann–Pick disease by stable, low level expression of lysosomal sphingomyelinase in the absence of secretory sphingomyelinase: relationship between brain intra-lysosomal enzyme activity and central nervous system function. Human molecular genetics, 2000. **9**(13): p. 1967-1976.

78. Horinouchi, K., et al., Acid sphingomyelinase deficient mice: a model of types A and B Niemann–Pick disease. Nature genetics, 1995. **10**(3): p. 288.

79. Wasserstein, M.P., et al., Successful within-patient dose escalation of olipudase alfa in acid sphingomyelinase deficiency. Molecular genetics and metabolism, 2015. **116**(1): p. 88-97.

80. McGovern, M.M., et al., Morbidity and mortality in type B Niemann–Pick disease. Genetics in Medicine, 2013. **15**(8): p. 618.

81. Wasserstein, M.P., et al., Olipudase alfa for treatment of acid sphingomyelinase deficiency (ASMD): safety and efficacy in adults treated for 30 months. Journal of inherited metabolic disease, 2018. **41**(5): p. 829-838.

82. Schuchman, E.H. and R.J. Desnick, Types a and B Niemann-pick disease. Molecular genetics and metabolism, 2017. **120**(1-2): p. 27-33.

83. Lee, C.Y., et al., Compound heterozygosity at the sphingomyelin phosphodiesterase-1 (SMPD1) gene is associated with low HDL cholesterol. Human genetics, 2003. **112**(5-6): p. 552-562.

84. Choi, H.Y., et al., Impaired ABCA1-dependent lipid efflux and hypoalphalipoproteinemia in human Niemann-Pick type C disease. Journal of Biological Chemistry, 2003. **278**(35): p. 32569-32577.

85. Wasserstein, M.P., et al., The natural history of type B Niemann-Pick disease: results from a 10-year longitudinal study. Pediatrics, 2004. **114**(6): p. e672-e677.

86. Zelcer, N., et al., LXR regulates cholesterol uptake through Idol-dependent ubiquitination of the LDL receptor. Science, 2009. **325**(5936): p. 100-104.

87. Boadu, E., et al., Correction of apolipoprotein AI-mediated lipid efflux and high density lipoprotein particle formation in human Niemann-Pick type C disease fibroblasts. Journal of Biological Chemistry, 2006. **281**(48): p. 37081-37090.

88. Lee, C.Y., et al., Increased sphingomyelin content impairs HDL biogenesis and maturation in human Niemann-Pick disease type B. Journal of lipid research, 2006. **47**(3): p. 622-632.

89. McGovern, M.M., et al., Lipid abnormalities in children with types A and B Niemann Pick disease. The Journal of pediatrics, 2004. **145**(1): p. 77-81.

90. Higgins, J.J., et al., A clinical staging classification for type C Niemann-Pick disease. Neurology, 1992. **42**(12): p. 2286-90.

91. Vanier, M.T. and G. Millat, Niemann-Pick disease type C. Clin Genet, 2003. **64**(4): p. 269-81.

92. Ioannou, Y.A., Multidrug permeases and subcellular cholesterol transport. Nat Rev Mol Cell Biol, 2001. **2**(9): p. 657-68.

93. Infante, R.E., et al., NPC2 facilitates bidirectional transfer of cholesterol between NPC1 and lipid bilayers, a step in cholesterol egress from lysosomes. Proc Natl Acad Sci U S A, 2008. **105**(40): p. 15287-92.

94. Pentchev, P.G., et al., A defect in cholesterol esterification in Niemann-Pick disease (type C) patients. Proc Natl Acad Sci U S A, 1985. **82**(23): p. 8247-51.

95. Schuchman, E.H. and R.J. Desnick, Types A and B Niemann-Pick disease. Mol Genet Metab, 2017. **120**(1-2): p. 27-33.

96. Hellerstein, M. and S. Turner, Reverse cholesterol transport fluxes. Current opinion in lipidology, 2014. **25**(1): p. 40-47.

97. Remaley, A.T., M. Amar, and D. Sviridov, HDL-replacement therapy: mechanism of action, types of agents and potential clinical indications. Expert review of cardiovascular therapy, 2008. **6**(9): p. 1203-1215.

98. Kingwell, B.A., et al., HDL-targeted therapies: progress, failures and future. Nature reviews Drug discovery, 2014. **13**(6): p. 445.

99. Kuai, R., et al., High-density lipoproteins: nature's multifunctional nanoparticles. ACS nano, 2016. **10**(3): p. 3015-3041.

100. Krause, B.R. and A.T. Remaley, Reconstituted HDL for the acute treatment of acute coronary syndrome. Current opinion in lipidology, 2013. **24**(6): p. 480-486.

101. Schwendeman, A., et al., The effect of phospholipid composition of reconstituted HDL on its cholesterol efflux and anti-inflammatory properties. J Lipid Res, 2015. **56**(9): p. 1727-37.

102. Tang, J., et al., Influence of route of administration and lipidation of apolipoprotein A-I peptide on pharmacokinetics and cholesterol mobilization. J Lipid Res, 2017. **58**(1): p. 124-136.

103. Remaley, A.T., et al., Synthetic amphipathic helical peptides promote lipid efflux from cells by an ABCA1-dependent and an ABCA1-independent pathway. J Lipid Res, 2003. **44**(4): p. 828-836.

104. D'Souza, W., et al., Structure/function relationships of apolipoprotein a-I mimetic peptides: implications for antiatherogenic activities of high-density lipoprotein. Circ Res, 2010. **107**(2): p. 217-27.

105. Tricoci, P., et al., Infusion of Reconstituted High-Density Lipoprotein, CSL112, in Patients With Atherosclerosis: Safety and Pharmacokinetic Results From a Phase 2a Randomized Clinical Trial. Journal of the American Heart Association, 2015. **4**(8): p. e002171.

106. Bisgaier, C.L., et al., ApoA-IMilano phospholipid complex (ETC-216) infusion in human volunteers. Insights into the phenotypic characteristics of ApoA-IMilano carriers. Pharmacological research, 2016. **111**: p. 86-99.

107. Miles, J., et al., P105 Single-dose Tolerability, Pharmacokinetics, and Cholesterol Mobilization in Hdl-c Fraction Following Intravenous Administration of Etc-642, a 22-mer Apoa-i Analogue and Phospholipids Complex, in Atherosclerosis Patients. Arteriosclerosis, Thrombosis, and Vascular Biology: Journal of the American Heart Association, 2004. **24**(5): p. e-19.

108. Amar, M.J., et al., 5A apolipoprotein mimetic peptide promotes cholesterol efflux and reduces atherosclerosis in mice. J Pharmacol Exp Ther, 2010. **334**(2): p. 634-41.

109. Bourdi, M., et al., Intravenous toxicity and toxicokinetics of an HDL mimetic, Fx-5A peptide complex, in cynomolgus monkeys. Regulatory Toxicology and Pharmacology, 2018.

110. Praggastis, M., et al., A murine Niemann-Pick C1 I1061T knock-in model recapitulates the pathological features of the most prevalent human disease allele. J Neurosci, 2015. **35**(21): p. 8091-106.

111. Schultz, M.L., et al., Coordinate regulation of mutant NPC1 degradation by selective ER autophagy and MARCH6-dependent ERAD. Nat Commun, 2018. **9**(1): p. 3671.

112. Chopra, R., et al., Protein kinase C activity is a protective modifier of Purkinje neuron degeneration in cerebellar ataxia. Hum Mol Genet, 2018. **27**(8): p. 1396-1410.

113. Moore, L.R., et al., Evaluation of Antisense Oligonucleotides Targeting ATXN3 in SCA3 Mouse Models. Mol Ther Nucleic Acids, 2017. **7**: p. 200-210.

114. Freudiger, C.W., et al., Label-free biomedical imaging with high sensitivity by stimulated Raman scattering microscopy. Science, 2008. **322**(5909): p. 1857-61.

115. Brown, M.S., S.E. Dana, and J.L. Goldstein, Receptor-dependent hydrolysis of cholesteryl esters contained in plasma low density lipoprotein. Proceedings of the National Academy of Sciences, 1975. **72**(8): p. 2925-2929.

116. Garber, D.W., K.R. Kulkarni, and G. Anantharamaiah, A sensitive and convenient method for lipoprotein profile analysis of individual mouse plasma samples. Journal of lipid research, 2000. **41**(6): p. 1020-1026.

117. Fisher, E.A., et al., High-density lipoprotein function, dysfunction, and reverse cholesterol transport. Arterioscler Thromb Vasc Biol, 2012. **32**(12): p. 2813-20.

118. Ohvo-Rekilä, H., et al., Cholesterol interactions with phospholipids in membranes. Progress in lipid research, 2002. **41**(1): p. 66-97.

119. Ramstedt, B. and J.P. Slotte, Interaction of cholesterol with sphingomyelins and acyl-chain-matched phosphatidylcholines: a comparative study of the effect of the chain length. Biophysical journal, 1999. **76**(2): p. 908-915.

120. Di Bartolo, B.A., et al., The apolipoprotein A-I mimetic peptide ETC-642 exhibits anti-inflammatory properties that are comparable to high density lipoproteins. Atherosclerosis, 2011. **217**(2): p. 395-400.

121. Acton, S., et al., Identification of scavenger receptor SR-BI as a high density lipoprotein receptor. Science, 1996. **271**(5248): p. 518-520.

122. Vance, J.E. and B. Karten, Niemann-Pick C disease and mobilization of lysosomal cholesterol by cyclodextrin. J Lipid Res, 2014. **55**(8): p. 1609-21.

123. Rosenbaum, A.I., et al., Endocytosis of beta-cyclodextrins is responsible for cholesterol reduction in Niemann-Pick type C mutant cells. Proc Natl Acad Sci U S A, 2010. **107**(12): p. 5477-82.

124. Demais, V., et al., Reversal of Pathologic Lipid Accumulation in NPC1-Deficient Neurons by Drug-Promoted Release of LAMP1-Coated Lamellar Inclusions. J Neurosci, 2016. **36**(30): p. 8012-25.

125. Peake, K.B. and J.E. Vance, Normalization of cholesterol homeostasis by 2-hydroxypropyl-beta-cyclodextrin in neurons and glia from Niemann-Pick C1 (NPC1)-deficient mice. J Biol Chem, 2012. **287**(12): p. 9290-8.

126. Gelsthorpe, M.E., et al., Niemann-Pick type C1 I1061T mutant encodes a functional protein that is selected for endoplasmic reticulum-associated degradation due to protein misfolding. J Biol Chem, 2008. **283**(13): p. 8229-36.

127. Yu, T., et al., Ryanodine receptor antagonists adapt NPC1 proteostasis to ameliorate lipid storage in Niemann-Pick type C disease fibroblasts. Hum Mol Genet, 2012. **21**(14): p. 3205-14.

128. Neufeld, E.B., et al., The ABCA1 transporter modulates late endocytic trafficking: insights from the correction of the genetic defect in Tangier disease. J Biol Chem, 2004. **279**(15): p. 15571-8.

129. Azuma, Y., et al., Retroendocytosis pathway of ABCA1/apoA-I contributes to HDL formation. Genes Cells, 2009. **14**(2): p. 191-204.

130. Koivusalo, M., et al., Amiloride inhibits macropinocytosis by lowering submembranous pH and preventing Rac1 and Cdc42 signaling. J Cell Biol, 2010. **188**(4): p. 547-63.

131. Chen, F.W., C. Li, and Y.A. Ioannou, Cyclodextrin induces calcium-dependent lysosomal exocytosis. PLoS One, 2010. **5**(11): p. e15054.

132. Higashi, Y., et al., Cerebellar degeneration in the Niemann-Pick type C mouse. Acta Neuropathol, 1993. **85**(2): p. 175-84.

133. Elrick, M.J., et al., Conditional Niemann-Pick C mice demonstrate cell autonomous Purkinje cell neurodegeneration. Hum Mol Genet, 2010. **19**(5): p. 837-47.

134. Aye, I.L., A.T. Singh, and J.A. Keelan, Transport of lipids by ABC proteins: interactions and implications for cellular toxicity, viability and function. Chem Biol Interact, 2009. **180**(3): p. 327-39.

135. Ridgway, N.D., Interactions between metabolism and intracellular distribution of cholesterol and sphingomyelin. Biochim Biophys Acta, 2000. **1484**(2-3): p. 129-41.

136. Brady, R.O., et al., The metabolism of sphingomyelin. II. Evidence of an enzymatic deficiency in Niemann-Pick diseae. Proc Natl Acad Sci U S A, 1966. **55**(2): p. 366-9.

137. Tecedor, L., et al., CLN3 loss disturbs membrane microdomain properties and protein transport in brain endothelial cells. J Neurosci, 2013. **33**(46): p. 18065-79.

138. Schultz, M.L., et al., Modulating membrane fluidity corrects Batten disease phenotypes in vitro and in vivo. Neurobiol Dis, 2018. **115**: p. 182-193.

139. Orringer, D.A., et al., Rapid intraoperative histology of unprocessed surgical specimens via fibre-laser-based stimulated Raman scattering microscopy. Nat Biomed Eng, 2017. **1**.

140. Choi, H.Y., et al., Impaired ABCA1-dependent lipid efflux and hypoalphalipoproteinemia in human Niemann-Pick type C disease. J Biol Chem, 2003. **278**(35): p. 32569-77.

141. Pagler, T.A., et al., Cholesterol efflux via HDL resecretion occurs when cholesterol transport out of the lysosome is impaired. J Lipid Res, 2007. **48**(10): p. 2141-50.

142. Lee, C.Y., et al., Increased sphingomyelin content impairs HDL biogenesis and maturation in human Niemann-Pick disease type B. J Lipid Res, 2006. **47**(3): p. 622-32.

143. Viana, M.B., et al., Very low levels of high density lipoprotein cholesterol in four sibs of a family with non-neuropathic Niemann-Pick disease and sea-blue histiocytosis. J Med Genet, 1990. **27**(8): p. 499-504.

144. Garver, W.S., et al., The National Niemann-Pick Type C1 Disease Database: correlation of lipid profiles, mutations, and biochemical phenotypes. J Lipid Res, 2010. **51**(2): p. 406-15.

145. Boadu, E., et al., Correction of apolipoprotein A-I-mediated lipid efflux and high density lipoprotein particle formation in human Niemann-Pick type C disease fibroblasts. J Biol Chem, 2006. **281**(48): p. 37081-90.

146. Boadu, E., R.C. Nelson, and G.A. Francis, ABCA1-dependent mobilization of lysosomal cholesterol requires functional Niemann-Pick C2 but not Niemann-Pick C1 protein. Biochim Biophys Acta, 2012. **1821**(3): p. 396-404.

147. Chen, W., et al., Preferential ATP-binding cassette transporter A1-mediated cholesterol efflux from late endosomes/lysosomes. J Biol Chem, 2001. **276**(47): p. 43564-9.

148. Zanoni, P., et al., Endocytosis of lipoproteins. Atherosclerosis, 2018. **275**: p. 273-295.

149. Takahashi, K., et al., Endocytic pathway of high density lipoprotein via trans-Golgi system in rat resident peritoneal macrophages. Lab Invest, 1989. **61**(3): p. 270-7.

150. Sun, B., et al., Quantitative analysis of SR-BI-dependent HDL retroendocytosis in hepatocytes and fibroblasts. J Lipid Res, 2006. **47**(8): p. 1700-13.

151. Ramstedt, B. and J.P. Slotte, Membrane properties of sphingomyelins. FEBS letters, 2002. **531**(1): p. 33-37.

152. Beaudet, A.L. and A.A. Manschreck, Metabolism of sphingomyelin by intact cultured fibroblasts: differentiation of Niemann-Pick disease types A and B. Biochemical and biophysical research communications, 1982. **105**(1): p. 14-19.

153. Acuña, M., et al., Epidemiological, clinical and biochemical characterization of the p.(Ala359Asp) SMPD1 variant causing Niemann–Pick disease type B. European Journal of Human Genetics, 2016. **24**(2): p. 208.

154. Puri, V., et al., Cholesterol modulates membrane traffic along the endocytic pathway in sphingolipid-storage diseases. Nature cell biology, 1999. **1**(6): p. 386.

155. Levade, T., et al., Sphingomyelin-degrading pathways in human cells: role in cell signalling. Chemistry and physics of lipids, 1999. **102**(1): p. 167-178.

156. Schwendeman, A., et al., The effect of phospholipid composition of reconstituted HDL on its cholesterol efflux and anti-inflammatory properties. Journal of lipid research, 2015. **56**(9): p. 1727-1737.

157. Santamarina-Fojo, S., et al., Regulation and intracellular trafficking of the ABCA1 transporter. Journal of lipid research, 2001. **42**(9): p. 1339-1345.

158. Tardy, C., et al., HDL and CER-001 inverse-dose dependent inhibition of atherosclerotic plaque formation in apoE-/-mice: evidence of ABCA1 down-regulation. PLoS One, 2015. **10**(9): p. e0137584.

159. Tang, J., et al., Influence of route of administration and lipidation of apolipoprotein AI peptide on pharmacokinetics and cholesterol mobilization. Journal of Lipid Research, 2017. **58**(1): p. 124-136.

160. Fawaz, M.V., et al., Synthetic High-Density Lipoprotein Cholesterol Scavengers for the Treatment of Niemann-Pick C Disease. Arteriosclerosis, Thrombosis, and Vascular Biology, 2018. **38**(Suppl_1): p. A164-A164.

161. Yancey, P.G., et al., Efflux of cellular cholesterol and phospholipid to lipid-free apolipoproteins and class A amphipathic peptides. Biochemistry, 1995. **34**(24): p. 7955-7965.

162. Amar, M.J., et al., 5A apolipoprotein mimetic peptide promotes cholesterol efflux and reduces atherosclerosis in mice. Journal of Pharmacology and Experimental Therapeutics, 2010. **334**(2): p. 634-641.

163. Di Bartolo, B.A., et al., The apolipoprotein AI mimetic peptide, ETC-642, reduces chronic vascular inflammation in the rabbit. Lipids in health and disease, 2011. **10**(1): p. 224.

164. Miles, J., et al. Single-dose tolerability, pharmacokinetics, and cholesterol mobilization in HDL-C fraction following intravenous administration of ETC-642, a 22-mer ApoA-I analogue and phospholipids complex, in atherosclerosis patients. in Arteriosclerosis Thrombosis and Vascular Biology. 2004. Arteriosclerosis Thrombosis and Vascular Biology (Lippincott Williams & Wilkins 530 Walnut St, Philadelphia, PA 19106-3621 USA).

165. Patel, H., et al., Characterization of apolipoprotein AI peptide phospholipid interaction and its effect on HDL nanodisc assembly. International journal of nanomedicine, 2019. **14**: p. 3069.

166. Banerjee, A. and H. Onyuksel, Peptide delivery using phospholipid micelles. Wiley Interdisciplinary Reviews: Nanomedicine and Nanobiotechnology, 2012. **4**(5): p. 562-574.

167. Asztalos, B.F., et al., Differential effects of HDL subpopulations on cellular ABCA1-and SR-BI-mediated cholesterol efflux. Journal of lipid research, 2005. **46**(10): p. 2246-2253.

168. Andrews, J., et al., Effect of serial infusions of reconstituted high-density lipoprotein (CER-001) on coronary atherosclerosis: rationale and design of the CARAT study. Cardiovascular diagnosis and therapy, 2017. **7**(1): p. 45.

169. Nicholls, S.J., et al., Effect of serial infusions of CER-001, a pre-β high-density lipoprotein mimetic, on coronary atherosclerosis in patients following acute coronary syndromes in the CER-001 atherosclerosis regression acute coronary syndrome trial: a randomized clinical trial. JAMA cardiology, 2018. **3**(9): p. 815-822.

170. Davidson, W.S., et al., The effect of high density lipoprotein phospholipid acyl chain composition on the efflux of cellular free cholesterol. Journal of Biological Chemistry, 1995. **270**(11): p. 5882-5890.

171. Bolin, D.J. and A. Jonas, Sphingomyelin inhibits the lecithin-cholesterol acyltransferase reaction with reconstituted high density lipoproteins by decreasing enzyme binding. Journal of Biological Chemistry, 1996. **271**(32): p. 19152-19158.

172. Sparks, D.L., P.G. Frank, and T.A.-M. Neville, Effect of the surface lipid composition of reconstituted LPA-I on apolipoprotein AI structure and lecithin:

cholesterol acyltransferase activity. Biochimica et Biophysica Acta (BBA)-Lipids and Lipid Metabolism, 1998. **1390**(2): p. 160-172.

173. Dasseux, J.-L., et al., Apolipoprotein AI agonists and their use to treat dyslipidemic disorders. 2000, Google Patents.

174. Remaley, A.T., et al., Apolipoprotein specificity for lipid efflux by the human ABCAI transporter. Biochemical and biophysical research communications, 2001. **280**(3): p. 818-823.

175. Navab, M., et al., Apolipoprotein AI mimetic peptides and their role in atherosclerosis prevention. Nature Reviews Cardiology, 2006. **3**(10): p. 540.

176. Sethi, A.A., et al., Asymmetry in the Lipid Affinity of Bihelical Amphipathic Peptides A structural determinant for the specificity of abca1-dependent cholesterol efflux by peptides. Journal of Biological Chemistry, 2008. **283**(47): p. 32273-32282.

177. Wool, G.D., C.A. Reardon, and G.S. Getz, Apolipoprotein AI mimetic peptide helix number and helix linker influence potentially anti-atherogenic properties. Journal of lipid research, 2008. **49**(6): p. 1268-1283.

178. Vecoli, C., et al., Apolipoprotein A-I mimetic peptide L-4F prevents myocardial and coronary dysfunction in diabetic mice. Journal of cellular biochemistry, 2011. **112**(9): p. 2616-2626.

179. Bielicki, J.K., et al., A new HDL mimetic peptide that stimulates cellular cholesterol efflux with high efficiency greatly reduces atherosclerosis in mice. Journal of lipid research, 2010. **51**(6): p. 1496-1503.

180. Khan, M., et al. Single-dose intravenous infusion of ETC-642, a 22-Mer ApoA-I analogue and phospholipids complex, elevates HDL-C in atherosclerosis patients. in Circulation. 2003. Lippincott Williams & Wilkins 530 Walnut St, Philadelphia, PA 19106-3621 USA.

181. Assmann, G., et al., Phosphatidylcholine substrate specificity of lecithin: cholesterol acyltransferase. Scandinavian Journal of Clinical and Laboratory Investigation, 1978. **38**(sup150): p. 16-20.

182. Subbaiah, P.V., et al., Altered positional specificity of human plasma lecithin-cholesterol acyltransferase in the presence of sn-2 arachidonoyl phosphatidyl cholines. Mechanism of formation of saturated cholesteryl esters. Biochimica et Biophysica Acta (BBA)-Lipids and Lipid Metabolism, 1992. **1128**(1): p. 83-92.

183. Small, D.M., Handbook of Lipid Research: The Physical Chemistry of Lipids: From Alkanes to Phospholipids. 1986.

184. Parks, J. and A. Gebre, Long-chain polyunsaturated fatty acids in the sn-2 position of phosphatidylcholine decrease the stability of recombinant high density lipoprotein apolipoprotein AI and the activation energy of the lecithin: cholesterol acyltransferase reaction. Journal of lipid research, 1997. **38**(2): p. 266-275.

185. Sreerama, N. and R.W. Woody, Estimation of protein secondary structure from circular dichroism spectra: comparison of CONTIN, SELCON, and CDSSTR methods with an expanded reference set. Analytical biochemistry, 2000. **287**(2): p. 252-260.

186. Reißer, S., et al., 3D hydrophobic moment vectors as a tool to characterize the surface polarity of amphiphilic peptides. Biophysical journal, 2014. **106**(11): p. 2385-2394.

187. Lomize, A.L., et al., Membranome: a database for proteome-wide analysis of single-pass membrane proteins. Nucleic acids research, 2016. **45**(D1): p. D250-D255.

188. Lomize, M.A., et al., OPM database and PPM web server: resources for positioning of proteins in membranes. Nucleic acids research, 2011. **40**(D1): p. D370-D376.

189. Homan, R., et al., A fluorescence method to detect and quantitate sterol esterification by lecithin: cholesterol acyltransferase. Analytical biochemistry, 2013. **441**(1): p. 80-86.

190. Krieger, M., Charting the fate of the “good cholesterol”: identification and characterization of the high-density lipoprotein receptor SR-BI. Annual review of biochemistry, 1999. **68**(1): p. 523-558.

191. Wang, N., et al., ATP-binding cassette transporters G1 and G4 mediate cellular cholesterol efflux to high-density lipoproteins. Proceedings of the National Academy of Sciences, 2004. **101**(26): p. 9774-9779.

192. Asztalos, B.F., et al., Role of LCAT in HDL remodeling: investigation of LCAT deficiency states. Journal of lipid research, 2007. **48**(3): p. 592-599.

193. Soutar, A.K., et al., Effect of the human plasma apolipoproteins and phosphatidylcholine acyl donor on the activity of lecithin. Cholesterol acyltransferase. Biochemistry, 1975. **14**(14): p. 3057-3064.

194. Sorci-Thomas, M., M. Kearns, and J. Lee, Apolipoprotein AI domains involved in lecithin-cholesterol acyltransferase activation. Structure: function relationships. Journal of Biological Chemistry, 1993. **268**(28): p. 21403-21409.

195. Anantharamaiah, G., et al., Use of synthetic peptide analogues to localize lecithin: cholesterol acyltransferase activating domain in apolipoprotein AI.

Arteriosclerosis: An Official Journal of the American Heart Association, Inc., 1990. **10**(1): p. 95-105.

196. Datta, G., et al., Effects of increasing hydrophobicity on the physical-chemical and biological properties of a class A amphipathic helical peptide. Journal of lipid research, 2001. **42**(7): p. 1096-1104.

197. Xu, B., et al., ABCA1-Derived Nascent High-Density Lipoprotein–Apolipoprotein AI and Lipids Metabolically Segregate. Arteriosclerosis, thrombosis, and vascular biology, 2017. **37**(12): p. 2260-2270.

198. Didichenko, S.A., et al., Enhanced HDL functionality in small HDL species produced upon remodeling of HDL by reconstituted HDL, CSL112: effects on cholesterol efflux, anti-inflammatory and antioxidative activity. Circulation research, 2016. **119**(6): p. 751-763.

199. Li, D., et al., Effect of Synthetic High Density Lipoproteins Modification with Polyethylene Glycol on Pharmacokinetics and Pharmacodynamics. Molecular pharmaceutics, 2017. **15**(1): p. 83-96.

200. Ditiatkovski, M., et al., Apolipoprotein AI Mimetic Peptides: Discordance Between In Vitro and In Vivo Properties—Brief Report. Arteriosclerosis, thrombosis, and vascular biology, 2017. **37**(7): p. 1301-1306.

201. Dal Magro, R., et al., ApoE-modified solid lipid nanoparticles: A feasible strategy to cross the blood-brain barrier. Journal of Controlled Release, 2017. **249**: p. 103-110.

202. Meng, Y., et al., A basic apoE-based peptide mediator to deliver proteins across the blood-brain barrier: long-term efficacy, toxicity, and mechanism. Molecular Therapy, 2017. **25**(7): p. 1531-1543.

203. Kreuter, J., et al., Covalent attachment of apolipoprotein AI and apolipoprotein B-100 to albumin nanoparticles enables drug transport into the brain. Journal of controlled release, 2007. **118**(1): p. 54-58.